Doctoral Thesis

Microengineered Hydrogel System for Complex 3D Tissue Engineering

Dongjin Lee

Department of Materials Science and Engineering

Graduate School of UNIST

2020

Microengineered Hydrogel System for Complex 3D Tissue Engineering

Dongjin Lee

Department of Materials Science and Engineering

Graduate School of UNIST

Microengineered Hydrogel System for Complex 3D Tissue Engineering

A thesis/dissertation
submitted to the Graduate School of UNIST
in partial fulfillment of the
requirements for the degree of
Doctor of Philosophy

Dongjin Lee

December/11/2019 of submission

Approved by

Advisor
Chaenyung Cha

Microengineered Hydrogel System for Complex 3D Tissue Engineering

Dongjin Lee

This certifies that the thesis/dissertation of Dongjin Lee is approved.

December/11/2019 of submission

signature

Advisor: Chaenyung Cha

signature

Prof. Jiyun Kim

signature

Prof. Hyun-Wook Kang

signature

Prof. Tae Eun Park

signature

Prof. Seung Yun Yang

signature.

Abstract

Tissue engineering is a multi-disciplinary field that bring into play expertise in biology and engineering to develop biomimetic tissue constructs. These days, it would be not enough to mimic the physical and biological properties of the native tissue because various cells possess different physical properties such as stiffness or diffusion. Therefore, we need to develop artificial tissues within 3D formation resembling the natural extracellular matrix (ECM) microenvironment in order to observe more closely to mimic native tissues. Hydrogel is very useful materials in that hydrophilic and good properties high swelling ratio. Also, it can be possible to control mechanical and chemical properties and applied for tissue engineering fields.

This thesis indicates the development of three-dimensional microfluidic devices for cellular studies based on applications such as high throughput cell encapsulated beads culture and cell-based assay. With microfluidics, we can generate cell encapsulated microgel which can be possible to observe cell morphology or drug test due to high diffusion compare to bulk size hydrogel. Microfluidics has a lot of benefits such as low cost, low consuming reagent, fast analysis and portable device and so on. I used this platform such as microfluidic chip in order to generate cell encapsulated beads with uniform size. I used Gelatin which is derived from collagen that is biocompatible polymer. I synthesis from gelatin to GelMa using some reagent during 48h. GelMa can react cross-linking by UV light due to cleavage double bond by radical reaction. And already GelMa has RGD site which can attach binding part with cell, therefore cell grows good environment likely ECM structure. And I can control the polymer stiffness using various GelMA concentration.

This thesis is organized as follows:

In chapter I is general introduction related to properties of basic microfluidics and microfluidic fabrication.

In chapter II is introduction of tissue engineering, hydrogel and various cells.

In chapter III is that Generated macrophage encapsulated beads using microfluidic chip and observed cell morphology by different stiffness and stimulated protein such as LPS (lipopolysaccharide).

In chapter IV is that Co-culture system with macrophage and MCF-7 in order to obtain more cohesive spheroid in microgel. In chapter V is that Generation of breast cancer such as MDA-MB-231, MCF-7, SK-BR-3 encapsulated beads and observed cell morphology by different stiffness and two kind of chemotherapeutics such paclitaxel and cisplatin.

Finally, I presented hollow fiber to mimic blood vessel using endothelial cell and observed cell morphology and viability in chapter VI.

List of Contents

List of Figures

Part I : General Introduction

Part II : Introduction

Part III : Microfluidics-assisted fabrication of macrophage microtissues with tunable physical properties for developing in vitro multiplex tissue model

D3=160 μm, D4=200 μm.

Figure 3.6. Microfluidic generation of gel-precursor droplets at varying ratios of aqueous-to-oil flow rates (Q_{Aq}/Q_O). (a) Q_{Aq}/Q_O = 0.095, (b) Q_{Aq}/Q_O = 0.21, (c) Q_{Aq}/Q_O = 0.32, (d) Q_{Aq}/Q_O = 0.45 (scale bar: 200 μm).

Figure 3.7. The viability of cells encapsulated in droplets having various sizes measured before photo-crosslinking to develop cell-laden microgels. D1=100 μm, D2=120 μm, D3=160μm, D4=200 μm. (scale bar: 50 μm)

Figure 3.8. Cell viability and proliferation in microgels at C2 (Aq1/Aq2=9%/12%) (a) Microscopic (upper) and fluorescent (lower) images of macrophages encapsulated in microgels taken at various times. The cells were fluorescently stained to identify live (green) and dead (red) cells (scale bar: 50 μm). (b) viability of macrophages at various times during culture up to 7 days. (c) The normalized number of viable cells (N_t/N_0) in the microgels was measured over time. (d) The plot in (c) was fitted with a power-law model to obtain the proliferation rates (k_P) (*p<0.05).

Figure 3.9. Cell viability and proliferation in microgels at (a) C1 (Aq1/Aq2 = 7% / 10%) and (b) C3(Aq1/Aq2 = 11% / 14%). Microscopic (upper) and fluorescent (lower) images of macrophages encapsulated in microgels taken at various times. The cells were fluorescently stained to identify live (green) and dead (red) cells (scale bar: 50 μm).

Figure 3.10. The viability of cells encapsulated in microgels with varying size at day 3 (scale bar: 50 μm). D1=100 μm, D2=120 μm, D3=160 μm, D4=200 μm.

Figure 3.11. (a) Differentiation of macrophages in microgels. (a) Microscopic images of macrophages in different microgels treated with LPS at day 7 (scale bar: 50 μm). Differentiated cells demonstrate sprouting formation. (b) The viability of macrophages at various times during culture up to 7 days. (c) The percentage of differentiated macrophages in the microgel.

Figure 3.12. Microscopic images of macrophage encapsulated in MGel microgels at varying concentrations (C1, C2 and C3) treated with LPS to induce Mϕ polarization (scale bar: 50 μm).

Figure 3.13. Microscopic images of macrophage cells cultured on the surfaces of MGel hydrogels at varying concentrations (C1, C2, and C3) which were prepared separately to assess the effects of culture conditions (2D vs. 3D) on the macrophage proliferation (scale bar: 200 μm). The initial cell adhesion and proliferation were monitored over time.

Figure 3.14. Immunocytochemical analysis of macrophage-laden microgels at different mechanical properties: (a) C1, (b) C2, (c) C3.

Figure 3.15. (a) Macrophage-laden microgels were embedded into a larger fibroblast tissue construct to fabricate multiplex tissue model. (b,c) The changes in their phenotypes were monitored over time (scale bar: 100 μm). The macrophages were treated with LPS prior to incorporation (untreated macrophages were used as a control). (d) A magnified view of the macrophages within the fibroblast tissue over time (scale bar: 50 μm).

Figure 3.16. (a,b) Macrophage-laden microgels were embedded into a larger hepatocarcinoma tissue construct to fabricate multiplex tissue model. The changes in their phenotypes were monitored over time (scale bar: 100 μm). The macrophages were treated with LPS prior to incorporation (untreated macrophages were used as a control). The arrow indicates the activated macrophages migrating out of the microgel. There was a significant decrease in hepatocarcinoma cell density surrounding the macrophage (highlighted area). (c) A magnified view of the macrophages within the hepatocarcinoma tissue over time (scale bar: 50 μm).

Part IV : Combined effects of co-culture and substrate mechanics on 3D tumor spheroid formation within microgels prepared via flow-focusing microfluidic fabrication

Figure 4.1. ^{1}H-NMR spectrum of methacrylic gelatin (MGel). Characteristic peaks (a and b) of methacrylate are noted.

Figure 4.2. Schematic illustration of double flow-focusing channel geometry of the microfluidic device used to generate cell-laden microgels.

Figure 4.3. (a) Schematic illustration of the fabrication of cell-laden microgels using a “double” flow focusing microfluidic device. Droplets of gel precursor solution dispersed with tumor cells are photo-crosslinked to generate the microgels. The cell-laden microgels are continuously cultured to allow the cells to proliferate and form spheroids. (b) A microscopic view of the microfluidic device (scale bar: 200 μm). (c) Representative optical (left) and fluorescent (right) images of cell-laden microgels (scale bar: 50 μm). The cells were fluorescently labeled to visualize live (green) and dead (red) cells.

Figure 4.4. (a) Elastic moduli (E) of MGel hydrogels at varying concentrations. (b) The viability of MCF-7 cells encapsulated in microgels at varying MGel concentrations, measured at various times up to 7 days.

Figure 4.5. Microscopic images of cell-laden microgels at various mechanical stiffness (from C1 to C5), controlled by MGel concentration, cultured over time (scale: 50 μm).

Figure 4.6. (a) The number of live MCF-7 cells at various times (N_t) normalized with the initial number of live cells (N_0) plotted over time. (b) The proliferation rate (k) obtained by fitting the plot in (a) with Eq.(1). (*p<0.05, n = 10)

Figure 4.7. The tumor spheroid formation within microgels with varying mechanics after 14 days of cell culture (scale: 50 μm). A collection of smaller spheroids was developed within the microgel.

Figure 4.8. (a) Schematic illustration of tumor microenvironment, consisting of multiple types of cells. Reprinted with permission from ref.[40]. Copyright 2016 Springer Nature. (b) Optical (left) and fluorescent (right) microscopic images of microgels encapsulated with varying amounts of macrophages co-cultured with MCF-7 cells (scale bar: 50 um). The cells were fluorescently labeled to

C5) exposed to paclitaxel and cisplatin, calculated from (a) and (b) (*p<0.05). Solid and dotted lines represent the viabilities of monolayer cultures of SK-BR-3 cells exposed to the same concentration at day 1 and 3, respectively.

Part VI : Facile generation hollow fiber to mimic blood vessel using human endothelial cells via GelMa and Alginate combination by controlled hydrogel stiffness in 3D culture

Figure 6.1. This schematic represents overall experiments. (a) Alginate and MGel mixed Ca^{2+} as a physical cross-linking using Alginate (Semi-IPN) after then chemical cross-linking by UV exposure using MGel (IPN). (b) IPN structure can be removed physically cross-linked Alginate by Sodium Citrate. (c) Generating of hollow fiber using same methods.

Figure 6.2. (a) and (c) Elastic moduli (E) and Swelling ratios (Q) of Alginate 0.5% and MGel mixed Semi-IPN and IPN (b) and (d) Elastic moduli (E) and Swelling ratios (Q) of Alginate 1% and MGel mixed Semi-IPN and IPN.

Figure 6.3. SEM images of IPN structure (Alginate 1% and MGel 8%, 10%, 12%, 15%) (scale bar: 10 μm)

Figure 6.4. Cell viability and proliferation in microgel. Representative microscopic(left) and fluorescent (right) images of 3T3 encapsulated in microgel taken at various times up to 7days. The cells were fluorescently stained to identify live (green) and dead (red) cells. (a) Semi-IPN structure (b) IPN structure (c) and (d) The normalized number of viable cells (N_t/N_0) in microgel was measured over time (N_t: number of viable cells at time, t, N_0: number of initial viable cells) Semi-IPN and IPN. (e) The plot in panel (c) and (d) were fitted with a power-law model to obtain the proliferation rate (k_P).

Figure 6.5. These images show the process which is removed alginate from IPN microgel in various time.

Figure 6.6. Scheme of generation of hollow fiber using alginate and MGel with HUVECs outer phase and inner phase 0.05M calcium chloride, 10% FBS, 25mM HEPES.

Figure 6.7. (a) Hollow fiber to mimic blood vessel using Alginate and MGel. (b) Microscopic image of hollow fiber.

Figure 6.8. Cell viability and proliferation in hollow fiber with HUVECs. Representative microscopic(left) and fluorescent (right) images of HUVECs encapsulated in microgel taken at various times up to 7days. These images show at 7days. The cells were fluorescently stained to identify live (green) and dead (red) cells. (a) Semi-IPN structure (b) IPN structure.

List of Tables

Part III : Microfluidics-assisted fabrication of macrophage microtissues with tunable physical properties for developing in vitro multiplex tissue model

Part IV : Combined effects of co-culture and substrate mechanics on 3D tumor spheroid formation within microgels prepared via flow-focusing microfluidic fabrication

Abbreviations

The abbreviations used extensively are :

BSA : Bovine serum albumin

Calcein-AM : Calcein acetoxymethylester

DMEM : Dulbecco's Modified Eagle's Medium

ECM : Extracellular matrix

ELISA : Enzyme Linked Immunosorbents Assay

FBS : Feral Bovine Serum

FITC : Fluorescein Isothiocyanate

GelMA : Gelatin Methacrylate

HEPES : 4-(2-hydroxyethyl)-1-piperazineethanesulfonic acid

ICC : Immunocytochemistry(Immunocytochemical)

MMP : Matrix metalloprotein

MSC : Mesenchymal stem cell (D1)

MTT : 3-(4,5-dimethylthiazol-2-yl)-2,5-diphenyl tetrazolium bromide

PBS : Phosphate Buffered Saline\

PI : Photo initiator

RGD : Arginine-glycine-aspartic acid

SD : Standard deviation

SDS : Sodium Dodesyl Sulfate

UV : Ultraviolet

PART I

General Introduction

1.1. Microfluidics Properties

1.1.1. Theoretical Study of Droplet Generation.

This chapter describes the theoretical background of the droplet formation mechanism using the microfluidic flow focusing method as well as the influence of other parameters on droplet generation. When two kind of immiscible liquids exposed each other in the microfluidic chip, the liquid breaking as a droplet formation via dripping, jetting and squeezing methods. Generally, at slow flow rate, the droplet can be made at dripping regime. However, at higher flow rate, the liquid can be divided via thin stream which is able to break in order to make droplet formation at jetting regime. And these studies can summary in that three kind of method such as dripping, jetting and squeezing.

1.1.1.1. Squeezing

In the squeezing regime case, very low capillary number of continuous phase and disperse phase as shown in Figure 1A. In order to maintain the constant flow rate, which increased the pressure apply to continuous phase streams. This result said that generating a neck of the dispersed phase of orifice channel. Finally, the narrowing neck can be unstable and breaks to droplet formation using disperse phase. [1] Droplets are formed at the equilibrium state between interface tension and hydrostatic pressure. Gastecki et al. introduced a rate of flow-controlled breakup model using flow focusing microfluidic chip at a low flow rate. [1-3] This model describes that the size of droplet is related to the flow rate ratio between dispersed phase and continuous phase at low flow rate.

1.1.1.2. Dripping.

In the dripping regime case, two kind of force, one is capillary force, another is viscous drag force, can be separated as a droplet formation via flow-focusing microfluidic chip. As shown in Figure 1B, a little bit increased the flow rate, the disperse phase can be unstable formation because of minimizing of the surface tension force by generated a droplet.[4] Continuous phase can overcome surface tension using shear force and finally droplet breaks up. Dripping regime examined based on shearing model. In this

case, the diameter of droplets is reversely related to the capillary number.

1.1.1.3. Jetting.

In the jetting regime case, there are two kind of method to generate jetting formation. One is Webber number (We) of disperse phase fluid is high. Another one is capillary number of the continuous phase is high. More detail explained, Weber number of the disperse phase is larger than 1 because of high flow rate or high density of disperse phase. In other words, inertia force is dominated rather than interfacial tension force. On the other hand, when capillary number of the continuous phase is high because of fast flow rate of continuous phase or high viscosity which can occur drag force of the outer continuous phase that can over the surface tension force of disperse phased.[2] This jetting stream is unstable because of unstable and breaking droplet at the downstream of the channel due to surface tension of the dispersed phase to minimize the surface area by generating a droplet as shown Figure 1C.

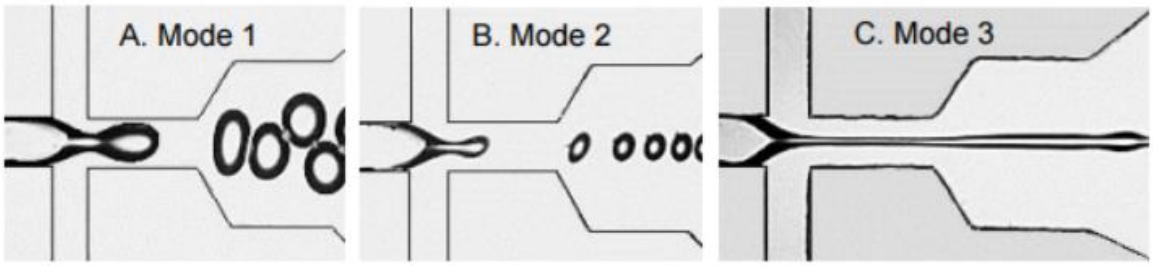

Figure 1.1 Droplet generating method in the flow focusing device. (A) Mode : squeezing regime at very low flow rate and low capillary number. (B) Mode : dripping regime at higher flow rate and modest capillary number. (C) Mode : jetting regime at high capillary number.

1.2. Microfabrication of Microfluidic chip formed Double Flow focusing Geometry

1.2.1. Microfluidic Chip Design

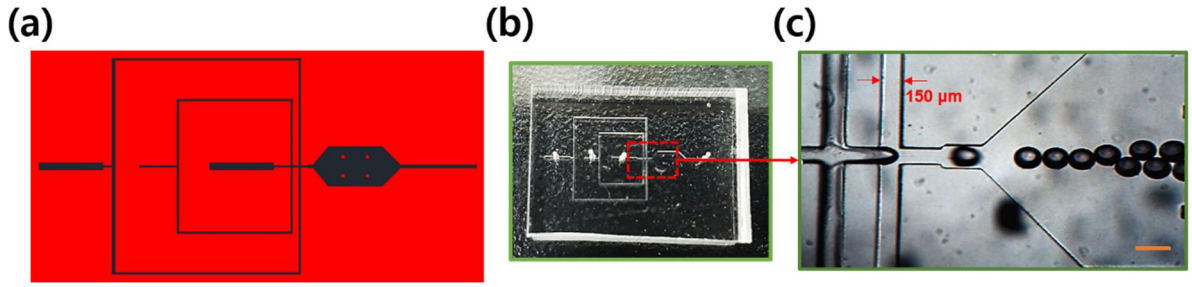

Figure 1.2 (a) This image is CAD file (b) Fabrication of microfluidic chip using PDMS (c) With microfluidic chip and generating droplet.

As shown the figure 1.2, we choose double flow focusing method in order to cell encapsulated beads with high cell viability. All channel width is 150 μm. And the high is 160 μm.

1.2.2. Mold Fabrication through MEMs Process

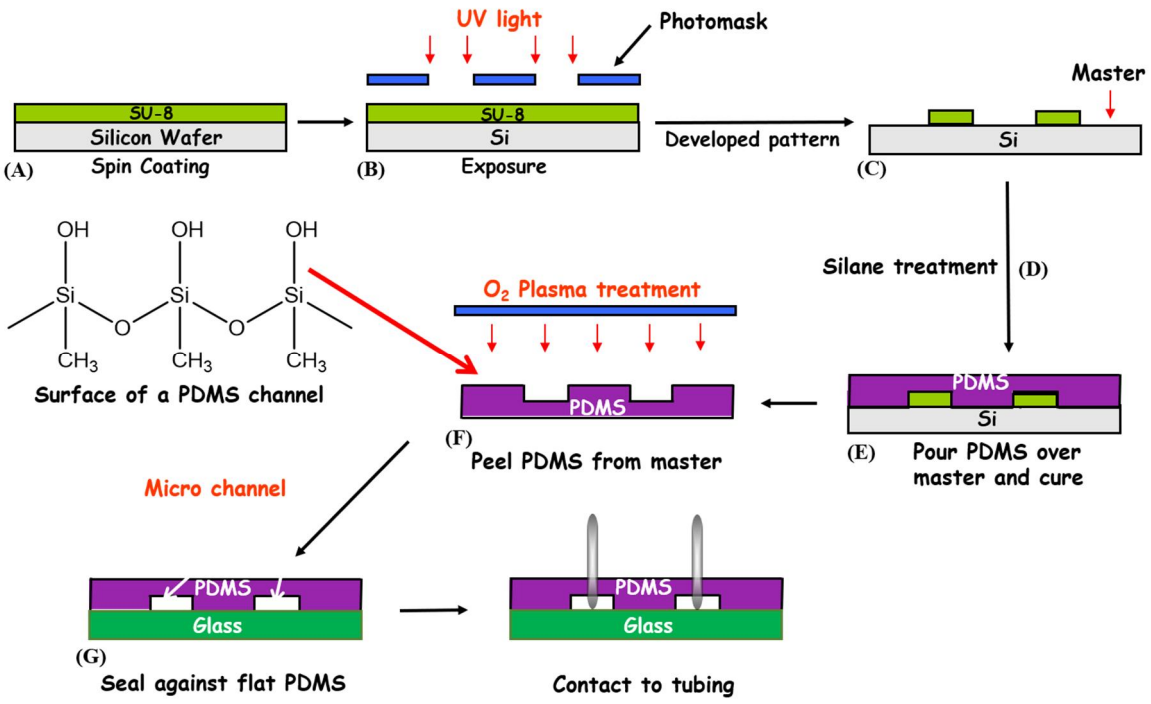

Figure 1.3 The process of PDMS microfluidic chip fabrication.

The fabrication process, as shown in Figure 1.3, begins with a silicon wafer, which is cleaned on the surface by pirhana treatment (H_2SO_4 : H_2O_2, 10:1) during 10 min. Fully remove the water on the wafer surface, coated with a UV-curable SU-8 100 (A). The process involves spin-coating the photoresist to control thickness, followed by baking to solidify the SU-8 100. Next, the SU-8 100 coated on the wafer and exposed to UV light through a photomask (B), which in the case of the most commonly used photoresist, SU-8 100, blocks light from the areas between fluidic channels. The UV exposure results in a crosslinking of the polymer's epoxide moieties and hardening of the exposed polymer regions, which remain in place during development in a SU-8 developer, while the unexposed polymer is washed off (C). This silicon wafer with hardened polymer features is used as a master mold and is coated with a fluorinated silane to aid demolding (D).

1.2.3. Microchannel Fabrication using PDMS

PDMS, typically mixed at a 10:1 ratio of monomer : curing agent, is poured over the mold to the desired height and allowed to polymerize at 60^{o}C for 1 or 2 hours (E). The molded PDMS is removed, via holes are punched out, and the device is completed by bonding the PDMS features to a glass slide using oxygen plasma treatment (F) of both glass and PDMS (G).

1.3. Reference

1. Nunes, J. K.; Tsai, S. S.; Wan, J.; Stone, H. A., Dripping and jetting in microfluidic multiphase flows applied to particle and fiber synthesis. *J Phys D Appl Phys* **2013,** *46* (11).
2. Garstecki, P.; Stone, H. A.; Whitesides, G. M., Mechanism for flow-rate controlled breakup in confined geometries: a route to monodisperse emulsions. *Phys Rev Lett* **2005,** *94* (16), 164501.
3. Nie, Z.; Seo, M.; Xu, S.; Lewis, P. C.; Mok, M.; Kumacheva, E.; Whitesides, G. M.; Garstecki, P.; Stone, H. A., Emulsification in a microfluidic flow-focusing device: effect of the viscosities of the liquids. *Microfluidics and Nanofluidics* **2008,** *5* (5), 585-594.
4. Lagus, T. P.; Edd, J. F., A review of the theory, methods and recent applications of high-throughput single-cell droplet microfluidics. *Journal of Physics D: Applied Physics* **2013,** *46* (11).

PART II

Introduction

2.1. Tissue Engineering

Tissue Engineering is interdisciplinary field which utilizes cell, biochemical, physical signals and biomaterials as well as they combined in order to mimic native tissue.[1] The purpose of tissue engineering is to offer biological substitutes which can keep, restore and develop the function of damaged tissues.[2] Tissue engineering applications combined to three kind of pillars : cells, signals and scaffolds. These are represented the triad of tissue engineering as shown Figure 2.1.

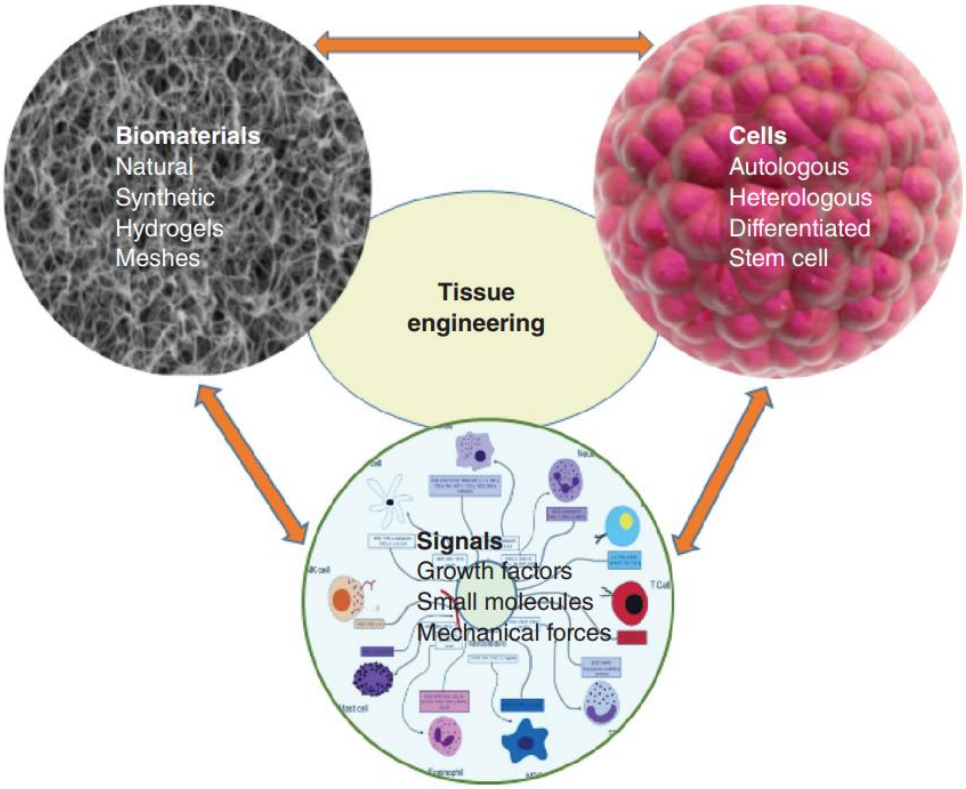

Figure 2.1. The three kind of part are related to tissue engineering. The combination of cells, signals and scaffolds is used to engineer functional tissues.

The scaffolds must be maintained biocompatible with both tissue specific cell types and the desired area environment within human body.[3] Therefore, it is important that various engineered tissues or organs necessitate unique designs and materials. Also, the scaffolds can fabricate with specific properties, for example, geometry, pore size, spatial distribution and permeability.[4] Artificial tissues

would be transplanted into the bodies of patients. The scaffolds are demanded to possess the geometric shape of the damaged tissue.[5-8] In addition, scaffolds have to provide appropriate mechanical properties or stability of shape to resist stresses. Hydrogel, as a scaffold, are usually used for cell encapsulated with maintained high biocompatibility and mild gelation conditions.[9] Scaffolds are obtained of natural or synthetic materials. And they can replicate the functions like natural three-dimensional environment in order to proliferate and organize into tissues which can maintain their specialized morphologies.[32] Tissue engineering aims to cure diseased or disfunctional tissues and organs. Appropriate sources of cells for tissue engineering can be identified. It is also important that finding suitable scaffolds for ECMs is challenged.

2.2. ECM Structure and Hydrogel Biomaterials

2.2.1. ECM Structure

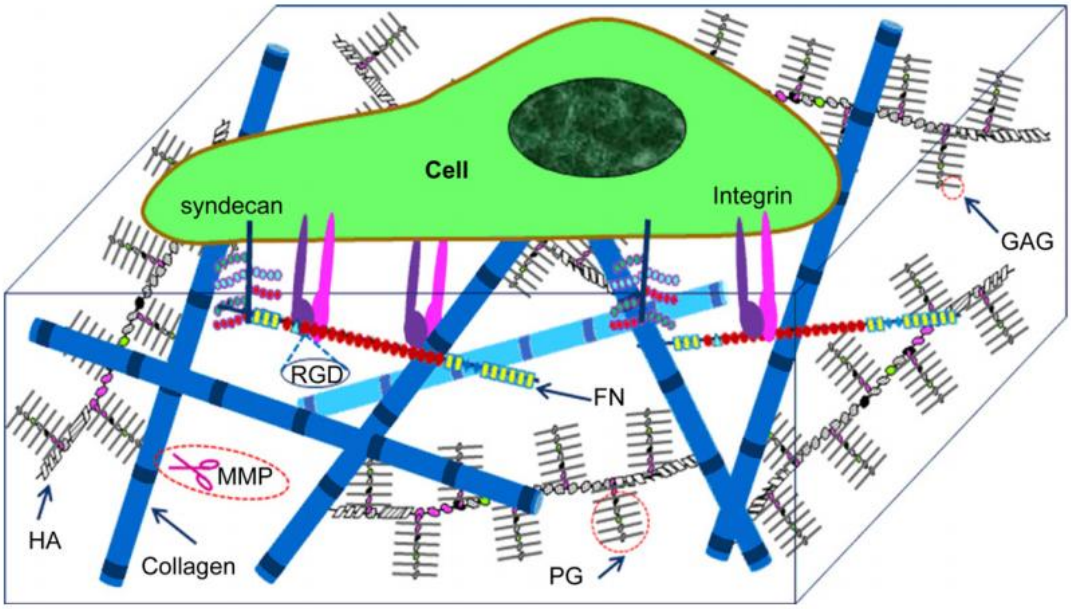

Figure 2.2. Complex three-dimensional structure of extracellular matrix (ECM) and ECM-cell interactions.

These days, some advanced techniques, such as 3D printing and electrospinning, have been improved to fabricate scaffolds that can imitate the extra cellular matrix (ECM).[10-12] The tissue of the human body included extracellular space which molecules are secreted by the cells to form a complex network. [13, 14] Generally, natural ECM such as collagen, elastin and fibrin consists of two classes of biomacromolecules, proteins and glycans.[15, 16] ECM proteins are embedded in negatively charged such as glycans which containing glycosaminoglycans (GAGs) and proteoglycans (PGs)[10, 16-18] GAGs are linear polymers of repeated disaccharide derivative with two types, such as sulfated and hyaluronic acid

(HA).[19] Most ECM proteins, containing collagen, FN(e.g., RGD, REDV and PHSRN), LN(e.g., YIGSR, LRE and IKLLI) and elastin(e.g., VAPG) have specific cleavage sites for degradation by enzymes, for example, matrix metalloproteinases (MMPs) plasmin and elastase.[20-24] MMPs are important role in morphogenesis, arthritis, angiogenesis, tumor invasion and metastasis.[25] There are two forms of RGD peptides, including linear RGD and cyclic RGD (cRGD). The RGD sequence in the cell binding domain of FN is exposed at the tip of a loop with a spatial constraint that results in increased affinity for cell binding[26] as shown Figure 2.2.

2.2.2. ECM property (Mechanotransduction)

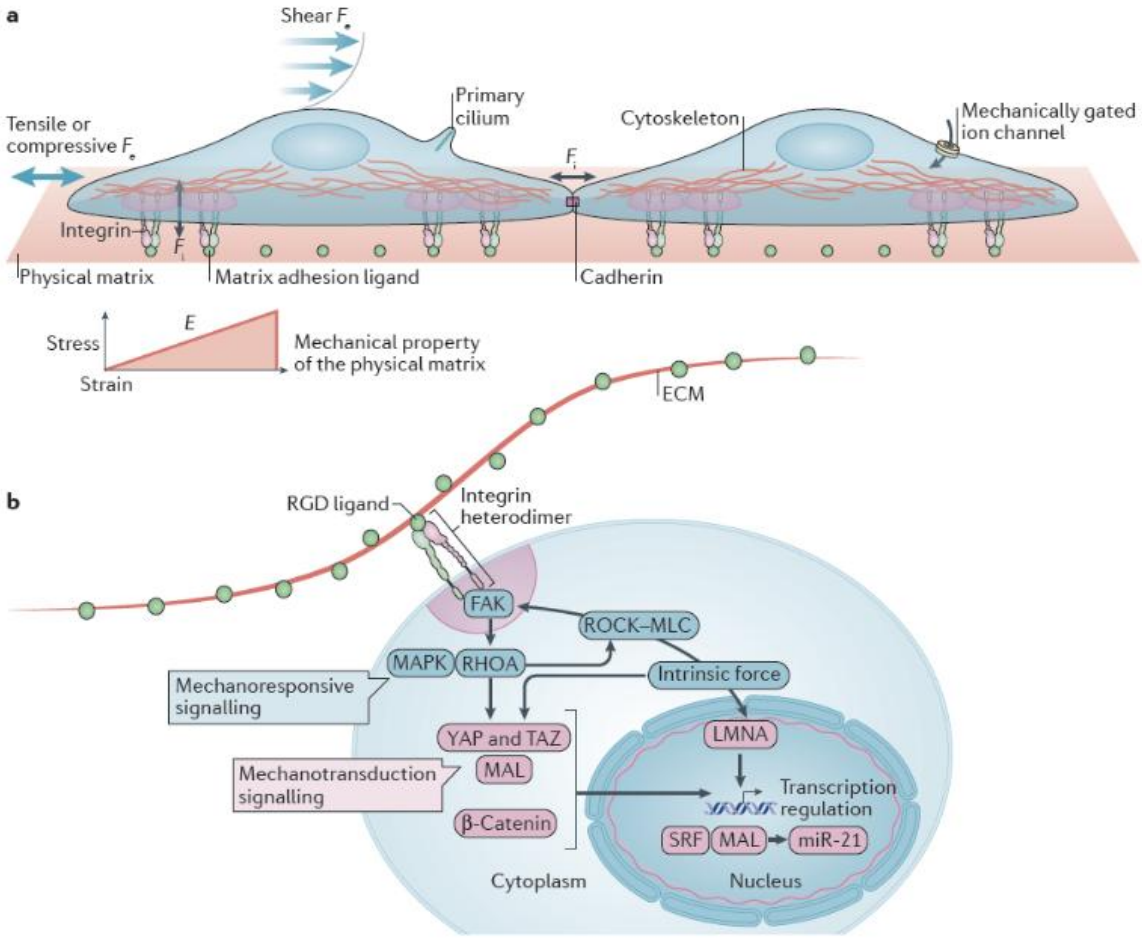

Figure 2.3. Stem cells exert forces and they are affected by external forces, which controlled their intracellular signaling pathways.[27]

Stem and cancer cells are interaction mechanically with their local area microenvironment, or niche, and these communications lead to develop the processes, direct cell fate, regulate tissue development, and are related to the progression of numerous diseases. It is possible that mechanical signals can be

used to modify disease progression and directly aid regeneration. There is a sensor called focal adhesion on the cell membrane that carries the physical signals from the ECM to the cell nucleus. We called this phenomenon 'mechanotransduction'. Figure 2.3 is well explained how to occur cell to ECM interaction through mechanotransduction.

2.2.3. Hydrogel biomaterials

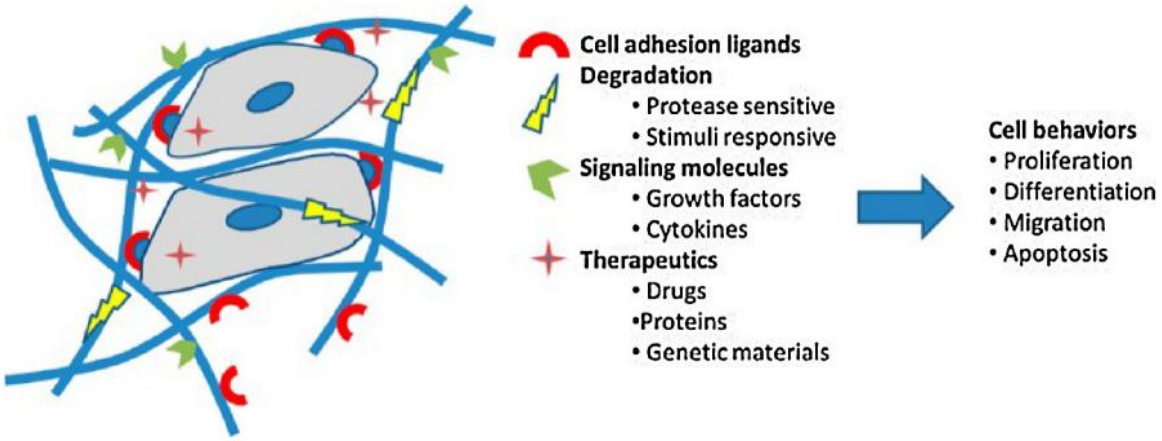

Figure 2.4. Important materials design considerations for tissue engineering, containing cell adhesion peptide, protease sensitive peptide for cell mediated matrix degradation, and presence of signaling molecules.

Hydrogel is attractive materials in that biocompatible and achieving mechanically robust networks with various enzymes. Various cell-matrix interaction, containing cell adhesion and matrix degradation are demanded for cell growth and migration.[28] Hybrid hydrogels can be employed to capture these properties (Figure 2.4) in a chemically and mechanically versatile substrate. Hydrogels are water-swollen polymeric materials that can be possible to support three-dimensional structure.

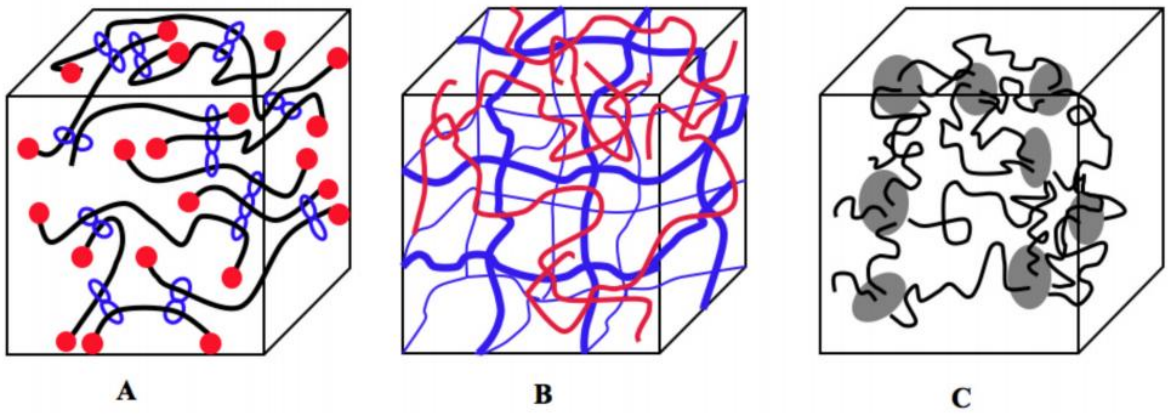

Figure 2.5 Synthesis hydrogels with good mechanical properties. (A) Topological sliding hydrogel.[29] (B) Double network hydrogels composed from two hydrophilic networks.[30] (C) Nanocomposite hydrogels synthesized by radical polymerization.[31]

Typical methods of biomaterials synthesis contained crosslinking polymerization using reactive polymer precursors. Hydrogels have been three main approaches, introduction of sliding crosslinking agent[29], double network hydrogels[30] and nanocomposite[31] hydrogels have noticeable enhanced mechanical properties of hydrogels as figure 2.5. Sliding crosslinking agent is a new concept of crosslinking. By chemically crosslinking two molecules, a sliding double ring crosslinking agent was produced. In this case, the hydrogel has outstanding mechanical properties. Double networks (DN) hydrogels are consist of interpenetrating networks (IPNs) formed by two kind of hydrophilic networks. Nanocomposite hydrogels are organic or inorganic hybrids. These hydrogels possessed extremely high surface hydrophobicity property.

2.3. Reference

1. Berthiaume, F.; Maguire, T. J.; Yarmush, M. L., Tissue engineering and regenerative medicine: history, progress, and challenges. *Annu Rev Chem Biomol Eng* **2011,** *2*, 403-30.

2. Langer, R.; Vacanti, J. P., Tissue Engineering. *SCIENCE* **1993,** *260*.

3. Langer, R., Perspectives and challenges in tissue engineering and regenerative medicine. *Adv Mater* **2009,** *21* (32-33), 3235-6.

4. Khademhosseini, A.; Langer, R.; Borenstein, J.; Vacanti, J. P., Microscale technologies for tissue engineering and biology. *PNAS* **2005,** *103*, 2480-2487.

5. Kadler, K., Matrix loading: assembly of extracellular matrix collagen fibrils during embryogenesis. *Birth Defects Res C Embryo Today* **2004,** *72* (1), 1-11.

6. Cukierman, E.; Pankov, R.; Stevens, D. R.; Yamada, K. M., Taking Cell-Matrix Adhesions to the Third Dimension. *SCIENCE* **2001,** *294*.

7. Abbott, A., Cell culture: Biology's new dimension. *Nature* **2003,** *424*, 870-872.

8. Lee, G. Y.; Kenny, P. A.; Lee, E. H.; Bissell, M. J., Three-dimensional culture models of normal and malignant breast epithelial cells. *Nat Methods* **2007,** *4* (4), 359-65.

9. Nicodemus, G. D.; Bryant, S. J., Cell encapsulation in biodegradable hydrogels for tissue engineering applications. *Tissue Eng Part B Rev* **2008,** *14* (2), 149-65.

10. Mi, H.-Y.; Jing, X.; Turng, L.-S., Fabrication of porous synthetic polymer scaffolds for tissue engineering. *Journal of Cellular Plastics* **2014,** *51* (2), 165-196.

11. Dutta, R. C.; Dey, M.; Dutta, A. K.; Basu, B., Competent processing techniques for scaffolds in tissue engineering. *Biotechnol Adv* **2017,** *35* (2), 240-250.

12. Holzwarth, J. M.; Ma, P. X., Biomimetic nanofibrous scaffolds for bone tissue engineering. *Biomaterials* **2011,** *32* (36), 9622-9.

13. Smith, R. L.; Lin, J.; M.C, T.; Shida, J.; Kajiyama, G.; Vu, T.; A.R, H.; M.C, v. d. M.; Goodman, S. B.; Schurman, D. J.; D.R, C., Time-dependent effects of intermittent hydrostatic pressure on articular c on rocyte type II collagen and aggrecan mRNA expression. *J Rehabil Res Dev.* **2000,** *37*, 153-61.

14. Lee, J. H.; Fitzgerald, J. B.; Dimicco, M. A.; Grodzinsky, A. J., Mechanical injury of cartilage explants causes specific time-dependent changes in chondrocyte gene expression. *Arthritis Rheum* **2005,** *52* (8), 2386-95.

15. Gailit, J.; Clark, R. A., Wound repair in the context of exratcellular matrix. *Curr Opin Cell Biol.* **1994,** *6*, 717-25.

16. Scott, J. E., Extracellular matrix, supramolecular organisation and shape. *J Anat.* **1995,** *187*, 259-269.

17. Papagiannopoulos, A.; Waigh, T. A.; Hardingham, T. E., The viscoelasticity of self-assembled proteoglycan combs. *Faraday Discuss* **2008,** *139*, 337-57; discussion 399-417, 419-20.

18. Rhodes, J. M.; Simons, M., The extracellular matrix and blood vessel formation: not just a scaffold. *J Cell Mol Med* **2007,** *11* (2), 176-205.

19. Dudhia, J., Aggrecan, aging and assembly in articular cartilage. *Cell Mol Life Sci* **2005,** *62* (19-20), 2241-56.

20. Ogura, Y.; Matsunaga, Y.; Nishiyama, T.; Amano, S., Plasmin induces degradation and dysfunction of laminin 332 (laminin 5) and impaired assembly of basement membrane at the dermal-epidermal junction. *Br J Dermatol* **2008,** *159* (1), 49-60.

21. Mydel, P.; Shipley, J. M.; Adair-Kirk, T. L.; Kelley, D. G.; Broekelmann, T. J.; Mecham, R. P.; Senior, R. M., Neutrophil elastase cleaves laminin-332 (laminin-5) generating peptides that are chemotactic for neutrophils. *J Biol Chem* **2008,** *283* (15), 9513-22.

22. Chang, C.; Werb, Z., The many faces of metalloproteases: cell growth, invasion, angiogenesis and metastasis. *TRENDS in Cell Biology 11*, S37-S43.

23. Giannelli, G.; Falk-Marzillier, J.; Schiraldi, O.; Stetler-Stevenson, W. G.; Quaranta, V., Induction of Cell Migration by Matrix Metalloprotease–2 Cleavage of Laminin-5. *SCIENCE* **1997,** *277*.

24. Seiki, M., The cell surface: the stage for matrix metalloproteinase regulation of migration. *Current Opinion in Cell Biology* **2002,** *14*, 624-632.

25. Amano, S.; Akutsu, N.; Matsunaga, Y.; Nishiyama, T.; Champliaud, M. F.; Burgeson, R. E.; Adachi, E., Importance of balance between extracellular matrix synthesis and degradation in basement membrane formation. *Exp Cell Res* **2001,** *271* (2), 249-62.

26. Leahy, D. J.; Aukhil, I.; Erickson, H. P., 2.0 A˚ Crystal Structure of a Four-Domain Segment of Human Fibronectin Encompassing the RGD Loop and Synergy Region. *Cell* **1996,** *84*, 155-164.

27. Vining, K. H.; Mooney, D. J., Mechanical forces direct stem cell behaviour in development and regeneration. *Nat Rev Mol Cell Biol* **2017,** *18* (12), 728-742.

28. Lau, H. K.; Kiick, K. L., Opportunities for multicomponent hybrid hydrogels in biomedical applications. *Biomacromolecules* **2015,** *16* (1), 28-42.

29. Okumura, Y.; Ito, K., The Polyrotaxane Gel: A Topological Gel by Figure-of-Eight Cross-links. *Adv Mater* **2001,** *13*.

30. Gong, J. P.; Katsuyama, Y.; Kurokawa, T.; Osada, Y., Double-Network Hydrogels with Extremely High Mechanical Strength. *Advanced Materials* **2003,** *15* (14), 1155-1158.

31. Haraguchi, K.; Takehisa, T., Nanocomposite Hydrogels: A Unique Organic-Inorganic Network Structure with Extraordinary Mechanical, Optical, and Swelling/De-swelling Properties. Adv Mater 2002, 14.

32. Lanza R, Langer R, Vacanti JP. **2013**. *Principles of Tissue Engineering*. Atlanta, GA: Elsevier Acad. 4th ed.

PART III

Microfluidics-assisted fabrication of macrophage microtissues with tunable physical properties for developing in vitro multiplex tissue model

3.1. Introduction

There is a growing need to develop physiologically relevant and tunable tissue models for fundamental investigation of both normal and disease physiology as well as drug screening applications.[1-3] For this purpose, various tissue engineering approaches are being developed and applied to fabricate biocompatible materials with tunable physical and biological properties as scaffolds for culturing cells and tissue for desired outcomes.[1-5] This research trend is largely influenced by the ethical issues surrounding the use of animal models.[6] In addition, the variability and questionable efficacy of animal models for predicting human outcome have also accentuated the need for engineering more reproducible and scalable platforms mimicking human tissues.[1-3] Therefore, microfabrication technology such as lithography and deposition printing is utilized to develop more complex and physiologically relevant in vitro tissue models to account for the heterogeneous nature of a biological tissue.[7-10] In addition, a high-throughput technology such as microarray is applied to create multiplex tissue platforms for efficient multiple analyses.[11, 12] In recent years, microfluidics technology has provided a valuable platform for engineering a miniaturized tissue models. For example, "organ-on-a-chip" technology is being heavily investigated, in which small tissues are cultured within a microfluidic chip, mostly made from biocompatible elastomers, and their biochemical analyses are efficiently analyzed, often in situ.[13-15] The fluid channels and tissue chambers within a microfluidic chip can be designed to mimic the complexities of a natural tissue environment, with multiple analytical methods embedded in a single chip platform. Alternatively, microfluidics is also being utilized to develop emulsion particles ("droplets") with varying size and shape in micrometer scale resolutions for biomedical applications.[16-19] Large quantities of monodisperse droplets can be efficiently fabricated and embedded with biological molecules (e.g. genes and proteins) and cells for high-throughput screening and injectable delivery applications. The droplets can be further engineered to generate microgels by crosslinking the droplets consisting of gel-forming precursors, which further diversifies the material properties.[20-24] Inspired by the versatility of the microfluidics approach, we have adopted the droplet microfluidic technology to create microgels with varying mechanical properties for use as 3D cell culture platform. Using a microfluidic double flow-focusing

device, monodisperse droplets of photo-crosslinkable gelatin containing cells in the core region were generated and crosslinked to develop cell-laden microgels with high viability. There have been several previous studies using microfluidics assisted fabrication of cell-laden microgels.[21, 25, 26] Most of these studies, however, do not take into account the effect of material properties. Herein, the mechanical properties of the microgels were controlled by varying the concentration of gel-forming macromer. Using macrophage as a model cell system, which is well known to undergo proliferation as well as M1 (inflammatory) / M2 (resolving) polarization in response to chemical and biophysical stimuli from the surrounding, the macrophages were encapsulated in microgels having various mechanical rigidity, and its effect on their viability, proliferation, and differentiation was evaluated.[27-30] Ultimately, these macrophage 'microtissues' were then dispersed and incorporated into a larger tissue construct consisting of different cell types to develop a hydrogel-based 3D co-culture model. Most co-culture studies involve either a platform with a permeable membrane to allow paracrine effects or simple cell mixtures,[31] which do not represent a real tissue environment in which different cell types reside in separate but interactive 3D microenvironments. This "multiplex" tissue model allowed the monitoring of complex interactions between two different types of cells residing in adjacent, compartmentalized areas within a tissue. Using this model, the phenotypical changes of macrophages in microgels and the surrounding cells, either cancer cells or fibroblasts, based on the mutual interaction were monitored and analyzed.

3.2. Material and methods

3.2.1. Fabrication of silicon master

The standard photolithography was utilized to fabricate the silicon master for polydimethylsiloxane (PDMS)-based microfluidic device. Briefly, SU-8 2000 (MicroChem Corp.) was spin-coated on a silicon wafer (STC, Japan) and then bake at 95ºC to remove the solvent and harden the photoresist. A photomask with patterns for the microfluidic channels was placed on top of the wafer, and exposed to UV to cross-link the patterned area. After baking at 95 °C to further solidify the cross-linked photoresist, the wafer was cooled to room temperature, and placed in SU-8 developer to remove the unexposed photoresist. The wafer was then rinsed with isopropanol three times and dried. The schematic illustration of the silicon master is shown in Figure 3.1.

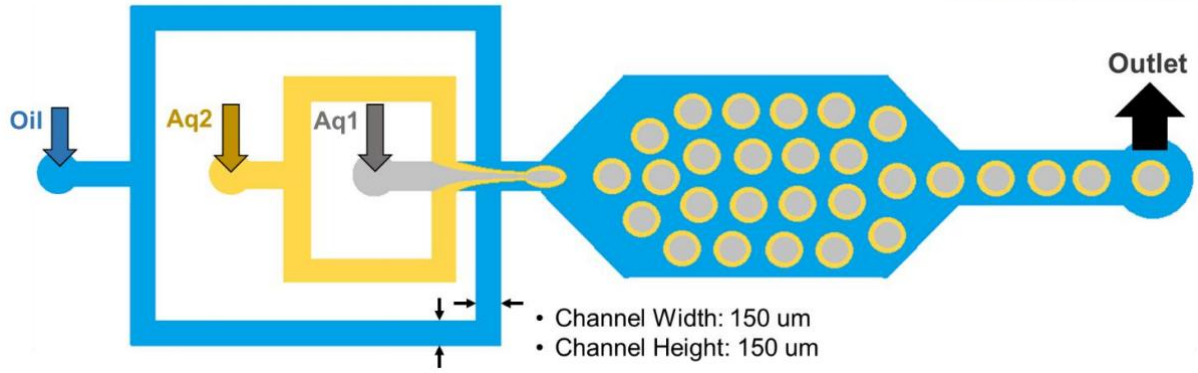

Figure 3.1. Schematics of the microfluidic device with double flow-focusing channel geometry to develop cell-laden microgels.

3.2.2. Fabrication of PDMS microfluidic flow-focusing device

PDMS elastomer was fabricated on top of the silicon master, by placing the mixture of silicone elastomer base and the curing agent (base: curing agent = 10:1, Sylgard®184 Silicone Elastomer Kit) on the master, degassing the PDMS mixture in a vacuum desiccator for 1 hour, and curing for 3 hours at 80 °C. Then, the PDMS elastomer with engraved microchannels was detached from the master, and fluid inlets and outlets were created using a hole punch (0.5 mm diameter). Finally, a glass slide was irreversibly bonded to the PDMS by treating their surfaces with oxygen plasma for 30 seconds to fabricate the PDMS microfluidic device.

3.2.3. Determination of droplet concentrations

The droplets obtained by a microfluidic double flow-focusing device consisted of core and shell regions at different concentrations. The overall concentration of the droplet after the core and shell regions merged was estimated by relative sizes of core and shell regions of a droplet. Briefly, the microscopic image was taken after the droplet was formed, which showed the clear demarcation between the core and shell regions before merging. The volumes of the core (V_c) and the shell (V_s) was calculated, and their relative portions were used to calculate the overall concentration (C_T),

$$V_C = \frac{4}{3}\pi r_C^3, \quad V_S = V_T - V_C, \quad C = \frac{V_C}{V_T}C_C + \frac{V_S}{V_T}C_S$$

V_T was the total droplet volume, C_c and C_s were the concentrations of core and shell, respectively, and r_c was the radius of the core. In this double microfluidic flow-focusing geometry, the average V_c/V and V_s/V were 0.52 and 0.48. The concentrations for C1, C2 and C3 are calculated as follows.

Conditions	C_c (%)	C_s (%)	C_T (%)
C1	7	10	8.4
C2	9	12	10.4
C3	11	14	12.4

Table 3.1 Overall concentration of calculated MGel at C1, C2 and C3.

3.2.4. Synthesis of photo-crosslinkable gelatin

Conjugation of methacrylic functional group to gelatin (i.e. methacrylic gelatin (MGel)) was accomplished following a previously published report. Briefly, gelatin (10 g, from porcine skin, Sigma Aldrich), 4-dimethylaminopyridine (1g, Sigma Aldrich), and 4-methoxyphenol (0.1g, Sigma Aldrich) were first dissolved in 100mL dimethyl sulfoxide at 50 °C. Glycidyl methacrylate (4 mL, Sigma Aldrich) was slowly added to the mixture, and the reaction was continued for 48 hours at 50 °C under N_2. The mixture was extensively dialysis against deionized water and lyophilized to obtain the final product. The chemical structure of methacrylate on gelatin was confirmed by ^{1}H-NMR (400-MR DD2, Agilent) Figure 3.2.

3.2.5. Mechanical properties of hydrogels

MGel precursor solutions at various concentrations, from 6 to 14 % (w/v), with 0.2 % (w/v) Irgacure 2959 as a photo-initiator in PBS were prepared. Each solution was placed in a thin glass mold (1 mm spacing) and irradiated with UV for 2 minutes (intensity: 200mW, distance: 5 cm, Model S1500, Omnicure®) to fabricate the hydrogel. Hydrogel disks were punched out (8 mm diameter) and incubated in PBS overnight before mechanical characterization. The mechanical properties of MGel hydrogels were assessed by measuring elastic moduli from uniaxial compression tests (Model 3343, Instron). Each hydrogel disk was compressed at a fixed rate (1 mm min^{-1}.), and a stress-strain relationship was obtained. The elastic modulus was calculated as the slope of the stress-strain curve at the region of elasticity (i.e. initial 10 % strain).

3.2.6. Fabrication of cell-laden microgels

The concentrations of MGel in the primary (Aq1) and secondary (Aq2) aqueous were 7 and 10, 9 and 12, and 11 and 14 % (w/v), respectively. The concentration of Aq2 which becomes the outer layer of the droplet was kept higher than that of Aq1, in order to minimize the Aq1 with cells in the core from moving outward via diffusion. The macrophage (RAW264.7 cell line purchased from ATCC®) cells

were dispersed in the Aq1 at 1 × 10^7 cells mL^{-1}. Both Aq1 and Aq2 contained 0.2 % (w/v) Irgacure 2959® as a photo initiator. Mineral oil supplemented with 20 % (v/v) Span80 (Sigma Aldrich) was used as the oil phase (O). The fluids were injected into the microfluidic device in controlled rates via electronic pumps (Legato®100, KD Scientific). To control the size of the droplets, the flow rate of Aq was varied from 80 to 150 µL hr^{-1}, while keeping the flow rate of O at 500 µL hr^{-1}. The droplets generated from the microfluidic device was exposed to UV for 2 minutes (intensity: 200mW, distance: 5 cm, Model S1500, Omnicure®) to crosslink the droplets to form microgels. The collected cell-laden microgels were incubated in the cell culture media (Dulbecco's Modified Eagle Medium supplemented with 10 % fetal bovine serum and 1 % penicillin/streptomycin, all purchased from Thermo Fisher) at 37 °C under 5 % atmospheric CO_2.

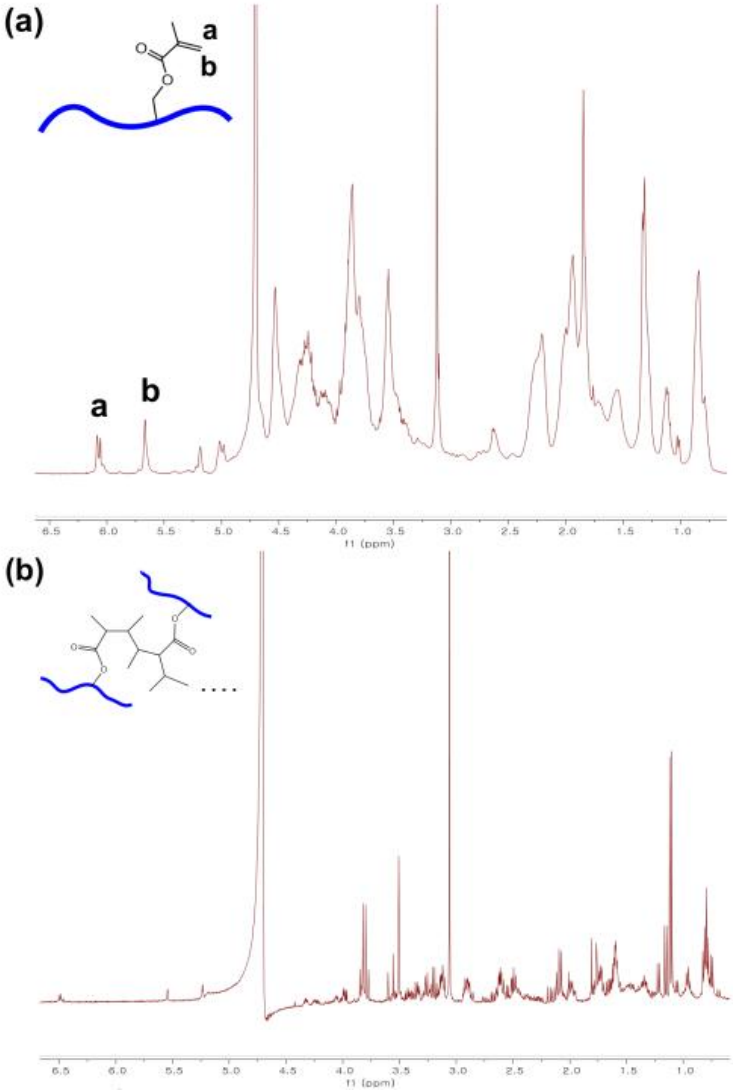

Figure 3.2 ^{1}H-NMR spectra of (a) MGel and (b) degraded MGel hydrogel. The methacrylic peaks (**a**, **b**) disappeared after gelation.

3.2.7. Fabrication of in vitro multi-tissue model

The microgel-based macrophage tissues were embedded into a larger tissue construct consisting of different types of cells to fabricate in vitro multi-tissue model. The macrophage-laden microgels were suspended in a precursor solution consisting of cells with the density of 1 x 10^6 cells mL^{-1} dispersed in 8 % (w/v) MGel and 0.2 % (w/v) Irgacure 2959®. The solution was placed in a thin glass mold (0.5 mm spacing) and irradiated with UV for 2 minutes (intensity: 200 W, distance: 5 cm, Model S1500, Omnicure®) to develop the multi-tissue construct. The cell types used for the large tissue constructs were fibroblasts (NIH-3T3), hepatocarcinoma (HepG2) all purchased from ATCC®.

3.2.8. In vitro evaluation

The viability of cells encapsulated in the microgels was measured using LIVE/DEAD Cell Viability Assay (Thermo Fisher). Briefly, microgel samples at designated time points were taken and treated with calcein AM and ethidium homodimer-1 to fluorescently label live (green) and dead (red) cells, respectively. The cells were visualized under an inverted fluorescent microscope (XDS-3FL, Optika), and the numbers of live and dead cells were counted. The viability was reported as the percentage of live cells. For each condition, the average value of viability results in 15 microgels was reported. To induce differentiation of the macrophages in microgels, they were treated with lipopolysaccharide (LPS, 1 μg mL^{-1}, Sigma Aldrich) included in the cell culture medium. The medium was replenished every two days. The change in cellular morphology over time was monitored with the microscope. To visualize the change in biomarkers of macrophage cells undergoing differentiation, immunofluorescent labeling of the characteristic protein markers (e.g. CD80 for M1 phenotype and CD206 for M2 phenotype) was performed. Hamster anti-mouse CD80 and rat anti-mouse CD206 were used as primary antibodies (1:250 dilution). AlexaFluor568-linked anti-hamster IgG and AlexaFluor488-linked goat anti-rat IgG were used as secondary antibodies for the hamster anti-mouse CD80 and rat anti-mouse CD206 antibodies, respectively (1:250 dilution). 4',6-diamidino-2-phenylindole (DAPI, 100 ng mL^{-1}, Sigma Aldrich) was also used in conjunction to stain the nuclei. After staining, the fluorescent images of the cells within the microgels were then visualized using a confocal microscope (FV1000, Olympus)

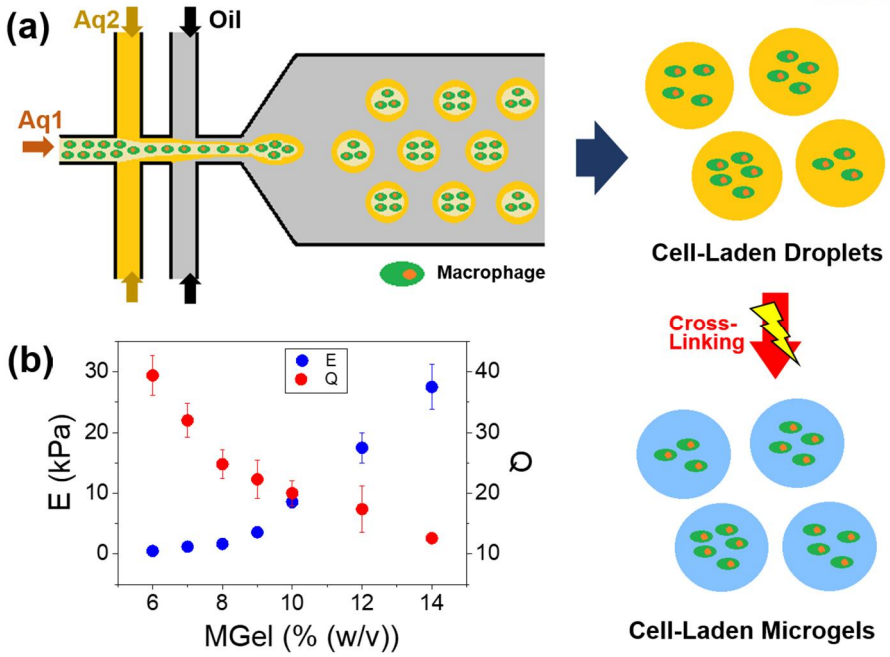

Figure 3.3 (a) Schematic illustration of a double flow-focusing microfluidic fabrication of macrophage-laden microgels. (b) Elastic moduli (E) and swelling ratios (Q) of photo-crosslinked MGel hydrogels at various concentrations.

3.3. Results and Discussion

3.3.1. Fabrication of macrophage-laden microgels

In this study, a microfluidic device having a flow-focusing geometry was used to generate cell-laden microgels. It allows the formation of monodisperse droplets of gel precursor solution infused with cells, after which photo-crosslinking scheme was employed to generate cell-laden microgels (Figure 3.3a). This particular "double" flow-focusing microfluidic device was chosen, based on our previous study, because it allows the generation of droplets with core-shell morphology, with cells being mostly in the core region, to enhance the biocompatibility of the droplet and subsequent microgel fabrication.[21, 26] In this device, the cells included in the primary aqueous phase ('Aq1') could be directed to the core region of the droplet, surrounded by the secondary aqueous phase ('Aq2') making up the shell region which acted as a buffering zone against the surrounding continuous oil phase (O) which is known to cause cytotoxic effects.[21, 32] To further enhance the biocompatibility, the concentration of methacrylic gelatin (MGel) in Aq2 was kept higher than that of Aq1, so initially the outer shell of Aq2 would have higher viscosity than the inner core of Aq1, and then it would make the cells in the core more difficult to move toward the shell having higher viscosity. This experiment design thereby increased the likelihood of maintaining the cells within Aq1. Initially, there was a noticeable delineation between core and shell regions of a droplet, as expected. But the core and shell regions of the droplet eventually merged over time via diffusion.(Figure 3.4) More significantly, even after the droplet formation, the cells mostly

stayed within the core region, demonstrating the effectiveness of this design, because the polymer chains moving into the core region have greater effect on keeping the cells within the core region, as compared with the water moving out to the shell region pushing the cells out. The extent of the photo-crosslinking reaction was also determined by the characteristic methacrylic peaks of MGel in ^{1}H-NMR spectra, which disappeared after gelation, demonstrating that the photo-crosslinking reaction went to completion. (Figure 3.2)

3.3.2. Physical properties of microgels

The mechanical properties of the microgels could be conveniently controlled by the concentration of MGel. Here, three different sets of concentrations for Aq1 and Aq2 were tested; 7 % and 10 % ('C1'), 9 % and 12 % ('C2'), and 11 % and 14 % ('C3'). Due to the difficulty of directly measuring the mechanical properties of the microgels, larger MGel hydrogels at varying concentrations were separately fabricated using the same photo-crosslinking scheme and their elastic moduli were obtained by uniaxial compression. Since two aqueous solutions with different concentrations (e.g. Aq1 and Aq2) were used to develop the microgels, the overall concentration of the microgels was estimated by the relative amounts of Aq1 and Aq2 making up to core and shell regions of the microgels, which was determined from the microscopic image taken during the droplet formation.

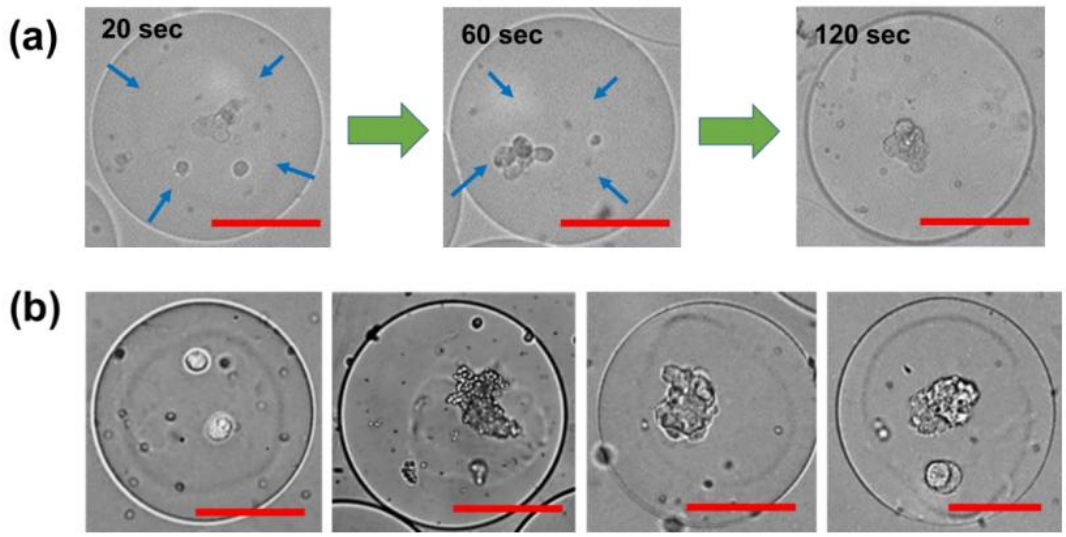

Figure 3.4 A microscopic image of a cell-encapsulated droplet showing a distinct core-shell interface right after formation(left). The border between core and shell, identified with arrows, disappear soon after, and the droplet become homogeneous (from left to right). (b) Microscopic images of cell-laden microgels fabricated before core-shell regions of the droplets merged. The interface between core and shell regions are clearly shown. (scale bar: 50 μm)

The volume ratio of Aq1 and Aq2 was determined to be 52:48, and thus the overall concentrations of C1, C2, and C3 were 8.4 %, 10.4 %, and 12.4 %, respectively. The elastic moduli at those concentrations were 1.8, 10.2, and 18.5 kPa, for C1, C2 and C3, respectively. (Figure 3.3(b), Table 3.2) The trend in swelling ratio was opposite to that of elastic modulus, as expected, since the porosity within the hydrogel becomes reduced with increasing crosslinking density. The size of the microgels could also be controlled by the ratio of flow rates of Aq and O (Q_{Aq}/Q_O) during the droplet formation (Figure 3.5(a), Figure 3.6)

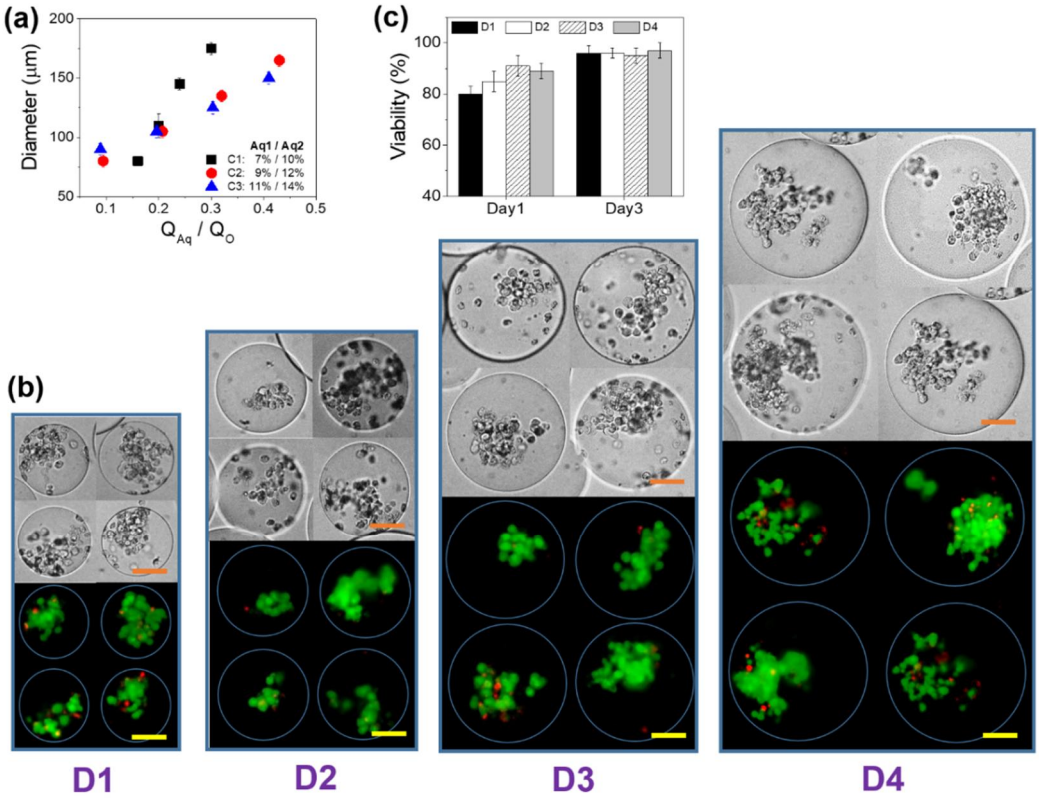

Figure 3.5. (a) Control of droplet diameters by ratios of aqueous-to-oil flow rates (Q_{Aq}/Q_O). (b) Phase contrast and fluorescent images of macrophage-laden microgels with varying size. (c) The viability of cells encapsulated in microgels with varying size (scale bar: 50 μm) at day 1. D1=100 μm, D2=120 μm, D3=160 μm, D4=200 μm.

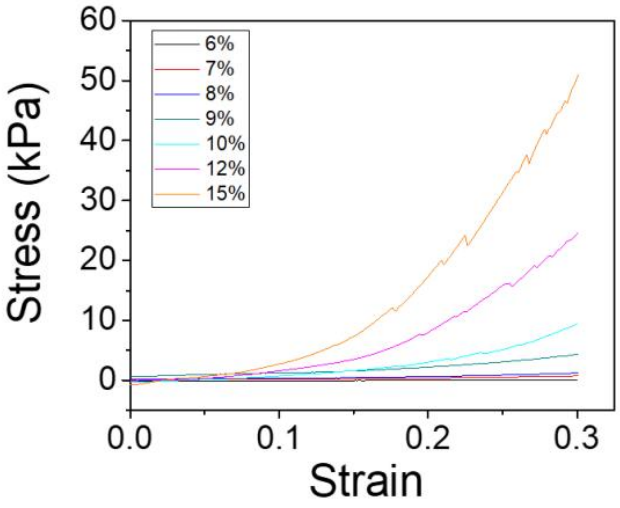

MGel(%)	E (kPa)
6	0.5
7	1.2
8	1.7
9	3.6
10	8.6
12	17.5
15	22.5

Table 3.2 Stress-strain curves of MGel hydrogels at various concentrations obtained by uniaxial compression. The table lists the average elastic moduli (E) of MGel hydrogels calculated from the curves.

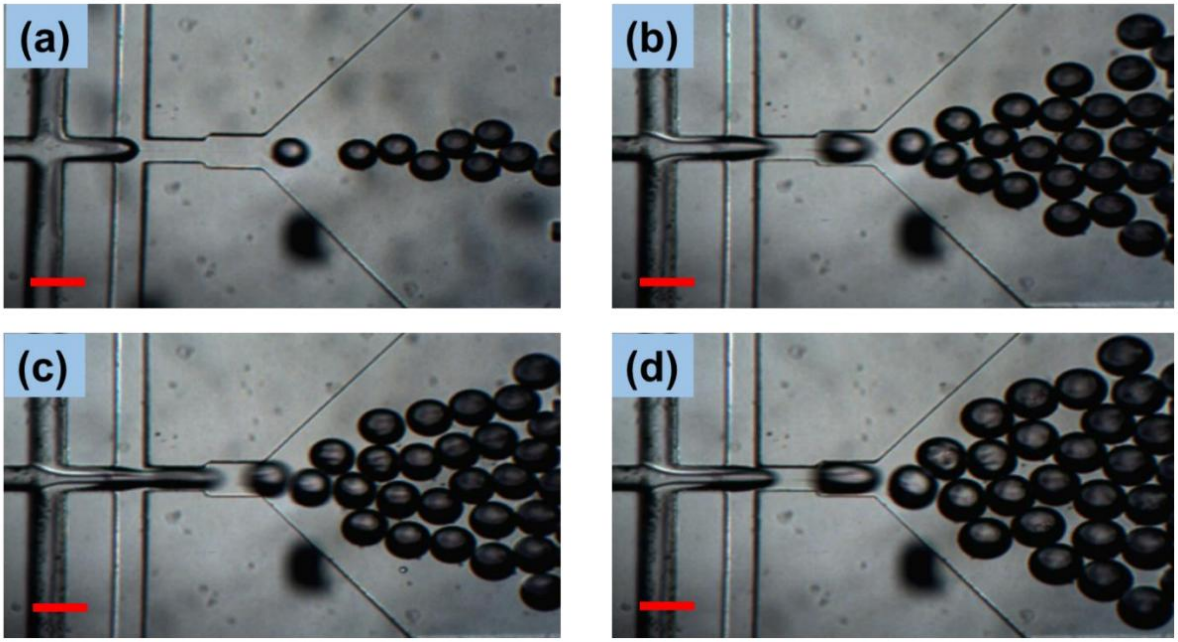

Figure 3.6 Microfluidic generation of gel-precursor droplets at varying ratios of aqueous-to-oil flow rates (Q_{Aq}/Q_O). (a) $Q_{Aq}/Q_O = 0.095$, (b) $Q_{Aq}/Q_O = 0.21$, (c) $Q_{Aq}/Q_O = 0.32$, (d) $Q_{Aq}/Q_O = 0.45$ (scale bar: 200 μm).

Due to the increasing viscosity of Aq phases with MGel concentration, the range of microgel diameter controlled under the given Q_{Aq}/Q_O became higher with degreasing MGel concentration. In this microfluidic channel dimensions, the diameter could be controlled from 80 to 165 um. It is suggested that larger microgels could be generated from a microfluidic device with larger channel dimensions. On the other hand, the droplets smaller than the lower limit could not be pinched off at lower Q_{Aq}/Q_O due

to the high viscosity of Aq phase opposing smaller droplet formation. After the microgel was immersed in buffered formation, there was approximately 20 % increase diameter for all microgel conditions due to swelling behavior of the microgels, as expected.

3.3.3. Biocompatibility of macrophage-laden microgels

3.3.3.1. Effect of microgel size

The biocompatibility of the microfluidic process to fabricate microgels and the microenvironment of the microgels as a 3D cell culture platform was assessed by measuring the viability and proliferation of the encapsulated cells over time. The viability here was defined as the percentage of live cells at a given time point. First, the effect of microgel size was evaluated by measuring the viability at microgels with four different diameters, 100 μm ('D1'), 120 μm ('D2'), 160 μm ('D3'), and 200 μm ('D4'), while keeping the concentration constant at C2. First, the viability of cells encapsulated in droplets prior to the photo-crosslinking step was measured, which showed that the cell viability was well maintained, demonstrating the biocompatibility of the microfluidic process to generate droplets. (Figure 3.7) After photo-crosslinking to synthesize cell-laden microgels, the initial viability of cells in microgels measured at day 1 also revealed that the viability remained high, above 80%, for all conditions. However, the viability was higher at larger microgels to a small degree (e.g. 90 % for D3 and D4, 85 % for D2, and 80 % for D1). (Figure 3.5(b), (c)) At lower Q_{Aq}/Q_O to generate smaller droplets, the pinch-off occurred more immediately with less jetting, and as a result, the core-shell regions became less clearly defined and the shell was thinner. (Figure 3.6) This result likely led to the greater likelihood of cells exposed to the oil phase during the pinch-off to form the smaller droplet formation. It is also possible that the harmful effect of UV irradiation became more pronounced for the cells in smaller droplets due to greater extent of UV penetration. In any case, the viability was above 80 % for all conditions, indicating the microfluidic process to generate droplets as well as photo-crosslinking step. Further cell culture up to 3 days resulted in the proliferation of the encapsulated cells with high viability for all conditions, which further demonstrated the biocompatibility of the microgels regardless of the size of microgels (Figure 3.10)

3.3.3.2. Effect of microgel mechanics

It is well established that the mechanical cues imparted by the surrounding matrices exert significant effects on residing cells by sigmal transduction through focal adhesion.[33] Therefore, it was hypothesized that the mechanical properties of the microgels, controlled by the concentration of MGel, would influence the macrophage activities. The viability of macrophage cells encapsulated within the

microgels having different rigidity was assessed at various time points (Figure 3.8(a), Figure 3.7).

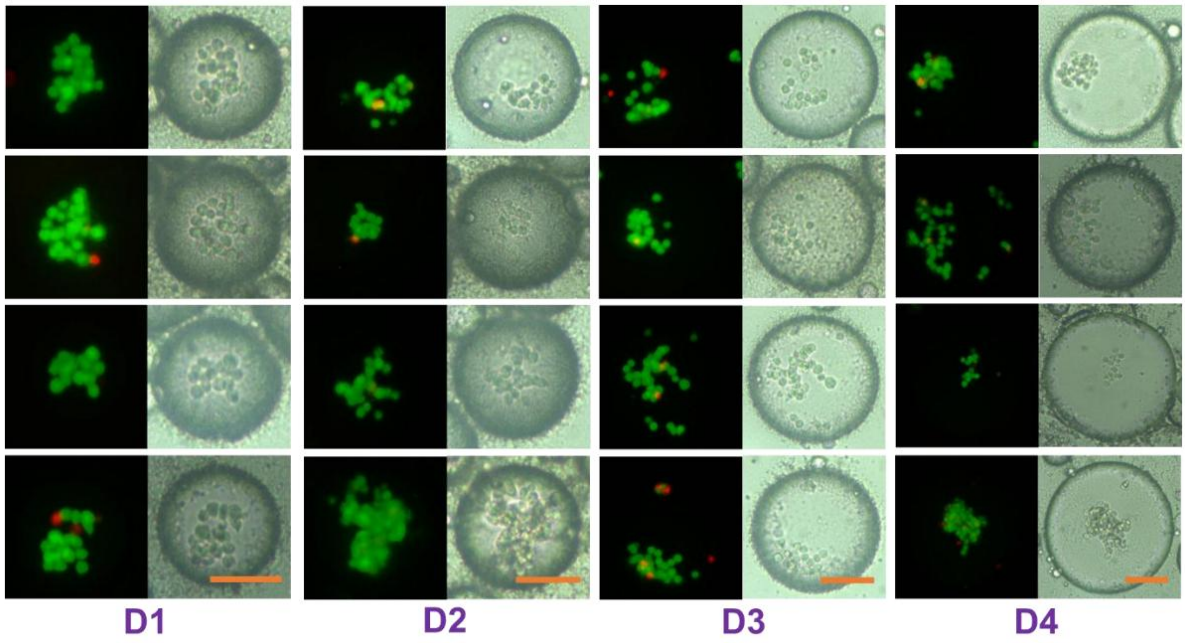

Figure 3.7 The viability of cells encapsulated in droplets having various sizes measured before photo-crosslinking to develop cell-laden microgels. D1=100 μm, D2=120 μm, D3=160μm, D4=200 μm. (scale bar: 50 μm)

The size of the microgel was fixed at 120 μm diameter. The initial viability, taken at day 1, was the highest at 85 % at the lowest MGel concentration (C1), and decreased to a small degree with increasing concentration (e.g. 77 % at C2, 72 % at C3) (Figure 3.8(b)). It was estimated that it was due to an increased level of radicals within the microgels during the gelation with greater amounts of reactants.

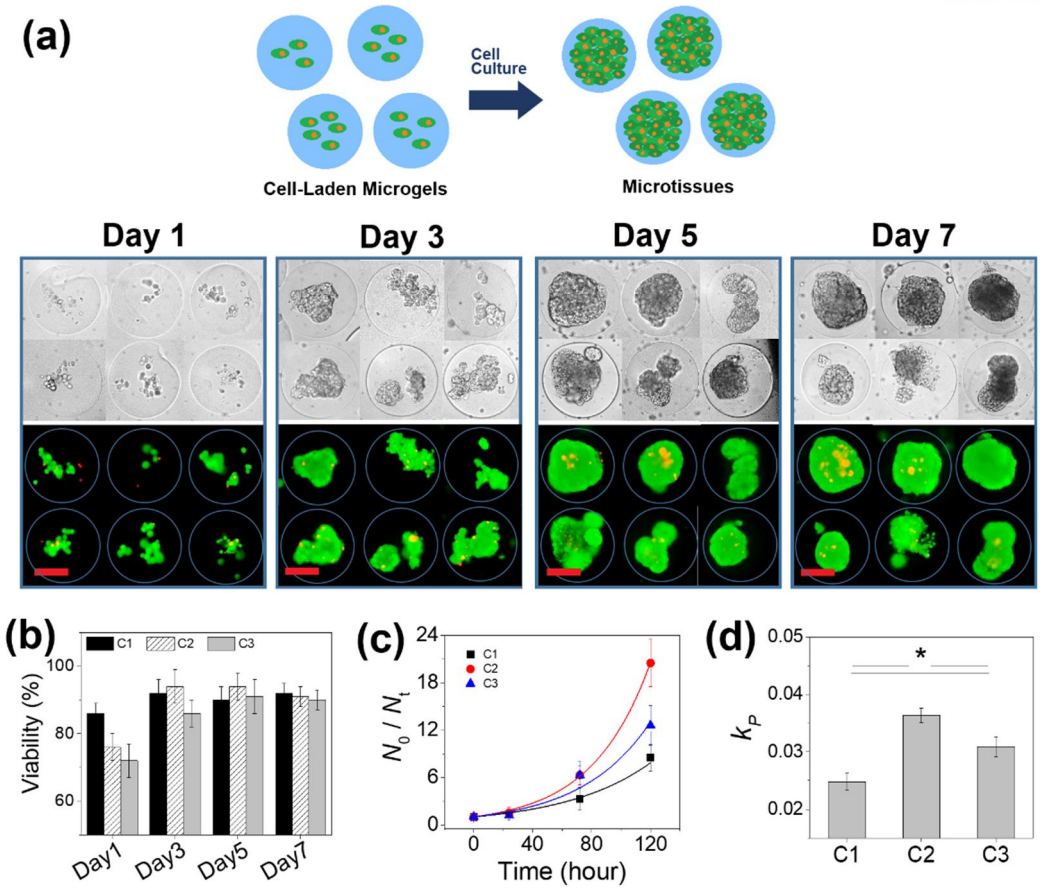

Figure 3.8 Cell viability and proliferation in microgels at C2 (Aq1/Aq2=9%/12%) (a) Microscopic (upper) and fluorescent (lower) images of macrophages encapsulated in microgels taken at various times. The cells were fluorescently stained to identify live (green) and dead (red) cells (scale bar: 50 μm). (b) viability of macrophages at various times during culture up to 7 days. (c) The normalized number of viable cells (N_t/N_0) in the microgels was measured over time. (d) The plot in (c) was fitted with a power-law model to obtain the proliferation rates (k_P) (*p<0.05).

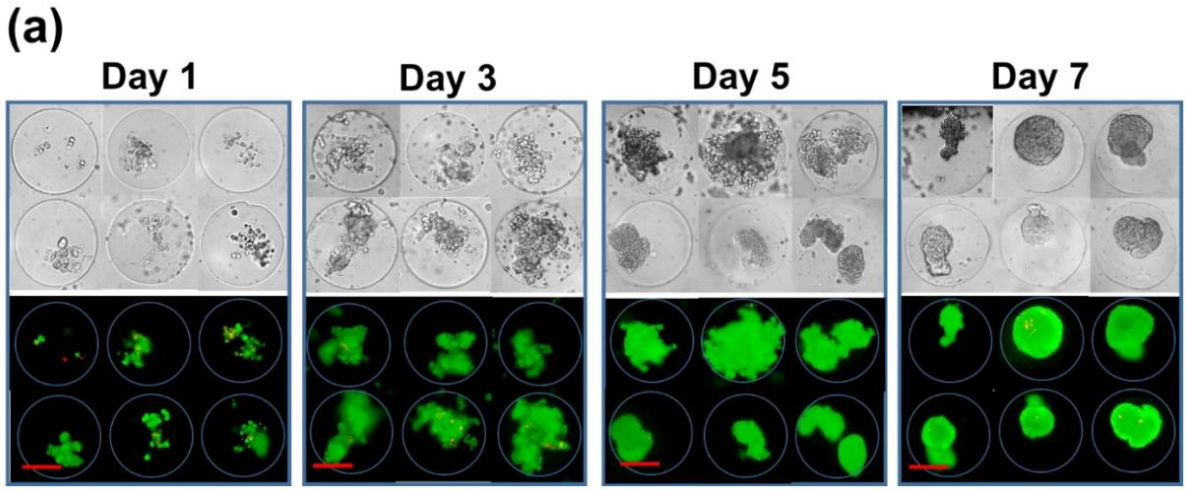

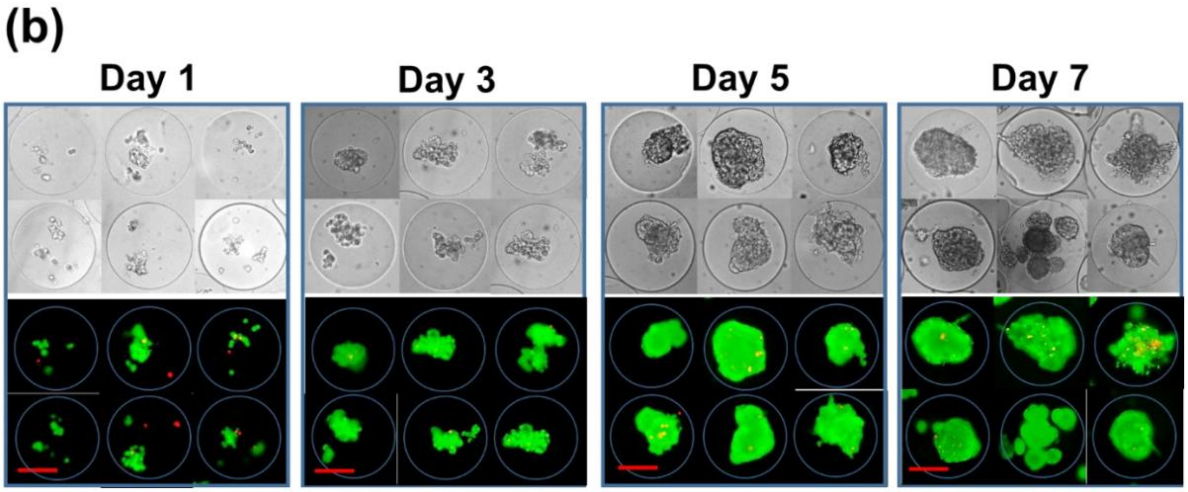

Figure 3.9 Cell viability and proliferation in microgels at (a) C1 (Aq1/Aq2 = 7% / 10%) and (b) C3(Aq1/Aq2 = 11% / 14%). Microscopic (upper) and fluorescent (lower) images of macrophages encapsulated in microgels taken at various times. The cells were fluorescently stained to identify live (green) and dead (red) cells (scale bar: 50 μm).

Nonetheless, the cells within the microgels at all conditions proliferated and formed high-density cell spheroids within the structure during the seven days of culture. The significant increase in the number of live cells, coupled with low number of dead cells, signified the biocompatibility of the microgels. It is interesting to note that the size of spheroids increased dramatically over the course of culture that they occupied the majority of the microgel, but the microgel itself did not expand nor fractured by increased internal pressure. This result further demonstrated the cells were able to significantly remodel the inner environment of the microgels to accommodate the increased cell density. This was made possible because the microgel consisted of crosslinked network of gelatin, which is derived from natural collagen and retains cell responsive moieties such as RGD peptide and MMP recognition domains.[34, 35] The macrophage cells used in this study have been shonw to express MMPs.[36] Hydrogels made from synthetic polymers, on the other hand, generally are not conducive towards this level of remodeling. The proliferation rate of macrophages in microgels at various MGel concentrations were calculated to assess the effect of mechanical properties on the encapsulated cells (Figure 3.8(c)). The increase in number of live cells (N_t/N_0) were counted at different times up to 5 days, after which it was not feasible to due to many overlaps (Figure 3.8(c)). The proliferation rate (k_P) was obtained by fitting the plot with a power-law model (Figure 3.8(d)). Interestingly, the k_P was significantly larger at C2 than both C1 and C3, suggesting there was an optimal mechanical environment for the encapsulated cells for proliferation. The increase in k_P from C1 to C2 indicated that increased rigidity of the microgel had a significant impact on improving the proliferation of cells in 3D environment. However, further increase in MGel concentration from C2 to C3 resulted in diminished k_P, though it was still larger than that at C1. This

could be a result of diminished permeability of the microgels with increased crosslinking density. Similar combined effects of mechanical and diffusional properties of hydrogels on the cells in 3D environment have been previously demonstrated.[21, 37] To evaluate the effect of different cell culture dimensions (2D vs. 3D), the same macrophage cells were separately cultured on the surface of MGel hydrogels at varying concentrations, and their proliferation behavior was measured and compared with that as shown above (Figure 3.13). Interestingly, initial cell adhesion was more pronounced at lower rigidity.[38]

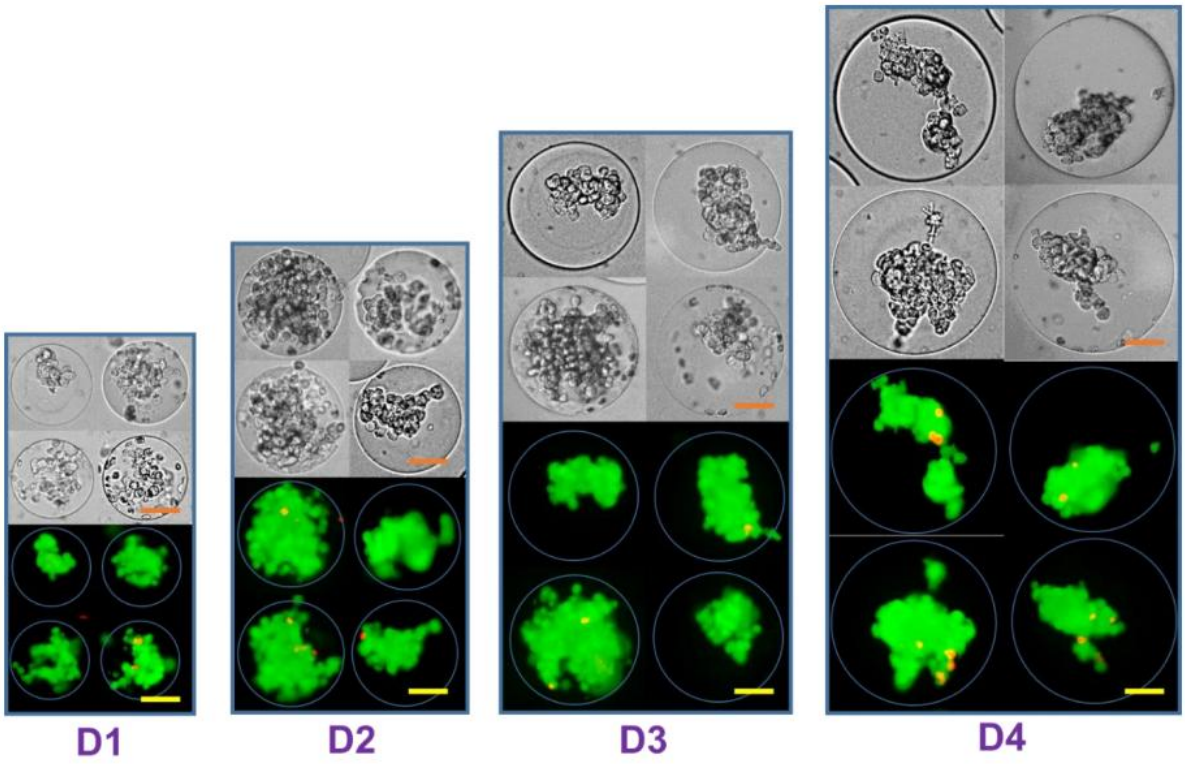

Figure 3.10 The viability of cells encapsulated in microgels with varying size at day 3 (scale bar: 50 μm). D1=100 μm, D2=120 μm, D3=160 μm, D4=200 μm.

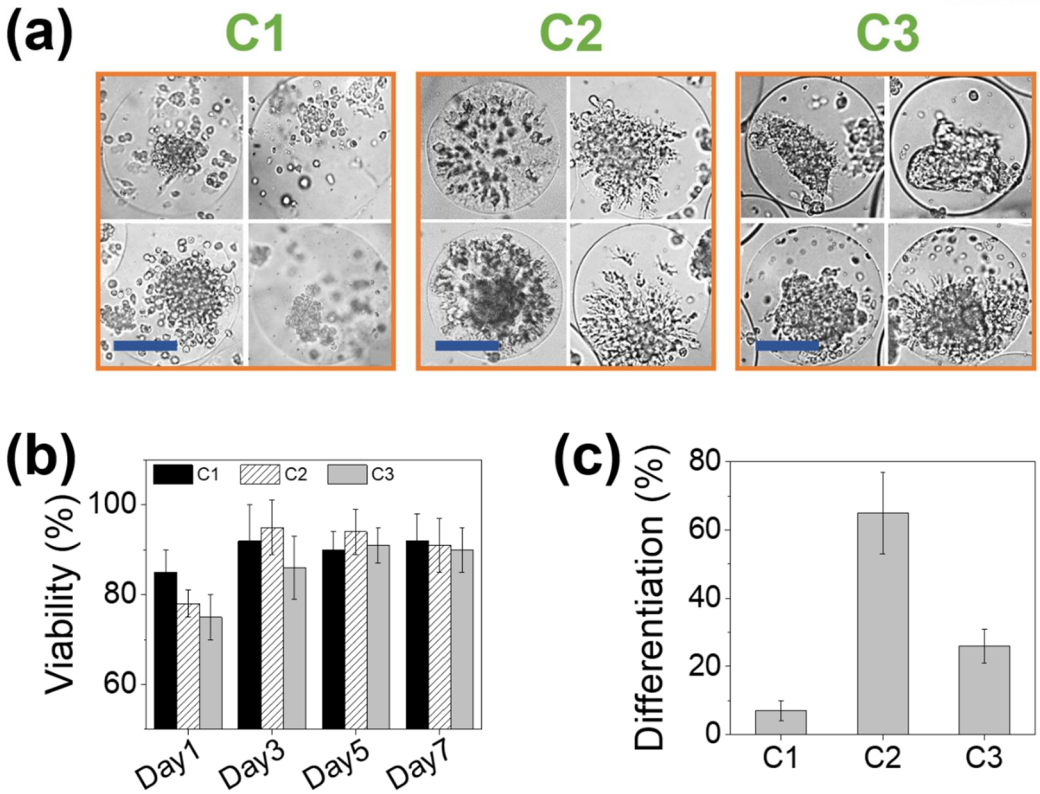

Figure 3.11 (a) Differentiation of macrophages in microgels. (a) Microscopic images of macrophages in different microgels treated with LPS at day 7 (scale bar: 50 μm). Differentiated cells demonstrate sprouting formation. (b) The viability of macrophages at various times during culture up to 7 days. (c) The percentage of differentiated macrophages in the microgel.

3.3.4. Induction of macrophage differentiation in microgels

The macrophages can be classified into M1 and M2 phenotypes, depending on their physiological functions.[27-30] Generally, M1 macrophages promote inflammatory response, whereas M2 macrophages promote tissue repair, as identified by their different cytokine expression profiles and morphologies. M1/M2 transition ('Mϕ polarization') is stimulated by various cytokines produced from surrounding tissue in response to physiological changes such as tumor, inflammation and wound healing, or from microbial toxins such as lipopolysaccharide (LPS). Therefore, the effect of mechanical properties of microgels on the differentiation of encapsulated macrophages undergoing Mϕ polarization, the cell-laden microgels were exposed to LPS during the culture, and their morphological transformation was monitored (Figure 3.11, Figure 3.12).

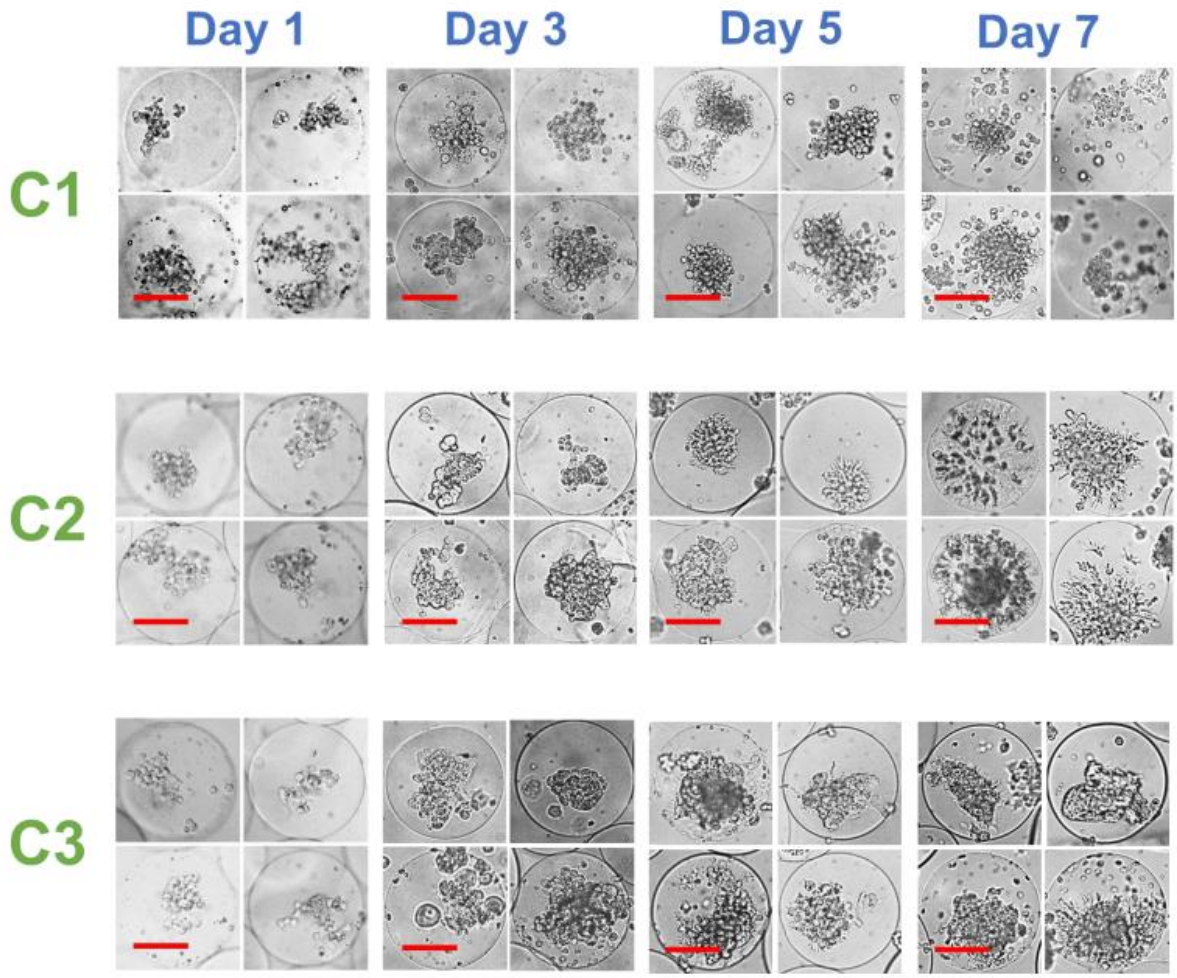

Figure 3.12 Microscopic images of macrophage encapsulated in MGel microgels at varying concentrations (C1, C2 and C3) treated with LPS to induce Mϕ polarization (scale bar: 50 μm).

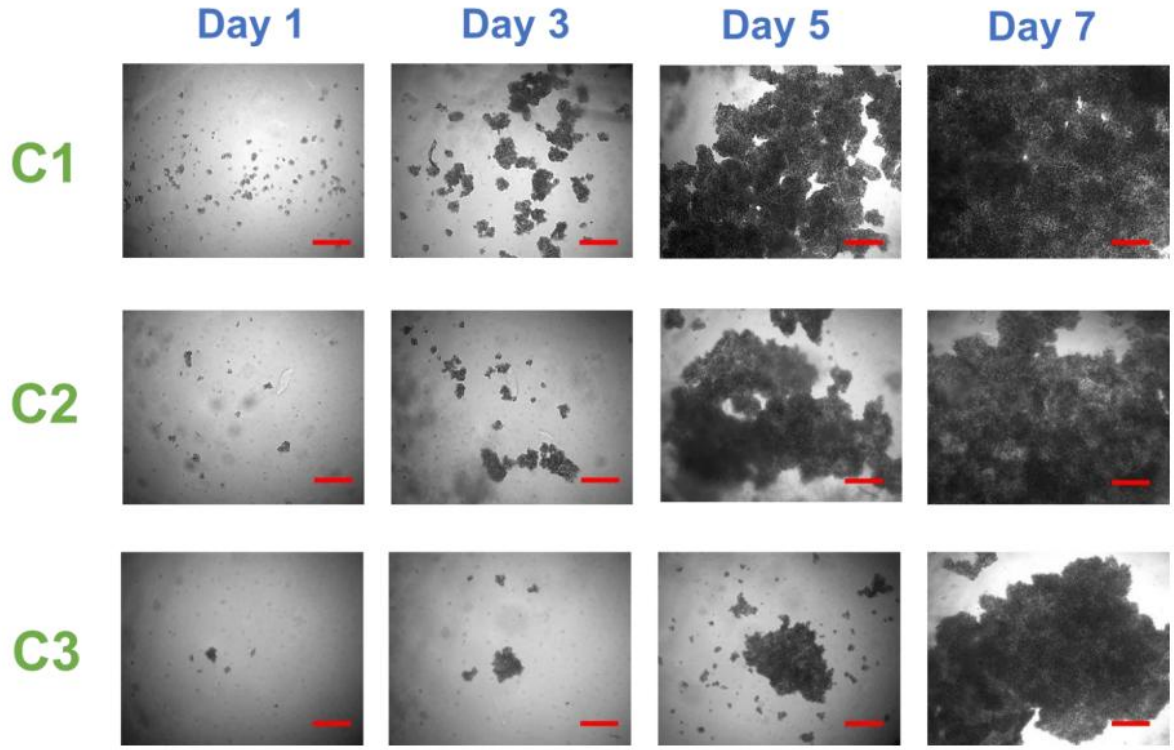

Figure 3.13 Microscopic images of macrophage cells cultured on the surfaces of MGel hydrogels at varying concentrations (C1, C2, and C3) which were prepared separately to assess the effects of culture conditions (2D vs. 3D) on the macrophage proliferation (scale bar: 200 μm). The initial cell adhesion and proliferation were monitored over time.

Previous studies have shown that the macrophage cell type used in this study (RAW264.7) demonstrates dendritic morphology, with increased expression of cell surface markers associated with M1 phenotype (e.g. CD80, CD86) as opposed to M2 phenotype (e.g. CD206, CD163).[39, 40] The mechanical properties of microgels were controlled with MGel concentrations; C1, C2 and C3. With the induction by LPS, the level of proliferation on all conditions diminished over time as compared to normal culture conditions as shown in Figure 3.8, as the number of cells did not significantly increase after 3 days, while maintaining their viability Figure 3.11(b), Figure 3.12. The cells demonstrating "dendrite"-like morphology (i.e. filopodial projections), began to appear soon after, and the number of differentiated cells reached maximum around day 7 of culture Figure 3.11(a). The macrophage cells acquiring filopodia, a hallmark of cellular migration, in response to LPS have been demonstrated.[41-44] The number of differentiated cells was highest at C2 in which over 60 % of the cells residing in the microgels showed filopodial projections Figure 3.11(c). On the other hand, the degrees of differentiation at other conditions were remarkably low, especially at C1 (> 7 %). This result demonstrated that the mechanical properties of the microgels had significant influence over the LPS-induced activation of the encapsulated macrophages. This type of biphasic trend was similar to the macrophage proliferation in

Figure 3.8. In regards to previous studies, in which macrophage proliferation and LPS-induced activation were promoted by the rigidity of substrate for 2D culture, the result shown here also showed the positive effect of increased rigidity on the encapsulated macrophages from C1 to C2.[45] However, the effect of diffusion likely came into play with 3D culture, as extensively reduced permeability of the microgel at higher stiffness (at C3) meant limited inner space to allow the cellular growth as well as cell spreading to take place.

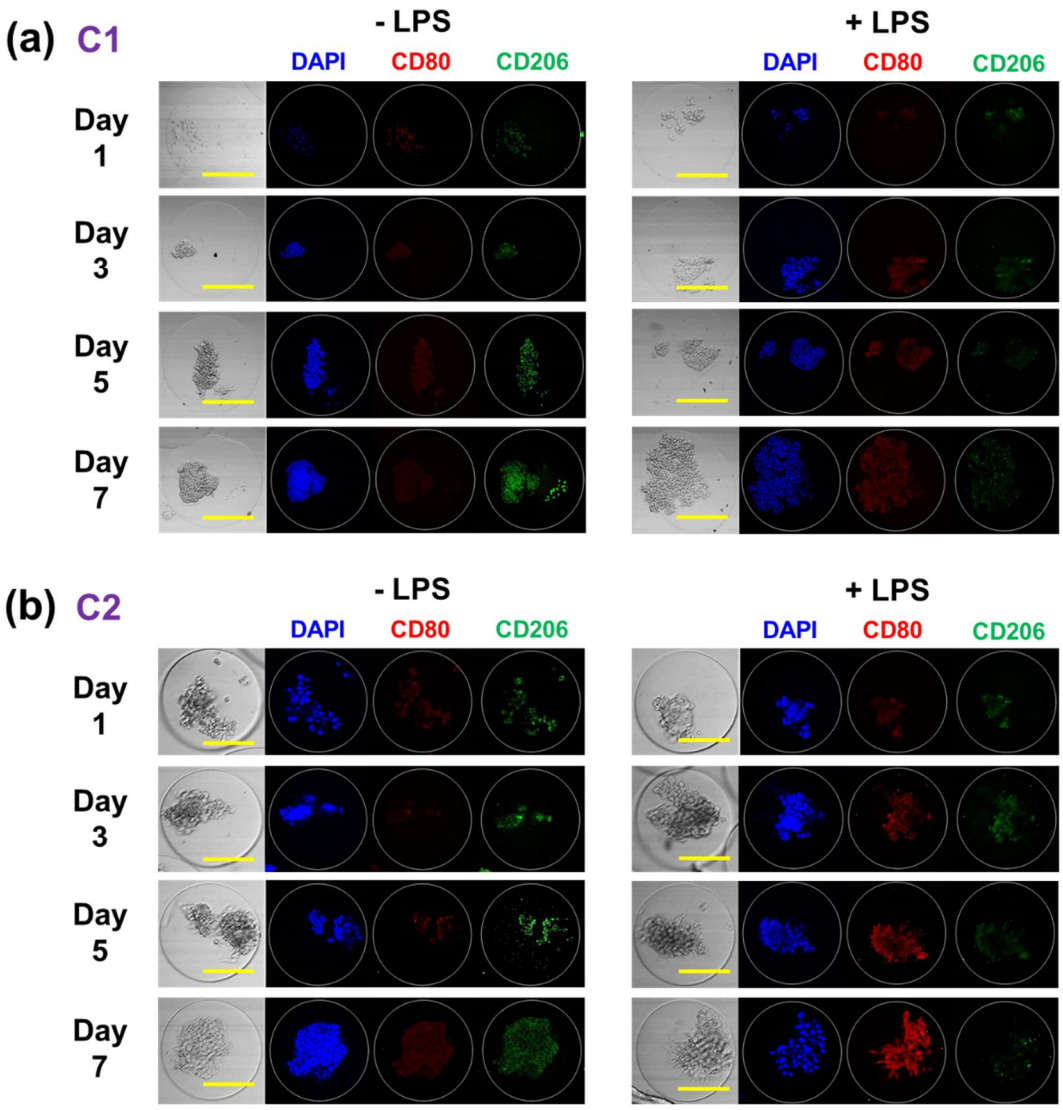

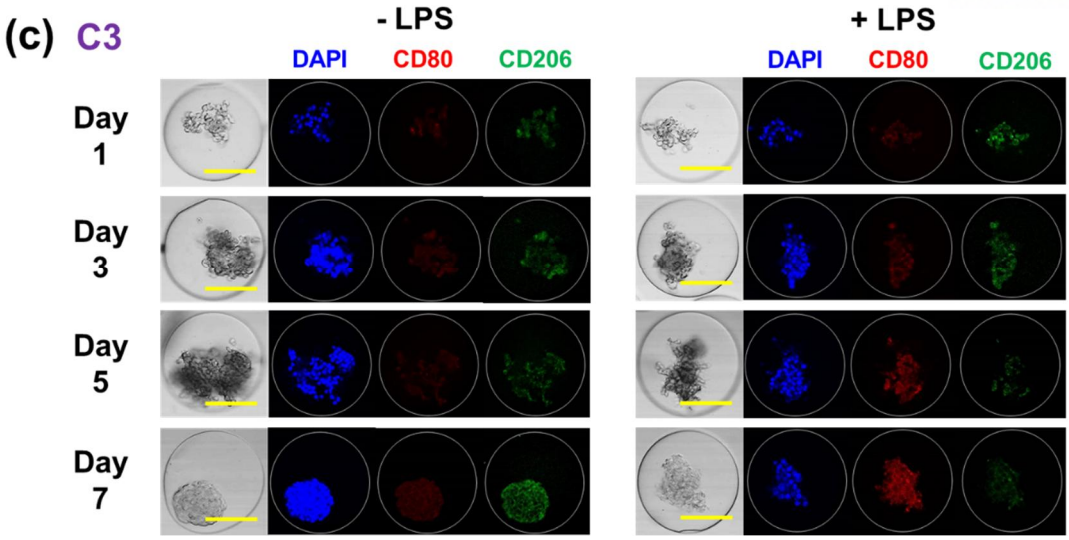

Figure 3.14 Immunocytochemical analysis of macrophage-laden microgels at different mechanical properties: (a) C1, (b) C2, (c) C3. The cells were treated with LPS to induce Mϕ polarization. At various time points, the characteristic cell surface markers, CD80 (red) and CD206 (green), on the cells encapsulated in the microgels were fluorescently labeled and monitored (scale bar: 50 μm). DAPI was used to label cell nuclei (blue).

Immuno-cytochemical analysis of the LPS-induced activation of encapsulated macrophages was performed to further characterize the different levels of activation in response to varying mechanical properties of the microgels Figure 3.14. The cellular expressions of CD80 and CD206, which are known to be characteristic biomarkers for M1 and M2 phenotypes, respectively, were monitored over the duration of cell culture. The levels of expressions were compared with those from untreated cells as a negative control. Also, the effect of mechanical properties of the microgels (e.g. C1, C2, and C3) on the biomarker expression was also explored. For untreated cells within the microgels, the expressions of CD80 and CD206 did not significantly change over time, maintaining their initial basal levels at day 1, at the highest microgel rigidity (at C3) Figure 3.14(b) and 3.14(c). However, at C1 and C2, there was noticeable increase in CD206 expression over time, while simultaneously showing decrease in CD80, suggesting the polarization favored M2 even without external stimuli at lower mechanical rigidity of the microgel Figure 3.14(a). This result indicated that the cells without any external stimuli did not show preferential polarization at higher substrate rigidity, but at lower rigidity the cells increased their anti-inflammatory potential. For the cells treated with LPS to induce M1 polarization, the level of CD80 expression correlated well with the number of cells undergoing morphological changes shown in Figure 3.11. The CD80 expression increased significantly over time and much greater than the untreated cells at C2, with simultaneous decrease in CD206 expression Figure 3.14(b). Similar expression profiles were shown for C3, though to a lesser extent Figure 3.14(c). For C1, the increase in CD80 expression was not as apparent as in other microgel conditions, similarly demonstrated by the lack of

morphological change, but the decrease in CD206 expression over time was more clearly demonstrated Figure 3.14(a). Taken together, the expressions of cellular markers for M1/M2 polarization of the macrophages encapsulated in microgels in response to LPS closely correlated with the morphological changes of the cells. Furthermore, the LPS induction of the encapsulated cells for M1 polarization was largely influenced by the mechanical properties of the microgels, highlighting the importance of tuning the substrate properties for desired phenotype.

3.3.5. In vitro multiplex tissue model

In recent years, considerable research efforts are being made to engineer in vitro tissue models to replace animal models for ethical concern over animal usage as well as creating more scalable, reproducible, and controllable testing platform.[7-10] Therefore, various tissue engineering approaches are adopted for this purpose, but it is still a substantial challenge to recreate more complex microenvironment consisting of multiple cell types. Herein, the macrophage-laden microgels developed in this study were incorporated into a larger hydrogel-based tissue constructs to fabricate a "multiplex" tissue model consisting of different cell types tissues. Due to their miniature size, the microgel-based tissue constructs could be viewed as dispersible and injectable tissue units capable of being incorporated into other tissue models. In addition, compared to conventional co-culture systems such as semi-permeable separating membrane and a simple cell mixture, in which a given culture condition (e.g. medium compositions, substrate properties) applies to all cell types, the microgel conditions could be controlled to optimize the encapsulated cells separate from other constituting cell types to fabricate more complex tissues. Using this in vitro tissue model, the effect of mutual interaction between macrophage and surrounding cells on the changes in their behavior were explored.

3.3.5.1. Fibroblast tissue

Previous studies using various co-culture systems have demonstrated that fibroblast activities are heavily influenced by various cytokines produced by macrophages in different physiological states. For example, during inflammation macrophages express pro-inflammatory cytokines (e.g. interleukin (IL)-1, 6, 12, tumor necrosis factor (TNF)-α, macrophage colony stimulating factor (M-CSF)) which induce proliferation and migration of fibroblasts. On the other hand, the macrophages are also able to influence fibroblasts to express extracellular matrix components during wound healing process by releasing growth factors such as FGF, platelet-derived growth factor (PDGF) and transforming growth factor (TGF)-β1. Therefore, macrophage-laden microgels were first incorporated into larger fibroblast-laden tissue constructs to monitor their phenotypical changes Figure 3.15(a). The macrophages were treated with LPS for 1 day prior to the incorporation to assess the effect of M1 activation on the surrounding

cells. For macrophages in microgels without LPS treatment, the cells proliferated over time in a similar rate to those cultured separately as shown in Figure 3.8, Figure 3.15(b). Unlike those macrophages which proliferated confined to the microgels, the cells in this multiplex system were able to eventually break and migrate out of the microgel after 7 days of culture, forming a colony at the periphery of the microgel, within the interstitial space between the microgel and the surrounding hydrogel. This suggested that the extracellular matrix (ECM) degradation and the growth potential of macrophages was enhanced by the presence of neighboring fibroblasts. However, the fibroblasts did not show any significant physiological change during the period.

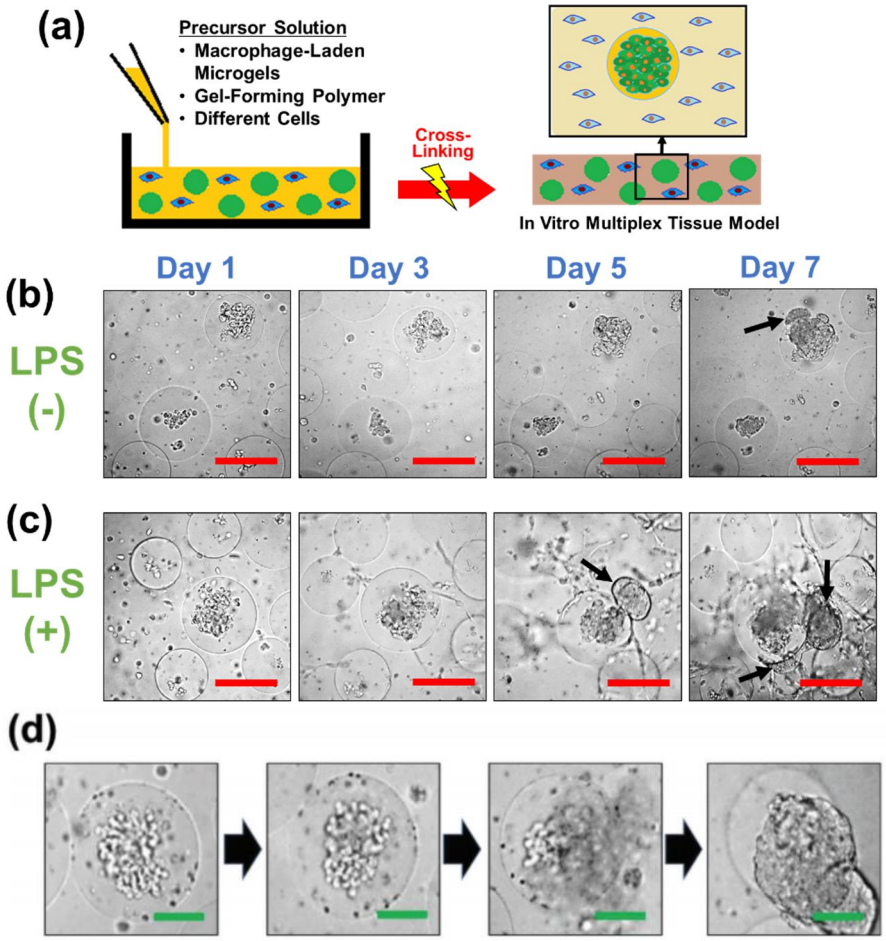

Figure 3.15 (a) Macrophage-laden microgels were embedded into a larger fibroblast tissue construct to fabricate multiplex tissue model. (b,c) The changes in their phenotypes were monitored over time (scale bar: 100 μm). The macrophages were treated with LPS prior to incorporation (untreated macrophages were used as a control). (d) A magnified view of the macrophages within the fibroblast tissue over time (scale bar: 50 μm).

When the macrophages were treated with LPS prior to multiplex tissue fabrication, the proliferation of the macrophages and their migration out of the microgels were more markedly pronounced, likely

due to the M1 activation enhancing their inflammatory potential Figure 3.15(c), 3.15(d). More interestingly, unlike the fibroblasts shown in Figure 3.15(b), which did not show any noticeable change, the surrounding fibroblasts began to spread at day 3 and proliferated around the macrophages, akin to the hypertrophic fibroblast growth in a wound healing process.[46] To the contrary, previous studies have shown that LPS-activated M1 macrophages suppress the fibroblast proliferation. Since the macrophages were only treated with LPS for 1 day prior to incorporation, and the normal culture condition was maintained throughout the culture, the macrophages did not undergo full M1 activation and both M1 and M2 characteristics were retained, leading to both M1 activated macrophage proliferation and migration and fibroblast proliferation induced by M2 activated macrophages. This explanation was partly explained by the lack of macrophages showing dendritic morphology which is a hallmark of M1 activation. Overall, these results demonstrated the effect of macrophages at different stages of activation on the surrounding fibroblastic cells was well demonstrated and characterized by the multiplex tissue model.

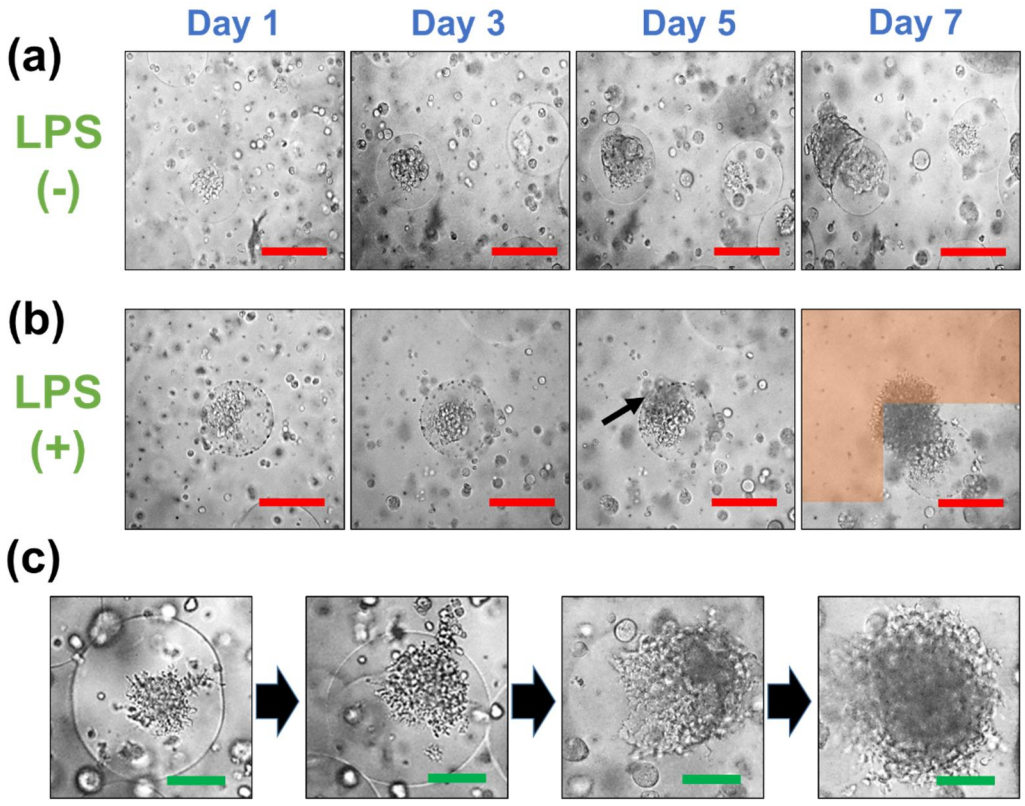

Figure 3.16 (a,b) Macrophage-laden microgels were embedded into a larger hepatocarcinoma tissue construct to fabricate multiplex tissue model. The changes in their phenotypes were monitored over time (scale bar: 100 μm). The macrophages were treated with LPS prior to incorporation (untreated macrophages were used as a control). The arrow indicates the activated macrophages migrating out of the microgel. There was a significant decrease in hepatocarcinoma cell density surrounding the macrophage (highlighted area). (c) A magnified view of the macrophages within the hepatocarcinoma tissue over time (scale bar: 50 μm).

3.3.5.2 Hepatocarcinoma Tissue

Macrophages play important and complex roles on the tumor tissue with both progression and suppression, due to their plasticity in regard to Mϕ polarization.[47-50] Macrophage cells are recruited by cancer cells, called tumor-associated macrophages (TAM), via paracrine effect and promote tumor progression by acquiring M2 phenotype and activate tumor tissue growth such as angiogenesis, immunosuppression and metastasis. In fact, tumor tissues generally consist of substantial portions of TAM. However, on the other hand, macrophages are also capable of promoting anti-cancer activities, such as proinflammatory cytokine expression (e.g. interleukins, TNF-a), antigen presentation and T cell activation, cytotoxic intermediates (e.g. nitric oxide, reactive oxygen species, by acquiring M1 phenotype via interferon-γ and co-stimuli. This anti-cancer effects of macrophages are now actively explored in cancer immunotherapy.[51, 52] To investigate the effect of reciprocal macrophages in microgels in cancer progression, macrophage-laden microgels were embedded in a hydrogel with hepatocarcinoma cells, and their behavior was monitored over time Figure 3.16. Similar to those surrounded with fibroblasts in Figure 3.15, the macrophage proliferated and eventually migrated out of the microgels and formed clusters at their periphery even without the LPS induction, indicating the surrounding hepatocarcinoma cells also similarly promoted the macrophage activation Figure 3.16(a). However, the surrounding hepatocarcinoma cells were not significantly affected during the culture period. When the macrophages were treated with LPS prior to tissue fabrication, there was a major difference in both macrophage and hepatocarcinoma cell activities Figure 3.16(b), (c). First, there were more macrophages displaying M1 phenotype (i.e. dendritic filopodia projection) generated over time than those surrounded by fibroblasts shown in Figure 6c. Furthermore, the dendritic M1 macrophages migrated out of the microgel and significantly increased in number. This result, along with that in fibroblast tissue model, highlighted that the LPS-induced M1 polarization was synergistically promoted by the presence of surrounding cancer cells, more so than normal cells,[41] likely due to paracrine effects. More importantly, there was extensive hepatocarcinoma cell death around the activated macrophage cluster, demonstrating that M1 activated macrophages showed anti-cancer activity highlighted area in Figure 3.16(b), which has been similarly demonstrated in previously published reports.[53-55] Since macrophages are not able to directly contact the cancer cells or activate T cells in this in vitro model, it was speculated that the activated M1 macrophages surrounded by cancer cells likely expressed elevated levels of inflammatory cytokines leading to anti-cancer effects. In sum, the results of phenotypical changes observed with the multiplex tissue model have successfully demonstrated the feasibility and effectiveness of this system as an in vitro tissue model to simultaneously study various biological processes for multiple cell types.

3.4. Conclusion

In this study, microfluidics-based fabrication of cell-laden microgels as microtissue constructs is presented, in which monodisperse aqueous droplets of a gel precursor solution generated from a microfluidic device with double flow-focusing channel geometry are crosslinked to generate the microgels. The biocompatibility of the microgels was well maintained regardless of their size, which was controlled by the flow rates during droplet generation. Mechanical properties of the microgels, controlled by the concentration of the gel-forming polymer, significantly influenced the proliferation and the LPS-induced differentiation ('Mϕ polarization') of encapsulated macrophages. Using these macrophage-laden microgels as dispersible microtissues, they were incorporated into a larger tissue construct to create "multiplex" tissue model, in which macrophage cells were compartmentalized within the microgel, but allowed to communicate with the surrounding tissue via diffusion. It could be argued that this model is more physiologically relevant and more closely mimic the real tissue than conventional co-culture systems. In this model, the macrophage proliferation, differentiation and migration were mediated by the type of surrounding cells, as well as LPS-induced activation. Conversely, the surrounding cells were also influenced by the state of macrophages. Taken together, the in vitro multiplex tissue model presented in this work could be applied to various types of tissues for analyzing complex and interdependent biological processes. In addition, the microgel-based tissue constructs may be used as an injectable form of implantable tissues for future clinical applications.

3.5. Reference

1. Elliott, N. T.; Yuan, F., A review of three-dimensional in vitro tissue models for drug discovery and transport studies. *J Pharm Sci* **2011,** *100* (1), 59-74.

2. Griffith, L. G.; Swartz, M. A., Capturing complex 3D tissue physiology in vitro. *Nat Rev Mol Cell Biol* **2006,** *7* (3), 211-24.

3. Yamada, K. M.; Cukierman, E., Modeling tissue morphogenesis and cancer in 3D. *Cell* **2007,** *130* (4), 601-10.

4. Lutolf, M. P.; Hubbell, J. A., Synthetic biomaterials as instructive extracellular microenvironments for morphogenesis in tissue engineering. *Nat Biotechnol* **2005,** *23* (1), 47-55.

5. Park, S.; Park, K. M., Engineered Polymeric Hydrogels for 3D Tissue Models. *Polymers (Basel)* **2016,** *8* (1).

6. Cheluvappa, R.; Scowen, P.; Eri, R., Ethics of animal research in human disease remediation, its institutional teaching; and alternatives to animal experimentation. *Pharmacol Res Perspect* **2017,** *5* (4).

7. Integration of Cell Culture and Microfabrication Technology. **2003**.

8. Chang, R.; Emami, K.; Wu, H.; Sun, W., Biofabrication of a three-dimensional liver micro-organ as an in vitro drug metabolism model. *Biofabrication* **2010,** *2* (4), 045004.

9. Kang, H. W.; Lee, S. J.; Ko, I. K.; Kengla, C.; Yoo, J. J.; Atala, A., A 3D bioprinting system to produce human-scale tissue constructs with structural integrity. *Nat Biotechnol* **2016,** *34* (3), 312-9.

10. Liaw, C. Y.; Ji, S.; Guvendiren, M., Engineering 3D Hydrogels for Personalized In Vitro Human Tissue Models. *Adv Healthc Mater* **2018,** *7* (4).

11. Casey, J.; Yue, X.; Nguyen, T. D.; Acun, A.; Zellmer, V. R.; Zhang, S.; Zorlutuna, P., 3D hydrogel-based microwell arrays as a tumor microenvironment model to study breast cancer growth. *Biomed Mater* **2017,** *12* (2), 025009.

12. Ma, Y.; Ji, Y.; Huang, G.; Ling, K.; Zhang, X.; Xu, F., Bioprinting 3D cell-laden hydrogel microarray for screening human periodontal ligament stem cell response to extracellular matrix. *Biofabrication* **2015,** *7* (4), 044105.

13. Bhise, N. S.; Ribas, J.; Manoharan, V.; Zhang, Y. S.; Polini, A.; Massa, S.; Dokmeci, M. R.; Khademhosseini, A., Organ-on-a-chip platforms for studying drug delivery systems. *J Control Release* **2014,** *190*, 82-93.

14. Caplin, J. D.; Granados, N. G.; James, M. R.; Montazami, R.; Hashemi, N., Microfluidic Organ-on-a-Chip Technology for Advancement of Drug Development and Toxicology. *Adv Healthc Mater* **2015,** *4* (10), 1426-50.

15. Huh, D.; Torisawa, Y. S.; Hamilton, G. A.; Kim, H. J.; Ingber, D. E., Microengineered physiological biomimicry: organs-on-chips. *Lab Chip* **2012,** *12* (12), 2156-64.

16. Guo, M. T.; Rotem, A.; Heyman, J. A.; Weitz, D. A., Droplet microfluidics for high-throughput biological assays. *Lab Chip* **2012,** *12* (12), 2146-55.

17. Joensson, H. N.; Andersson Svahn, H., Droplet microfluidics--a tool for single-cell analysis. *Angew Chem Int Ed Engl* **2012,** *51* (49), 12176-92.

18. Leng, X.; Zhang, W.; Wang, C.; Cui, L.; Yang, C. J., Agarose droplet microfluidics for highly parallel and efficient single molecule emulsion PCR. *Lab Chip* **2010,** *10* (21), 2841-3.

19. Mark, D.; Haeberle, S.; Roth, G.; von Stetten, F.; Zengerle, R., Microfluidic lab-on-a-chip platforms: requirements, characteristics and applications. *Chem Soc Rev* **2010,** *39* (3), 1153-82.

20. Cha, C.; Oh, J.; Kim, K.; Qiu, Y.; Joh, M.; Shin, S. R.; Wang, X.; Camci-Unal, G.; Wan, K. T.; Liao, R.; Khademhosseini, A., Microfluidics-assisted fabrication of gelatin-silica core-shell microgels for injectable tissue constructs. *Biomacromolecules* **2014,** *15* (1), 283-90.

21. Kim, S.; Oh, J.; Cha, C., Enhancing the biocompatibility of microfluidics-assisted fabrication of cell-laden microgels with channel geometry. *Colloids Surf B Biointerfaces* **2016,** *147*, 1-8.

22. Park, K.-S.; Kim, C.; Nam, J.-O.; Kang, S.-M.; Lee, C.-S., Synthesis and characterization of thermosensitive gelatin hydrogel microspheres in a microfluidic system. *Macromolecular Research* **2016,** *24* (6), 529-536.

23. Rossow, T.; Heyman, J. A.; Ehrlicher, A. J.; Langhoff, A.; Weitz, D. A.; Haag, R.; Seiffert, S., Controlled synthesis of cell-laden microgels by radical-free gelation in droplet microfluidics. *J Am Chem Soc* **2012,** *134* (10), 4983-9.

24. Zhao, X.; Liu, S.; Yildirimer, L.; Zhao, H.; Ding, R.; Wang, H.; Cui, W.; Weitz, D., Injectable Stem Cell-Laden Photocrosslinkable Microspheres Fabricated Using Microfluidics for Rapid Generation of Osteogenic Tissue Constructs. *Advanced Functional Materials* **2016,** *26* (17), 2809-2819.

25. Aikawa, T.; Konno, T.; Ishihara, K., Phospholipid polymer hydrogel microsphere modulates the cell cycle profile of encapsulated cells. *Soft Matter* **2013,** *9* (18).

26. Aikawa, T.; Konno, T.; Takai, M.; Ishihara, K., Spherical phospholipid polymer hydrogels for cell encapsulation prepared with a flow-focusing microfluidic channel device. *Langmuir* **2012,** *28* (4), 2145-50.

27. Labonte, A. C.; Tosello-Trampont, A. C.; Hahn, Y. S., The role of macrophage polarization in infectious and inflammatory diseases. *Mol Cells* **2014,** *37* (4), 275-85.

28. Martinez, F. O.; Sica, A.; Mantovani, A.; Locati, M., Macrophage activation and polarization. *Front Biosci* **2008,** *13*, 453-61.

29. McWhorter, F. Y.; Davis, C. T.; Liu, W. F., Physical and mechanical regulation of macrophage phenotype and function. *Cell Mol Life Sci* **2015,** *72* (7), 1303-16.

30. Sridharan, R.; Cameron, A. R.; Kelly, D. J.; Kearney, C. J.; O'Brien, F. J., Biomaterial based modulation of macrophage polarization: a review and suggested design principles. *Materials Today*

2015, *18* (6), 313-325.

31. Goers, L.; Freemont, P.; Polizzi, K. M., Co-culture systems and technologies: taking synthetic biology to the next level. *J R Soc Interface* **2014,** *11* (96).

32. Sikkema, J.; de Bont, J. A.; Poolman, B., Mechanisms of membrane toxicity of hydrocarbons. 32. *Microbiol Rev.* **1995,** *59*, 201-22.

33. Wang, N.; Tytell, J. D.; Ingber, D. E., Mechanotransduction at a distance: mechanically coupling the extracellular matrix with the nucleus.. *Nat Rev Mol Cell Biol.* **2009,** *10*.

34. Ugarte-Berzal, E.; Vandooren, J.; Bailon, E.; Opdenakker, G.; Garcia-Pardo, A., Inhibition of MMP-9-dependent Degradation of Gelatin, but Not Other MMP-9 Substrates, by the MMP-9 Hemopexin Domain Blades 1 and 4. *J Biol Chem* **2016,** *291* (22), 11751-60.

35. Vandooren, J.; Geurts, N.; Martens, E.; Van den Steen, P. E.; Jonghe, S. D.; Herdewijn, P.; Opdenakker, G., Gelatin degradation assay reveals MMP-9 inhibitors and function of O-glycosylated domain. *World J Biol Chem* **2011,** *2* (1), 14-24.

36. Murray, M. Y.; Birkland, T. P.; Howe, J. D.; Rowan, A. D.; Fidock, M.; Parks, W. C.; Gavrilovic, J., Macrophage migration and invasion is regulated by MMP10 expression. *PLoS One* **2013,** *8* (5), e63555.

37. Cha, C.; Jeong, J. H.; Shim, J.; Kong, H., Tuning the dependency between stiffness and permeability of a cell encapsulating hydrogel with hydrophilic pendant chains. *Acta Biomater.* **2011,** *7* (10), 3719-28.

38. Adlerz, K. M.; Aranda-Espinoza, H.; Hayenga, H. N., Substrate elasticity regulates the behavior of human monocyte-derived macrophages. *Eur Biophys J.* **2016,** *45* (4), 301-9.

39. Saxena, R. K.; Vallyathan, V.; Lewis, D. M., Evidence for lipopolysaccharide-induced differentiation of RAW264.7 murine macrophage cell line into dendritic like cells. *J Biosci.* **2003,** *28*, 129-34.

40. Zanganeh, S.; Hutter, G.; Spitler, R.; Lenkov, O.; Mahmoudi, M.; Shaw, A.; Pajarinen, J. S.; Nejadnik, H.; Goodman, S.; Moseley, M.; Coussens, L. M.; Daldrup-Link, H. E., Iron oxide nanoparticles inhibit tumour growth by inducing pro-inflammatory macrophage polarization in tumour tissues. *Nat Nanotechnol* **2016,** *11* (11), 986-994.

41. Jacquemet, G.; Hamidi, H.; Ivaska, J., Corrigendum to “Filopodia in cell adhesion, 3D migration and cancer cell invasion” *Curr. Opin. Cell Biol.* **2015**, 36, 23–31.

42. Pi, J.; Li, T.; Liu, J.; Su, X.; Wang, R.; Yang, F.; Bai, H.; Jin, H.; Cai, J., Detection of lipopolysaccharide induced inflammatory responses in RAW264.7 macrophages using atomic force microscope. *Micron* **2014,** *65*, 1-9.

43. Ploeger, D. T.; Hosper, N. A.; Schipper, M.; Koerts, J. A.; de Rond, S.; Bank, R. A., Cell plasticity in wound healing: paracrine factors of M1/ M2 polarized macrophages influence the phenotypical state of dermal fibroblasts. *Cell Commun Signal.* **2013,** *11*.

44. Williams, L. M.; Ridley, A. J., Lipopolysaccharide induces actin reorganization and tyrosine phosphorylation of Pyk2 and paxillin in monocytes and macrophages. *J Immunol* **2000,** *164* (4), 2028-36.

45. Patel, N. R.; Bole, M.; Chen, C.; Hardin, C. C.; Kho, A. T.; Mih, J.; Deng, L.; Butler, J.; Tschumperlin, D.; Fredberg, J. J.; Krishnan, R.; Koziel, H., Cell elasticity determines macrophage function. *PLoS One* **2012,** *7* (9), e41024.

46. METZGER, Z.; HOFFELD, J. T.; OPPENHEIM, J. J., Suppression of Fibroblast Proliferation by Activated Macrophages: involvement of H_20_2 and a Non-prostaglandin E Product of the Cyclooxygenase Pathway. *Cellular immunology* **1986,** *100*, 501-514.

47. Allavena, P.; Sica, A.; Garlanda, C.; Mantovani, A., The Yin-Yang of tumor-associated macrophages in neoplastic progression and immune surveillance. *Immunol Rev* **2008,** *222*, 155-61.

48. Allavena, P.; Sica, A.; Solinas, G.; Porta, C.; Mantovani, A., The inflammatory micro-environment in tumor progression: the role of tumor-associated macrophages. *Crit Rev Oncol Hematol* **2008,** *66* (1), 1-9.

49. Mantovani, A.; Sozzani, S.; Locati, M.; Allavena, P.; Sica, A., Macrophage polarization: tumor-associated macrophages as a paradigm for polarized M2 mononuclear phagocytes. *Trends Immunol* **2002,** *23*, 549-55.

50. Muller-Quernheim, U. C.; Potthast, L.; Muller-Quernheim, J.; Zissel, G., Tumor-cell co-culture induced alternative activation of macrophages is modulated by interferons in vitro. *J Interferon Cytokine Res* **2012,** *32* (4), 169-77.

51. De Palma, M.; Lewis, C. E., Macrophage regulation of tumor responses to anticancer therapies. *Cancer Cell* **2013,** *23* (3), 277-86.

52. Mills, C. D.; Lenz, L. L.; Harris, R. A., A Breakthrough: Macrophage-Directed Cancer Immunotherapy. *Cancer Res* **2016,** *76* (3), 513-6.

53. Cai, X.; Yin, Y.; Li, N.; Zhu, D.; Zhang, J.; Zhang, C. Y.; Zen, K., Re-polarization of tumor-associated macrophages to pro-inflammatory M1 macrophages by microRNA-155. *J Mol Cell Biol* **2012,** *4* (5), 341-3.

54. Genin, M.; Clement, F.; Fattaccioli, A.; Raes, M.; Michiels, C., M1 and M2 macrophages derived from THP-1 cells differentially modulate the response of cancer cells to etoposide. *BMC Cancer* **2015,** *15*, 577.

55. Yuan, A.; Hsiao, Y. J.; Chen, H. Y.; Chen, H. W.; Ho, C. C.; Chen, Y. Y.; Liu, Y. C.; Hong, T. H.; Yu, S. L.; Chen, J. J.; Yang, P. C., Opposite Effects of M1 and M2 Macrophage Subtypes on Lung Cancer Progression. *Sci Rep* **2015,** *5*, 14273.

PART IV

Combined effects of co-culture and substrate mechanics on 3D tumor spheroid formation within microgels prepared via flow-focusing microfluidic fabrication

4.1. Introduction

Tumor spheroids have been extensively investigated as a three-dimensional (3D) tissue model to study various aspects of cancer physiology as well as for high throughput screening applications, as they can mimic 3D solid tumor tissues more closely than conventional two-dimensional monolayers.[1-3] In addition, there are several methods available to efficiently develop spheroids in large quantities, both templated (e.g. microwells) and suspension (e.g. hanging drop) cultures.[4-6] This is possible due to the high proliferative nature and strong cell-cell interactions of various tumor cells, which are hallmarks of tumor progression, such that even under conventional in vitro cell culture conditions, the cells easily grow in numbers and often naturally aggregate to form spheroid structures. More recently, scaffold materials have been increasingly adopted to provide 3D tumor microenvironment resembling natural extracellular matrix (ECM), such as microgels (e.g. alginate and gelatin microbeads), to induce more complex cell-matrix as well as cell-cell interactions during spheroid formation.[7-10] Due to the advancement in microfabrication technology, the size and shape of these scaffolds can be fine-tuned to generate tumor spheroids with more complex and elaborate morphology. In addition, as the physical properties of tumor microenvironment have also been shown to influence the tumor formation and physiology, the mechanical properties of the scaffold are controlled to influence tumor spheroid formation.[11, 12] The use of scaffold also has the advantage of incorporating different types of cells in predefined numbers to generate heterogeneous spheroids.[13, 14] Furthermore, the topological features of the hydrogel surface have also been shown to influence the behavior of tumor cells.[15, 16] Flow-focusing microfluidics has recently gained significant interest in the field of biomaterials, as it can generate liquid droplets with controlled, monodisperse size and architecture in high yield and biocompatibility.[17-19] These droplets are used to encapsulate a wide array of biologically relevant molecules (e.g. therapeutic molecules, proteins) and species (e.g. bacterial and mammalian cells) for delivery applications. Moreover, the droplets consisting of gel-forming polymers can be crosslinked to develop microgels as cell culture platforms for tissue engineering applications.[20-25] In this study, a microfluidic device with double flow-focusing channel geometry was used to fabricate microgels encapsulated with tumor cells, in order to create uniform-sized, microgel-based 3D tumor spheroids. The aqueous droplets of methacrylic gelatin, a gel-forming polymer, dispersed with breast adenocarcinoma cells (i.e., MCF-7) were first generated by the microfluidic device, followed by photo-crosslinking to develop microgels

containing tumor cells. Gelatin-based hydrogels have long been widely used as 3D cell culture platforms for tissue engineering applications. For example, gelatin, which is derived from collagen, retains cell recognition domains such as cell adhesion ligands (e.g., Arg-Gly-ASP (RGD) peptide) and matrix metalloproteinase (MMP) domains that are crucial for cellular activities such as proliferation and migration.[21, 25-29] Due to the biocompatible and bioactive environment imparted by the crosslinked gelatin network, the cells would proliferate and eventually turn into spheroids within the microgels. There have been numerous studies on developing tumor spheroids using various cell sources, including the oft-used MCF-7 cells.[30-33] However, most of these studies were performed either in suspension culture or on 2D substrate, and tumor spheroid formation under 3D environment are not extensively investigated to date. This study not only allows the investigation of tumor spheroid formation within size-controlled microgels, but also the effect of mechanical environment of tumor spheroid formation could be further explored by controlling the mechanical properties of the microgels with the polymer concentration. Furthermore, the tumor cells were co-cultured with a different type of cells, either fibroblasts or macrophages which have been well known to be involved in tumor progression, to further influence the spheroid formation within the microgels. The results of this study would delineate the combined effects of co-culture and ECM mechanics on the tumor spheroid formation.

4.2. Materials and methods

4.2.1. Fabrication of a Microfluidic Device

The silicon master for the PDMS-based microfluidic device was fabricated on a silicon wafer using a standard photolithography. Briefly, SU-8 100 (MicroChem Corp.) as a photoresist was first spin-coated on a silicon wafer at 1750 rpm for 30 seconds, and then baked at 65 °C for 20 minutes, followed by 95 °C for 50 minutes to harden the photoresist. The height of the photoresist became approximately 150 μm. The photomask with a pattern for the microfluidic channel was placed on top of the wafer, and irradiated with UV to fabricate the patterned area. After baking at 95 °C to further strengthen the patterned area, the wafer was placed in SU-8 developer to remove the non-fabricated area. The wafer was washed with isopropanol and dried. The channel schematic is shown in Figure 4.2. PDMS elastomer was fabricated on top of the silicon master (base:curing agent = 10:1, Sylgard®184 Silicone Elastomer Kit, Midland, MI, USA). The PDMS mixture was first degassed under vacuum, and cured for 3 hours at 80 °C. The PDMS elastomer with the channel pattern engraved on the surface was detached from the master, and fluid inlets and outlets were created using a hole puncher (0.5 mm diameter). Finally, a glass slide and the PDMS were treated with oxygen plasma (Harrick Plasma) for 30 seconds and permanently bonded to each other to fabricate the PDMS microfluidic device. To inject fluids into and collect the fluid from the microfluidic device, plastic tubings (Tygon®, Saint-Gobain

Performance Plastics, Merrimack, NH, USA) were connected to the inlets and outlet of the microfluidic device.

4.2.2. Immunocytochemistry

Immunocytochemical labeling of cells encapsulated in microgels was performed to visualize the characteristic biomarkers. Briefly, a cell-laden microgel sample was first fixed in 4 % formaldehyde solution overnight at 4 °C. After washing with PBS, the sample was incubated in a PBS-DS (5 % donkey serum in PBS) as a blocking solution for 30 minutes. After removing the blocking solution, the sample was incubated with primary antibodies for 2 hours at room temperature. After removing the antibody solution and washing with PBS, the sample was postfixed with 4 % formaldehyde for 5 minutes. After washing with PBS, the sample was treated with 0.3% Triton X-100/PBS-DS (PBST-DS) for 30 min. After washing with PBS-DS, the sample was incubated with fluorophore-conjugated secondary antibodies and 4′,6-diamidino-2-phenylindole (DAPI, 100 ng mL−1) for 2 hours at room temperature. After removing the antibody solution and washing with PBST 3 times, the fluorescent image of the hydrogel surface was captured with a confocal microscope (FV1000, Olympus, Shinjuku, Tokyo, Japan).

4.2.3. Determination of droplet concentrations

The overall MGel concentration of the droplet after the merging of core and shell regions was estimated by the volumes of core and shell regions determined from the microscopic observation. Briefly, there was a clear border between core and shell regions, which are Aq1 and Aq2 phases, respectively, immediately after droplet formation. The volumes of the core (V_c) and the shell (V_s) was calculated, and their relative portions were used to calculate the overall concentration (C_T),

$$V_C = \frac{4}{3}\pi r_C^3, \quad V_S = V_T - V_C, \quad C_T = \frac{V_C}{V_T}C_C + \frac{V_S}{V_T}C_S \ ,$$

V_T was the total droplet volume, Cc and Cs were the concentrations of core and shell, respectively, and r_c was the radius of the core. In this study, the average V_c/V and V_s/V were 0.6 and 0.4. The C_T are calculated as follows:

Conditions	C_c (%)	C_s (%)	C_T (%)
C1	5	8	6.2
C2	7	10	8.2
C3	9	12	10.2
C4	11	14	12.2
C5	13	16	14.2

Table. 4.1 The concentrations of core (C_c) and shell (C_s) regions of droplets, and the final concentration of droplets after merging (C_T).

4.2.4. Synthesis of methacrylic gelatin (MGel)

The methacrylate conjugation to gelatin was accomplished following a previously published method.[21, 25, 34] In a typical experimental set-up, gelatin (10 g, Sigma Aldrich, St. Louis, MO, USA), 4-dimethylaminopyridine (1 g, Sigma Aldrich), and 4-methoxyphenol (0.1g, Sigma Aldrich) were dissolved in 100 mL dimethylsulfoxide at 50 °C. Then, glycidyl methacrylate (4 mL, S0.1gigma Aldrich) was slowly added and reacted for 2 days at 50 °C under dry N_2. The product was purified by dialysis against deionized water for 2 days, changing the water three times a day, and dried by lyophilization. The chemical structure of the product was analyzed using ^{1}H-NMR spectroscopy. (Figure 4.1)

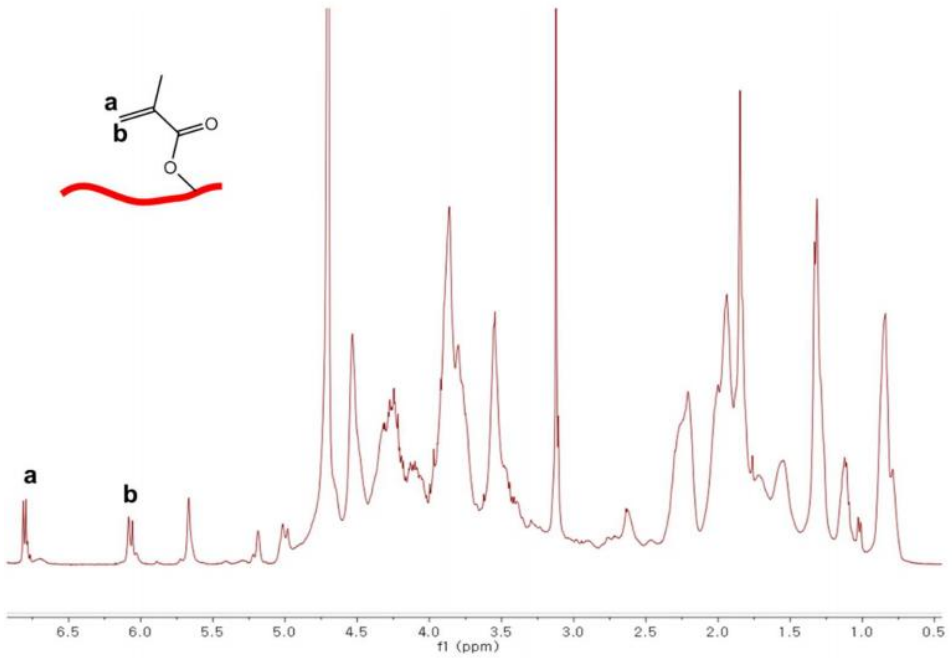

Figure 4.1 ^{1}H-NMR spectrum of methacrylic gelatin (MGel). Characteristic peaks (a and b) of methacrylate are noted.

4.2.5. Fabrication of cell-laden microgels

The polydimethylsulfoxane (PDMS)-based microfluidic device having a "double" flow-focusing channel was fabricated using a standard photolithography and PDMS (Sylgard®184 Silicone Elastomer, Dow Corning) molding technique (detailed processing steps and channel geometry are included in Figure 4.2). [21, 25] The channel consisted of two inlets for aqueous phases containing (*Aq*1 and *Aq*2) and one inlet for oil phase (*O*). *Aq*1 would become the core of a droplet, while *Aq*2 would become the shell (Figure 4.3(a), Figure 4.2). *Aq*1 and *Aq*2 consisted of MGel and 0.2 % (w/v) Irgacure 2959® as a photo-initiator in phosphate buffered saline (PBS, pH 7.4). The concentrations of MGel in *Aq*1 and *Aq*2 explored in this study were 5 and 8, 7 and 10, 9 and 12, 11 and 14, and 13 and 16 % (w/v), respectively. *O* consisted of 20 % Span®80 (Sigma Aldrich) as a surfactant in mineral oil. In *Aq*1, human breast adenocarcinoma cells, MCF-7 (ATCC®), were dispersed in the *Aq*1 at 1×10^7 cells mL^{-1}. For co-culture conditions, either fibroblasts (3T3, ATCC®) or macrophages (RAW264.7, ATCC®) were mixed with MCF-7 cells in varying ratios. The fluids were injected into the microfluidic device using electronic pumps (Legato®100, KD Scientific). The flow rate of *Aq*1 and *Aq*2 was 125 µL hr^{-1}, while keeping the flow rate of O at 500 µL hr^{-1}, resulting in droplets with 100 µm average diameter. The droplets were then irradiated with UV for 2 minutes (intensity: 200 mW, distance: 5 cm, emission filter: 250-450 nm, Model S1500, Omnicure®) to fabricate the cell-laden microgels. The microgels were washed extensively with PBS to remove residual oil, and incubated in the cell culture medium (RPMI 1640 supplemented with 10 % fetal bovine serum and 1 % penicillin/streptomycin, all purchased from Thermo Fisher) at 37 °C under 5 % atmospheric CO_2. Due to the difficulty of directly measuring the mechanical properties of microgels, larger MGel hydrogel disks (8 mm diameter, 1 mm thickness) at the same MGel concentrations were fabricated by placing the precursor solution in a custom-made mold and applying the same photo-crosslinking step used to develop the microgels, as stated above, and their elastic moduli were obtained from uniaxial compression experiments.[35, 36] Each hydrogel disk was compressed at a rate of 1 mm min^{-1} using a universal testing machine (Model 3343, Instron). The elastic modulus was calculated from the slope of a stress-strain curve at the elastic region (first 10 % strain).

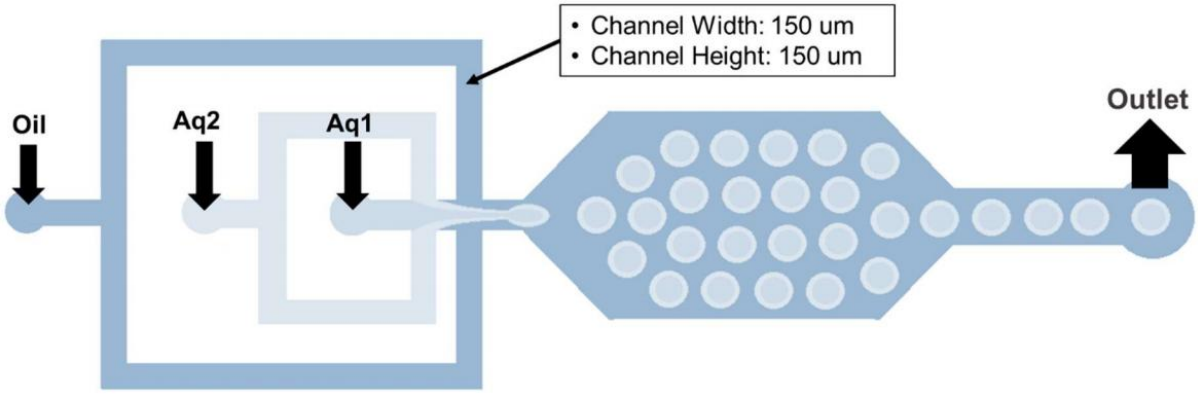

Figure 4.2 Schematic illustration of double flow-focusing channel geometry of the microfluidic device used to generate cell-laden microgels.

4.2.6. In vitro evaluation

4.2.6.1. Viability and proliferation

The viability of the cells encapsulated in the microgels were evaluated using LIVE/DEAD Cell Viability Assay kit (Thermo Fisher), following the manufacturer's instuctions. Briefly, the cell-laden microgels were treated with calcein-AM and ethidium homodimer-1 to fluorescently label live (green) and dead (red) cells. The cells were visualized with a fluorescent microscope (XDS-3FL, Optika) and counted. The viability was reported as the percentage of live cells from the total number of cells. The viability was measured at various time points. The proliferation rate (k_P) of encapsulated cells was determined by counting the number of live cells at various time points, and the plot of the normalized number of viable cells (N_t/N_0) vs. time (t) was fitted with the following power-law equation,

$$\frac{N_t}{N_0} = 2^{k_p \cdot t} \qquad (1)$$

N_t was the number of viable cells at time, t, and N_0 was the initial number of viable cells at t=0.[21, 37]

4.2.6.2. Immunostaining

To visualize the biomarker expression of cells encapsulated in microgels at different stages of growth, immunofluorescent labeling of CD80 for macrophage and E-cadherin (E-cad) for MCF-7 cells was performed (detailed immunocytochemistry protocol is described in 2.2 section).[38-41] Hamster anti-mouse CD80 and rat anti-mouse E-cad were used as primary antibodies (1:250 dilution). AlexaFluor®568-linked anti-hamster IgG and AlexaFluor®488-linked goat anti-rat IgG were used as secondary antibodies (1:250 dilution). The cell nuclei were stained with 4',6-diamidino-2-phenylindole (DAPI, Sigma Aldrich). The labeled cells within the microgels were imaged using a confocal fluorescence microscope (FV1000, Olympus).

4.3. Results and Discussion

4.3.1. Microfluidic fabrication of cell-laden microgels

The bioactive microgels encapsulated with spheroid-forming breast tumor cells (i.e. MCF-7) were fabricated by a microfluidic device with flow-focusing channel (Figure 4.3). The flow-focusing geometry of the microfluidic channel allows the formation of monodisperse aqueous droplets via shear stress applied by the oil flow. To fabricate cell-laden microgels, the aqueous droplets consisted of gel-

forming macromer, methacrylic gelatin (MGel), and photoinitiator in order to apply photocrosslinking scheme. Herein, the "double" flow-focusing microfluidic channel geometry was utilized, in which one aqueous phase (*Aq*1) is allowed to enter the second aqueous phase (*Aq*2) before being pinched off to form droplets. Our previous studies have demonstrated that this particular channel geometry could significantly enhance the viability of the encapsulated cells by directing the cells to the center of the droplets, and eventually the microgels, by including the cells only in *Aq*1. This strategy minimized the cells from contacting the oil phase containing surfactants, which is well known to cause cytotoxic effects.[39, 42]

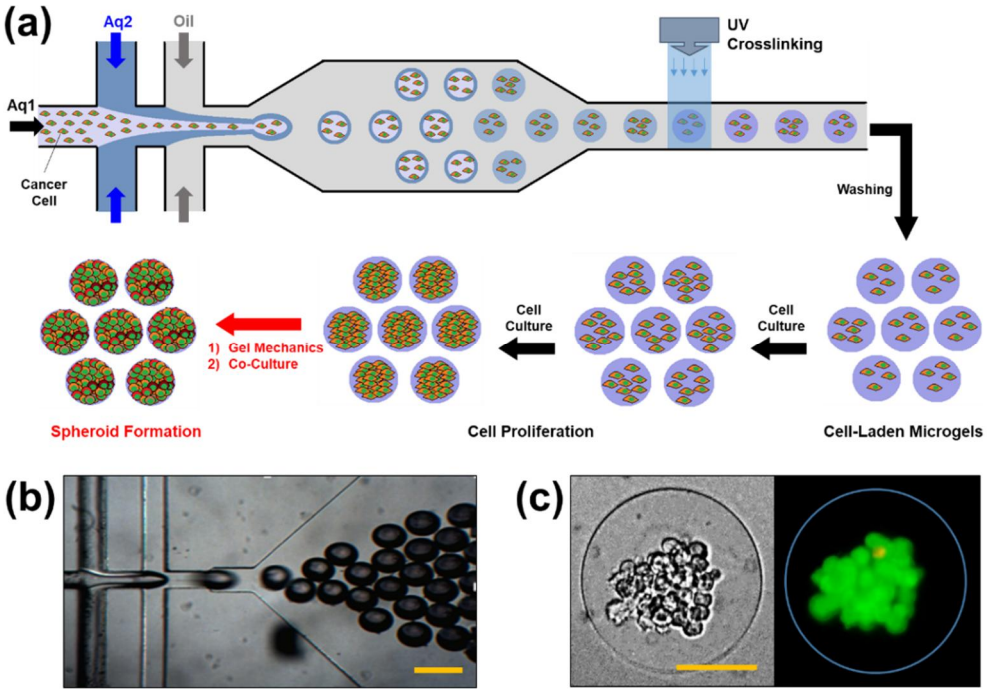

Figure 4.3 (a) Schematic illustration of the fabrication of cell-laden microgels using a "double" flow-focusing microfluidic device. Droplets of gel precursor solution dispersed with tumor cells are photocrosslinked to generate the microgels. The cell-laden microgels are continuously cultured to allow the cells to proliferate and form spheroids. (b) A microscopic view of the microfluidic device (scale bar: 200 μm). (c) Representative optical (left) and fluorescent (right) images of cell-laden microgels (scale bar: 50 μm). The cells were fluorescently labeled to visualize live (green) and dead (red) cells.

To help keep the cells within the core region of the droplets before employing photo-crosslinking, the MGel concentration in *Aq*2, which would become the shell region, was higher than that of *Aq*1, again following our previous studies.[21, 25] With the higher viscosity of shell region, the cells within the core region would more likely remain there than move outwards, further minimizing the chances of cells contacting the surrounding oil phase. The microscopic observation of resulting microgels indeed revealed that the cells generally remained within the core region, even after the core and shell regions eventually merged via diffusion and photo-crosslinked to form microgel (Figure 4.3c). One of the advantages of flow-focusing microfluidics in creating droplets is the precise control of size by simply

adjusting the flow rates of aqueous and oil phases. Also, the droplets are monodisperse in size under the given flow rates, as shown in Figure 4.3b, especially compared with those created by non-specific high shear (e.g. sonication) which results in wider size distributions.[43] Here, the ratio of aqueous to oil flows was kept at 0.2, which resulted in droplets with the average diameter of 100 μm.

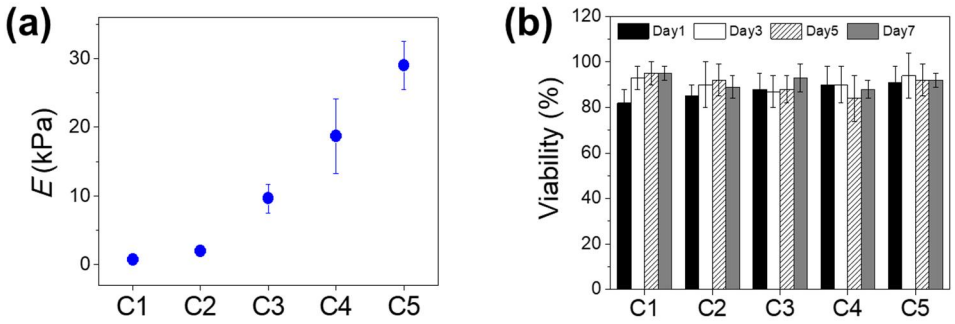

Figure 4.4 (a) Elastic moduli (*E*) of MGel hydrogels at varying concentrations. (b) The viability of MCF-7 cells encapsulated in microgels at varying MGel concentrations, measured at various times up to 7 days.

4.3.2. Effect of microgel mechanics on tumor spheroid formation

To investigate the effect of microgel mechanics on the viability and proliferation of the encapsulated cells, the mechanical properties of the microgels were controlled by varying the MGel concentrations. Five different sets of MGel concentrations for *Aq*1 and *Aq*2 were explored; 5 % and 8 % (C1), 7 % and 10 % (C2), 9 % and 12 % (C3), 11 % and 14 % (C4), and 13 % and 16% (C5). The overall MGel concentration after the merging of core and shell regions were estimated to be 6.2 % (C1), 8.2 % (C2), 10.2 % (C3), 12.2 % (C4) and 14.2 % (C5), determined based on the relative amounts of core and shell regions (detailed calculations are provided in Supporting Information). Due to the difficulty of directly measuring the mechanical properties of microgels, larger hydrogels at the same MGel concentrations via photo-crosslinking were separately fabricated, and their elastic moduli were obtained from uniaxial compression (Figure 4.4a). The moduli could be controlled in a wide range, from 0.7 kPa to 30 kPa, by varying the MGel concentration.

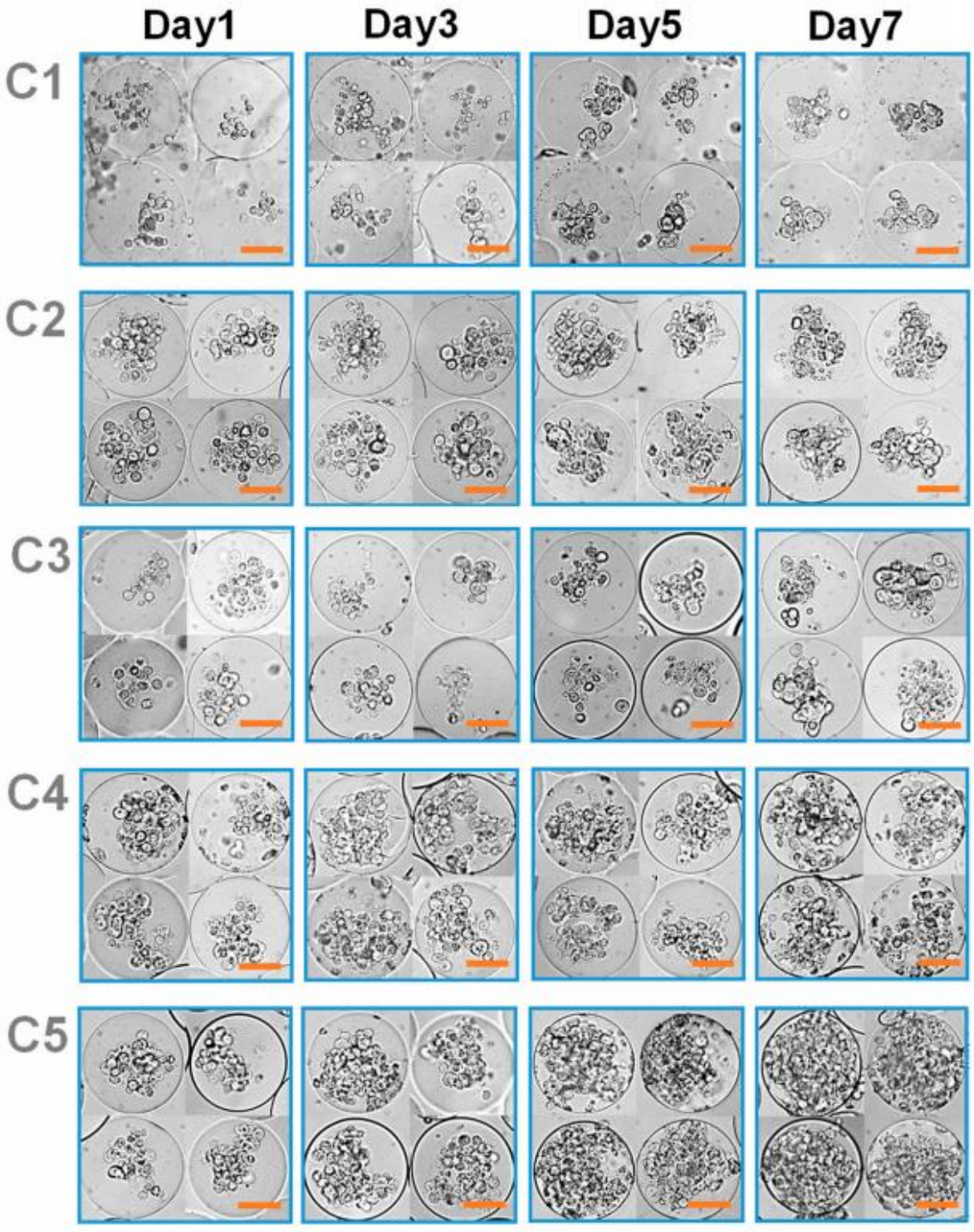

Figure 4.5 Microscopic images of cell-laden microgels at various mechanical stiffness (from C1 to C5), controlled by MGel concentration, cultured over time (scale: 50 μm).

The MCF-7 cells encapsulated in the microgels with varying mechanical stiffness were cultured, and

their viability and proliferation were measured. The cell viability was well maintained regardless of the microgel conditions, all above 80 %, demonstrating the biocompatibility of the microfluidic process and the 3D microenvironment provided by the microgels (Figure 4.3 and Figure 4.4). However, there was a significant difference in cell proliferation in response to varying mechanical stiffness of the microgels. The cell proliferation increased substantially with increasing mechanical stiffness, as identified by the microscopic observation (Figure 4.5). To further quantify the rate of proliferation at different microgels, the number of cells were counted at various times throughout the cell culture, and the plot of number of cells vs. time was fitted with a population doubling power-law model to obtain the proliferation rate (k) (Figure 4.6). In accordance with the microscopic images, the k values increased with mechanical stiffness of the microgels. Previous studies have similarly demonstrated that the proliferation of MCF-7 cells was enhanced on stiffer substrates.[44] However, the majority of the studies have been performed on the surface (2D). Since medium diffusion into the microgel and the available inner space in the microgel for cell growth becomes more limited at higher stiffness, which would be viewed as deterrent for cellular growth, the increase in proliferation under those circumstances revealed that the mechanotransduction imparted by the higher stiffness of the microgel had significant influence over proliferation. Moreover, the overall microgel dimension did not change during the proliferation, suggesting that the cells could remodel the internal structure to accommodate the increasing number of cells.

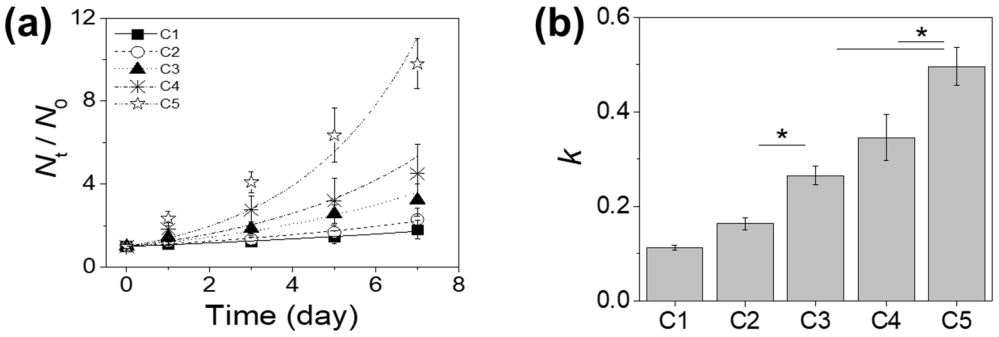

Figure 4.6 (a) The number of live MCF-7 cells at various times (N_t) normalized with the initial number of live cells (N_0) plotted over time. (b) The proliferation rate (k) obtained by fitting the plot in (a) with Eq.(1). (*p<0.05, n = 10)

With the continued cell culture up to 2 weeks, the cells formed a collection of smaller spheroids within the microgels, in which the cell clusters organized into more well defined spherical entities (Figure 4.7). The size of these spheroids was larger at higher microgel stiffness, suggesting that greater number of cells during the proliferation naturally led to the formation of larger spheroids. Especially at C4 and C5, the cells outgrew the size of the microgels, such that some of the cells could migrate out of the microgels. Overall, these results highlighted that the MCF-7 cells within the microgels showed higher proliferation

at greater microgel stiffness, and the cells eventually turned into spheroids. However, it should be noted that the continued cell proliferation did not lead to a singular large spheroid in a microgel, rather a number of smaller spheroids co-existing within the microgel.

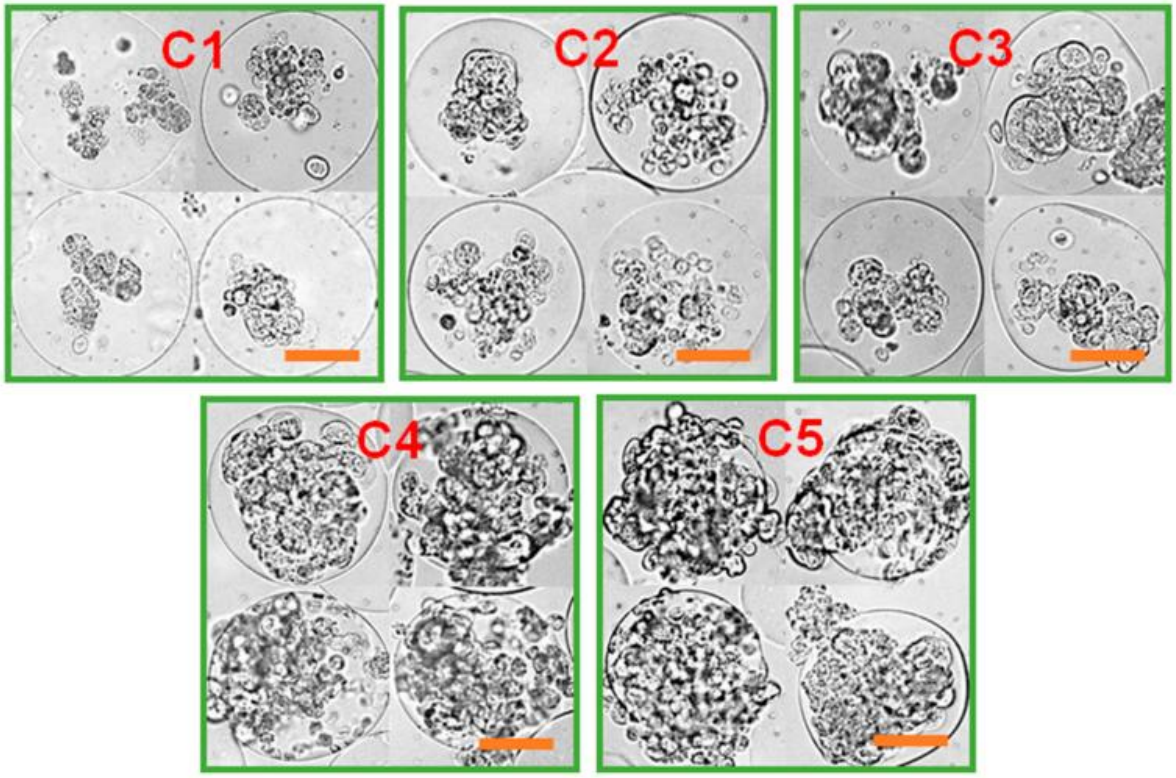

Figure 4.7 The tumor spheroid formation within microgels with varying mechanics after 14 days of cell culture (scale: 50 μm). A collection of smaller spheroids was developed within the microgel.

4.3.3. Effect of co-culture on tumor spheroid formation

It has been widely reported that the many tumor tissues contain a heterogeneous mixture of different cell types which help promote tumor growth and metastasis (Figure 4.8a).[45-47] For example, tumor-associated macrophages are found in most solid tumors, and involved with angiogenesis, immune suppression and tissue remodeling which help tumor progression.[45, 46] Fibroblasts are also similarly recruited by tumor cells and become activated as tumor-associated fibroblasts which similarly aid in tumor growth by promoting angiogenesis and tissue remodeling.[47, 48] Therefore, it was hypothesized that the presence of these supporting cells would help turn the MCF-7 cells into a larger and more mature (compact) tumor spheroid within a microgel. To investigate the role of supporting cells on the tumor spheroid formation within microgels, either macrophages or fibroblasts are co-cultured with MCF-7 cells within the microgels, and tumor spheroid formation was monitored.

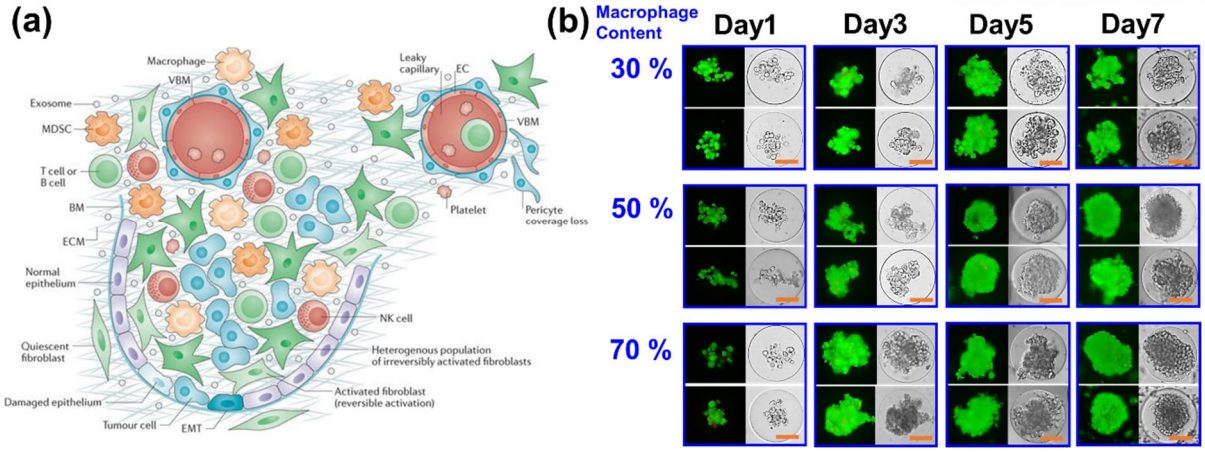

Figure 4.8 (a) Schematic illustration of tumor microenvironment, consisting of multiple types of cells. Reprinted with permission.[39] Copyright 2016 Springer Nature. (b) Optical (left) and fluorescent (right) microscopic images of microgels encapsulated with varying amounts of macrophages co-cultured with MCF-7 cells (scale bar: 50 um). The cells were fluorescently labeled to visualize live (green) and dead (red) cells.

First, the MCF-7 cells were co-cultured with macrophages (RAW264.7 cell line) in microgels at different macrophage contents (30 %, 50 % and 70 % macrophages) (Figure 4.8b). The MGel concentration of the microgel was fixed at C3. Regardless of the cell compositions, the viability of the cells was high and well maintained throughout the culture. In addition, the cells all underwent significant proliferation over the course of cell culture. At lower macrophage content (30 %), the cell proliferation and spheroid morphology was similar to those with only MCF-7 cell, in which several smaller tumor spheroids were formed within a microgel. When the amount of macrophages was increased (50 % and 70 %), the cells proliferated at faster pace and transformed into a large, single tumor spheroid with greater uniformity within a microgel. Remarkably, at the highest macrophage content (70 %), the tumor spheroids were more readily formed, only by day 3 of culture, further highlighting the role of macrophages in promoting tumor spheroid formation. In all conditions, there were filopodial projections the periphery of tumor spheroids, a hallmark of tumor invasion and metastatic potential.[49-51] This observation further gave evidence that the macrophages were actively involved with the tumor progression and spheroid formation. Next, MCF-7 cells were co-cultured with fibroblasts in the microgels at different ratios and the tumor spheroid formation was examined (Figure 4.9). At lower fibroblast content (30 %), the cell proliferation was not significantly different from that with only MCF-7 cells. In addition, the spheroids formed within a microgel were smaller than those co-cultured with macrophages. At higher fibroblast content (50 %), more well-defined and larger tumor spheroids were formed. However, the tumor spheroids were markedly smaller, and the proliferation was slower than those co-cultured with macrophages. Moreover, at the highest fibroblast content (70 %), the cell proliferation and tumor spheroid formation was reduced compared with those with lower fibroblast content. This result suggested that the effect of fibroblast on promoting tumor spheroid

formation may not have been as potent as the macrophages, and the initial reduced number of MCF-7 cells in the microgels with higher fibroblast content likely led to slower tumor progression. Taken together, the tumor spheroid formation was greatly aided by the presence of supporting cells, and this enhancement effect was varied depending on the cell type.

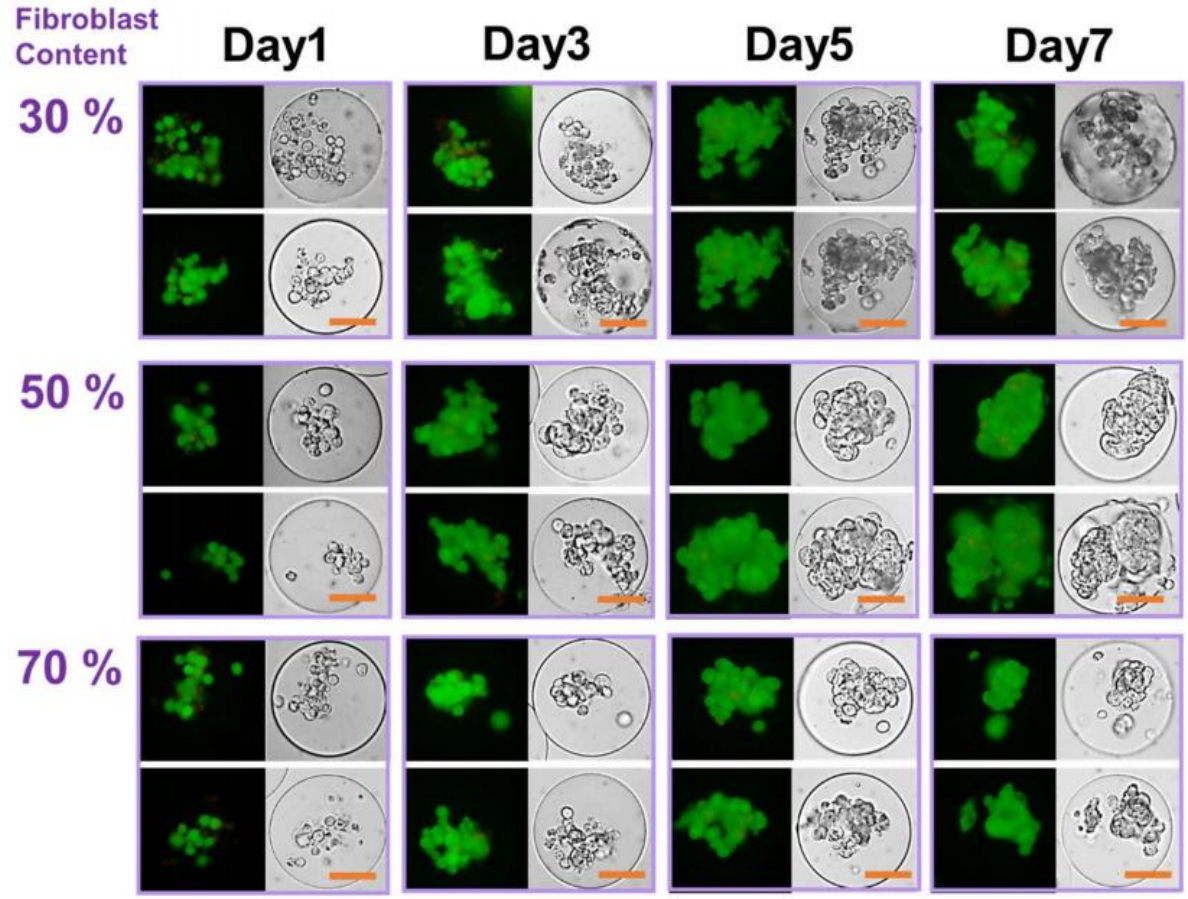

Figure 4.9 Optical (right) and fluorescent (left) microscopic images of microgels encapsulated with varying amounts of fibroblasts co-cultureed with MCF-7 cells (scale bar : 50 μm). The cells were fluorescently labeled to visualize live (green) and dead (red) cells.

4.3.4. Combined effect of co-culture and microgel mechanics on tumor spheroid formation

The results presented above clearly demonstrated that both the mechanical properties of the surrounding matrix and the presence of supporting cells play important roles in tumor spheroid formation within the microgels. Therefore, to elucidate their combined effects, the co-culture of MCF-7 cells with supporting cells within microgels with varying mechanical properties was performed, and the change in tumor spheroid formation was evaluated.

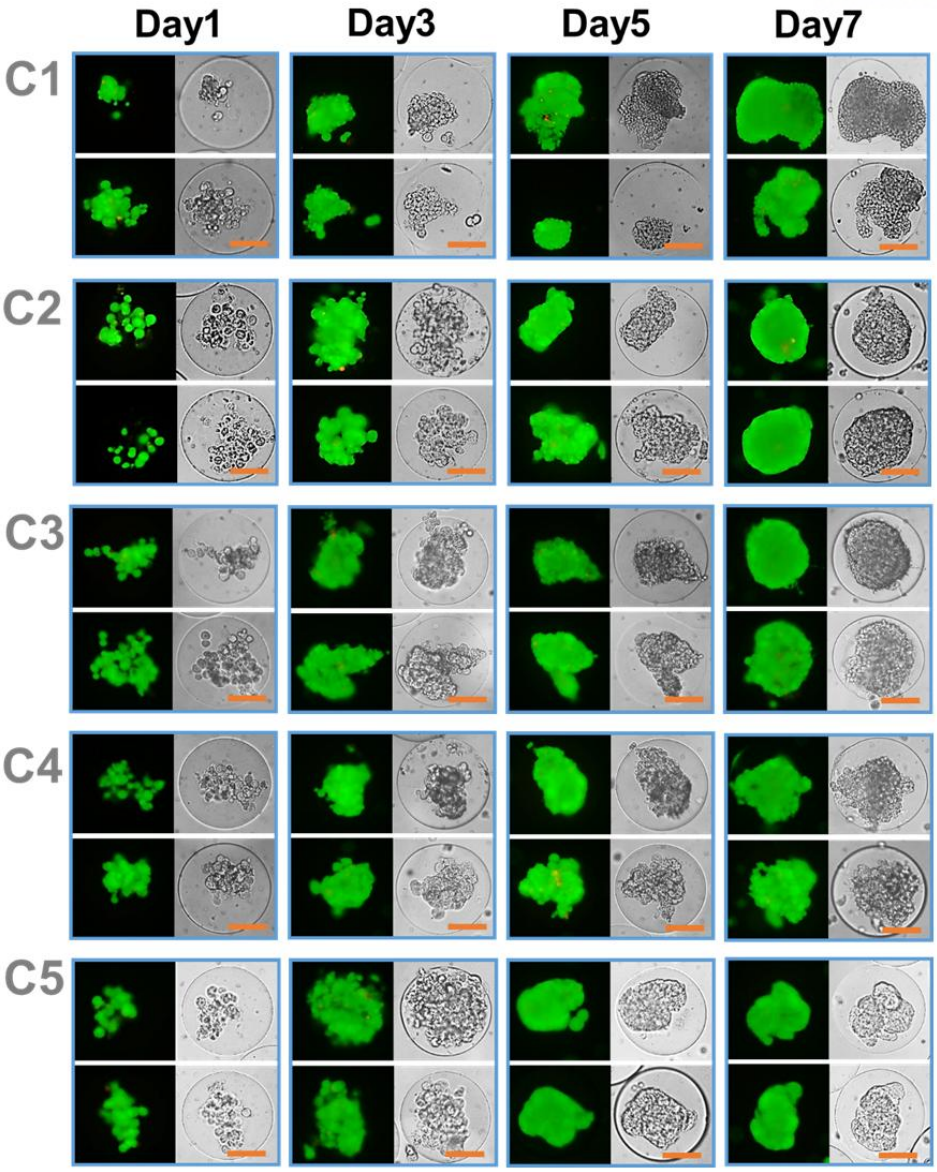

Figure 4.10 Optical (left) and fluorescent (right) microscopic images of MCF-7 cells and macrophages (5:5 ratio) co-encapsulated in the microgels with various mechanical stiffness (from C1 to C5) (scale bar: 50 um). The cells were fluorescently labeled to visualize live (green) and dead (red) cells.

The MCF-7 cells alone in microgels with varying mechanical stiffness demonstrated increase in proliferation with increasing mechanical stiffness, as demonstrated in Figure 4.5 and Figure 4.6. With the co-culture with macrophages, the trend in proliferation rate was similar, in which the cell proliferation increased with the mechanical stiffness of the microgels, but the cell proliferation was greatly enhanced at lower mechanical stiffness (C1 and C2) (Figure 4.10). In C1, the cells continue to proliferate and eventually broke out of the microgel, due to the structural weakness. But the cells were closer to aggregates that continue to spread without forming a compact, well-defined spherical form that defines tumor spheroids. However, beginning with C2, the larger tumor spheroid that covers the

entire microgel volume with the peripheral filopodial projection was shown. With increasing mechanical stiffness of the microgels, the tumor spheroids formed more quickly, such that larger tumor spheroids began to form only after day 3 of culture at C4 and C5. However, at the highest mechanical stiffness (C5), even though the tumor spheroid formation occurred earlier than other conditions, the size of spheroids were smaller, likely due to the increased mechanical strength of the microgels likely increased the metabolic stress and also acted as a physical barrier against forming larger spheroids.[11] Regardless, at a wide range of mechanical stiffness of the microgels, the cells all proliferated and formed a large, compact spheroid within the microgels rather than several smaller spheroids, further establishing the important role of co-cultured macrophage on the tumor spheroid formation. Immunocytochemical analysis of the characteristic biomarkers of MCF-7 cells and macrophages within the microgel was performed to further analyze their biochemical changes during the tumor spheroid formation (Figure 4.11). For MCF-7 cells, the expression of E-cadherin (E-cad), a calcium-dependent transmembrane protein responsible for cell-cell junction and communication and known biomarker for epithelial cells, was targeted and analyzed, since the expression behavior of E-cad in breast mammary cells is well known to be altered, often down-regulated, which leads to tumor progression via epithelial-to-mesenchymal transition.[52, 53] For macrophages, CD206 (an M2 phenotype marker) and CD80 (an M1 activation marker) were targeted to monitor the degree of macrophage activation during tumor spheroid formation. For tumor-associated macrophages, their M1 activation which is involved with inflammatory and tumor-suppressive activities is down-regulated and their anti-inflammatory and immune-suppressive potentials are up-regulated, helping tumor progression.[54] Regardless of the microgel stiffness, the E-cad expression per cell significantly decreased over time, which was in line with many previous studies demonstrating their down-regulation. This suggested that the MCF-7 cells within the microgels became highly tumorigenic during their proliferation and spheroid formation. In addition, the CD206 expression was generally much larger than that of CD80 from C1 to C3, which corroborate with previous reports showing tumor-associated macrophages acquire M2 phenotype to promote tumor progression. The concurrent decrease in CD80 expression over time and the generally diminished level of CD80 expression regardless of gel mechanics were also indicative of the M1 suppression, which coincided with the increased CD206 expression and further highlighted the tumor-promoting role of macrophages within tumor microenvironment. Interestingly, the relative expressions of CD206 and CD80 were dependent on the gel mechanics. For example, CD206 expression was much lower at higher gel stiffness (C4 and C5) as compared to lower stiffness (from C1 to C3). Also, the initial CD80 expression at day 1 was higher than CD206 expression at C4 and C5, although it decreased significantly afterwards and CD206 expression increased over time. This indicated that at higher gel stiffness, the macrophage favored M1 phenotype, but the presence of tumor cells influenced the Mφ polarization more towards tumor-promoting M2 phenotype. In addition, while the CD206 expression showed

increase over time at C4, it remained substantially low throughout the period at C5, possibly due to the limited permeability of microgels at higher stiffness suppressing Mφ polarization itself. These results highlight the gel mechanics as well as the presence of tumor cells combine to influence the macrophage activities. Taken together, these results evidently established the synergistic role of co-culture with macrophages and tunable mechanical properties of microgels on improving the tumor spheroid formation in microgels.

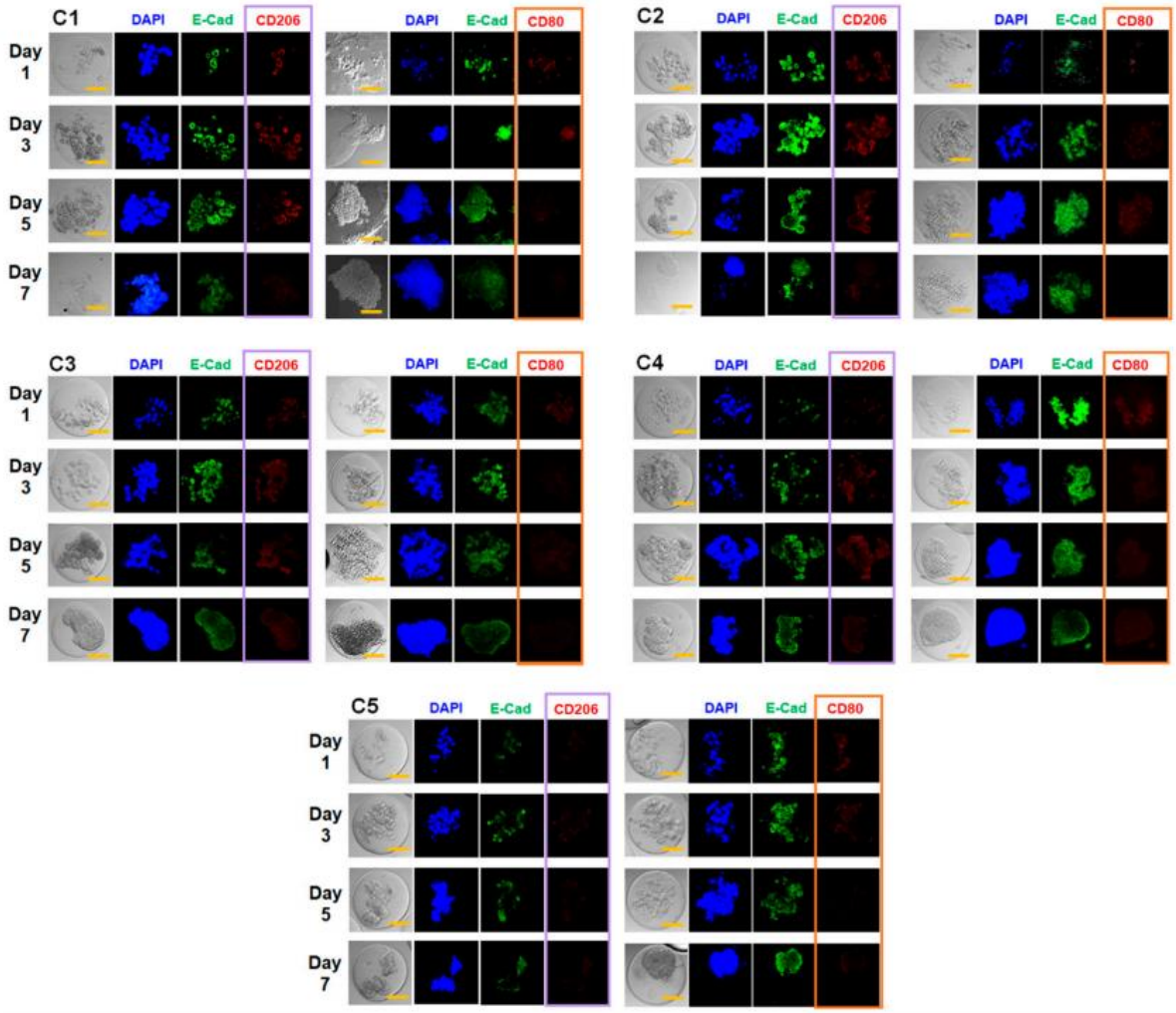

Figure 4.11 Immunocytochemical analysis of MCF-7 cells and macrophages encapsulated in microgels with varying mechanical properties (from C1 to C5). At various times up to 7 days, E-cadherin (E-cad), CD206 and CD80 were fluorescently labeled (scale bar: 50 μm). 4,6'-diamidino-2-phenylindole (DAPI) was used to label cell nuclei.

4.4. Conclusion

There is a growing interest in utilizing tumor spheroids as 3D sturctures as high-thoughput screening platforms for cancer therapeutic development, because tissue0based platforms provide more in-depth biological information than conventional target molecule-based platforms. In this study, tumor spheroids were developed within size-controlled microgels with tunable mechanical properties as a 3D cell culture platform via a flow-focusing microfluidic fabrication. The double flow-focusing channel geometry allowed biocompatible encapsulation of cells inside aqueous droplets of gel-forming precursor solution, which were then photo-crosslinked to form cell-laden microgels. With breast adenocarcinoma cells (MCF-7), the cells encapsulated inside the microgels showed high viability throughout the cell culture regardless of the mechanical properties of microgel. However, the rate of proliferation was highly dependent on their mechanical properties; the cells proliferated faster within microgels with higher mechanical stiffness. MCF-7 cells alone did not lead to a mature spheroid within a microgel, in which all the cells form a large, compact, and well-defined spherical cell cluster, but rather a collection of smaller cell aggregates were formed regardless of the microgel stiffness. However, when MCF-7 cells were co-cultured with supporting cells, macrophages or fibroblasts, well known to be involved with tumor progression, the cells within a microgel proliferated and turned into a mature spheroid regardless of the microgel stiffness, though their rate and extent of spheroid formation was dependent on the microgel stiffness. Taken together, the microfluidic fabrication of cell-laden microgels with varying mechanical properties coupled with providing supporting cells to control tumor spheroid formation is expected to be an efficient strategy of generating a wide array of heterogeneous 3D tumor spheroids as platform for drug screening applications as well as fundamental biological investigation.

4.5. Reference

1. Mehta, G.; Hsiao, A. Y.; Ingram, M.; Luker, G. D.; Takayama, S., Opportunities and challenges for use of tumor spheroids as models to test drug delivery and efficacy. *J. Control. Release* **2012,** *164* (2), 192-204.

2. Hirschhaeuser, F.; Menne, H.; Dittfeld, C.; West, J.; Mueller-Klieser, W.; Kunz-Schughart, L. A., Multicellular tumor spheroids: An underestimated tool is catching up again. *J. Biotechnol.* **2010,** *148* (1), 3-15.

3. Santini, M. T.; Rainaldi, G.; Indovina, P. L., Apoptosis, cell adhesion and the extracellular matrix in the three-dimensional growth of multicellular tumor spheroids. *Crit. Rev. Oncol. Hematol.* **2000,** *36* (2), 75-87.

4. Lin, R.-Z.; Chang, H.-Y., Recent advances in three-dimensional multicellular spheroid culture for biomedical research. *Biotechnol. J.* **2008,** *3* (9-10), 1172-1184.

5. Kelm, J. M.; Timmins, N. E.; Brown, C. J.; Fussenegger, M.; Nielsen, L. K., Method for generation of homogeneous multicellular tumor spheroids applicable to a wide variety of cell types. *Biotechnol. Bioeng.* **2003,** *83* (2), 173-180.

6. Gong, X.; Lin, C.; Cheng, J.; Su, J.; Zhao, H.; Liu, T.; Wen, X.; Zhao, P., Generation of multicellular tumor spheroids with microwell-based agarose scaffolds for drug testing. *PLOS One* **2015,** *10* (6), e0130348.

7. Wang, Y.; Wang, J., Mixed hydrogel bead-based tumor spheroid formation and anticancer drug testing. *Analyst* **2014,** *139* (10), 2449-2458.

8. Yu, L.; Chen, M. C. W.; Cheung, K. C., Droplet-based microfluidic system for multicellular tumor spheroid formation and anticancer drug testing. *Lab Chip* **2010,** *10* (18), 2424-2432.

9. Zhang, X.; Wang, W.; Yu, W.; Xie, Y.; Zhang, X.; Zhang, Y.; Ma, X., Development of an in vitro multicellular tumor spheroid model using microencapsulation and its application in anticancer drug screening and testing. *Biotechnol. Prog.* **2005,** *21* (4), 1289-1296.

10. Yu, L.; Grist, S. M.; Nasseri, S. S.; Cheng, E.; Hwang, Y.-C. E.; Ni, C.; Cheung, K. C., Core-shell hydrogel beads with extracellular matrix for tumor spheroid formation. *Biomicrofluidics* **2015,** *9* (2), 024118.

11. Cheng, G.; Tse, J.; Jain, R. K.; Munn, L. L., Micro-environmental mechanical stress controls tumor spheroid size and morphology by suppressing proliferation and inducing apoptosis in cancer cells. *PLOS One* **2009,** *4* (2), e4632.

12. Liang, Y.; Jeong, J.; DeVolder, R. J.; Cha, C.; Wang, F.; Tong, Y. W.; Kong, H., A cell-instructive hydrogel to regulate malignancy of 3D tumor spheroids with matrix rigidity. *Biomaterials* **2011,** *32* (35), 9308-9315.

13. Dolznig, H.; Rupp, C.; Puri, C.; Haslinger, C.; Schweifer, N.; Wieser, E.; Kerjaschki, D.; Garin-Chesa, P., Modeling colon adenocarcinomas in vitro: A 3d co-culture system induces cancer-relevant pathways upon tumor cell and stromal fibroblast interaction. *Am. J. Pathol.* **2011,** *179* (1), 487-501.

14. Hsiao, A. Y.; Tung, Y.-C.; Qu, X.; Patel, L. R.; Pienta, K. J.; Takayama, S., 384 hanging drop arrays give excellent Z-factors and allow versatile formation of co-culture spheroids. *Biotechnol. Bioeng.* **2012,** *109* (5), 1293-1304.

15. Kojima, T.; Moraes, C.; Cavnar, S. P.; Luker, G. D.; Takayama, S., Surface-templated hydrogel patterns prompt matrix-dependent migration of breast cancer cells towards chemokine-secreting cells. *Acta Biomater* **2015,** *13*, 68-77.

16. Kraning-Rush, C. M.; Reinhart-King, C. A., Controlling matrix stiffness and topography for the study of tumor cell migration. *Cell Adh Migr* **2012,** *6* (3), 274-9.

17. Schneider, T.; Kreutz, J.; Chiu, D. T., The potential impact of droplet microfluidics in biology. *Anal. Chem.* **2013,** *85* (7), 3476-3482.

18. Guo, M. T.; Rotem, A.; Heyman, J. A.; Weitz, D. A., Droplet microfluidics for high-throughput biological assays. *Lab Chip* **2012,** *12* (12), 2146-2155.

19. Teh, S.-Y.; Lin, R.; Hung, L.-H.; Lee, A. P., Droplet microfluidics. *Lab Chip* **2008,** *8* (2), 198-220.

20. Park, K.-S.; Kim, C.; Nam, J.-O.; Kang, S.-M.; Lee, C.-S., Synthesis and characterization of thermosensitive gelatin hydrogel microspheres in a microfluidic system. *Macromol. Res.* **2016,** *24* (6), 529–536.

21. Lee, D.; Lee, K.; Cha, C., Microfluidics-Assisted Fabrication of Microtissues with Tunable Physical Properties for Developing an In Vitro Multiplex Tissue Model. *Advanced Biosystems* **2018,** *2* (12).

22. Tumarkin, E.; Kumacheva, E., Microfluidic generation of microgels from synthetic and natural polymers. *Chem. Soc. Rev.* **2009,** *38* (8), 2161-2168.

23. Zhao, X.; Liu, S.; Yildirimer, L.; Zhao, H.; Ding, R.; Wang, H.; Cui, W.; Weitz, D., Injectable stem cell-laden photocrosslinkable microspheres fabricated using microfluidics for rapid generation of osteogenic tissue constructs. *Adv. Funct. Mater.* **2016,** *26* (17), 2809-2819.

24. Kumachev, A.; Greener, J.; Tumarkin, E.; Eiser, E.; Zandstra, P. W.; Kumacheva, E., High-throughput generation of hydrogel microbeads with varying elasticity for cell encapsulation. *Biomaterials* **2011,** *32* (6), 1477-1483.

25. Kim, S.; Oh, J.; Cha, C., Enhancing the biocompatibility of microfluidics-assisted fabrication of cell-laden microgels with channel geometry. *Colloids Surf B Biointerfaces* **2016,** *147*, 1-8.

26. Zhao, X.; Lang, Q.; Yildirimer, L.; Lin, Z. Y.; Cui, W.; Annabi, N.; Ng, K. W.; Dokmeci, M. R.; Ghaemmaghami, A. M.; Khademhosseini, A., Photocrosslinkable Gelatin Hydrogel for Epidermal Tissue Engineering. *Adv Healthc Mater* **2016,** *5* (1), 108-18.

27. Shu, X. Z.; Liu, Y.; Palumbo, F.; Prestwich, G. D., Disulfide-crosslinked hyaluronan-gelatin hydrogel films: a covalent mimic of the extracellular matrix for in vitro cell growth. *Biomaterials* **2003,** *24* (21), 3825-3834.

28. Cha, C.; Shin, S. R.; Gao, X.; Annabi, N.; Dokmeci, M. R.; Tang, X. S.; Khademhosseini, A., Controlling mechanical properties of cell-laden hydrogels by covalent incorporation of graphene oxide. *Small* **2014,** *10* (3), 514-23.

29. Nichol, J. W.; Koshy, S. T.; Bae, H.; Hwang, C. M.; Yamanlar, S.; Khademhosseini, A., Cell-laden microengineered gelatin methacrylate hydrogels. *Biomaterials* **2010,** *31* (21), 5536-44.

30. Byers, S. W.; Sommers, C. L.; Hoxter, B.; Mercurio, A. M.; Tozeren, A., Role of E-cadherin in the response of tumor cell aggregates to lymphatic, venous and arterial flow: measurement of cell-cell adhesion strength. *J. Cell Sci.* **1995,** *108* (5), 2053-2064.

31. Kenny, P. A.; Lee, G. Y.; Myers, C. A.; Neve, R. M.; Semeiks, J. R.; Spellman, P. T.; Lorenz, K.; Lee, E. H.; Barcellos-Hoff, M. H.; Petersen, O. W.; Gray, J. W.; Bissell, M. J., The morphologies of breast cancer cell lines in three-dimensional assays correlate with their profiles of gene expression. *Mol. Oncol.* **2007,** *1* (1), 84-96.

32. Amaral, J. B. d.; Rezende-Teixeira, P.; Freitas, V. M.; Machado-Santelli, G. M., MCF-7 cells as a three-dimensional model for the study of human breast cancer. *Tissue Eng. Part C Methods* **2011,** *17* (11), 1097-1107.

33. Yui, S.; Tomita, K.; Kudo, T.; Ando, S.; Yamazaki, M., Induction of multicellular 3-D spheroids of MCF-7 breast carcinoma cells by neutrophil-derived cathepsin G and elastase. *Cancer Sci.* **2005,** *96* (9), 560-570.

34. Kim, S.; Sim, S. B.; Lee, K.; Cha, C., Comprehensive examination of mechanical and diffusional effects on cell behavior using a decoupled 3D hydrogel system. *Macromol. Biosci.* **2017,** *17* (9), 1700162.

35. Kim, M.; Cha, C., Modulation of functional pendant chains within poly(ethylene glycol) hydrogels for refined control of protein release. *Sci. Rep.* **2018,** *8* (1), 4315.

36. Jang, J.; Hong, J.; Cha, C., Effects of precursor composition and mode of crosslinking on mechanical properties of graphene oxide reinforced composite hydrogels. *J. Mech. Behav. Biomed. Mater.* **2017,** *69*, 282-293.

37. Chu, C.; Schmidt, J. J.; Carnes, K.; Zhang, Z.; Kong, H. J.; Hofmann, M.-C., Three-dimensional synthetic niche components to control germ cell proliferation. *Tissue Eng. Part A* **2009,** *15* (2), 255-262.

38. Bracke, M. E.; Vyncke, B. M.; Bruyneel, E. A.; Vermeulen, S. J.; De Bruyne, G. K.; Van Larebeke, N. A.; Vleminckx, K.; Van Roy, F. M.; Mareel, M. M., Insulin-like growth factor I activates the invasion suppressor function of E-cadherin in MCF-7 human mammary carcinoma cells in vitro. *Brit. J. Cancer* **1993,** *68*, 282.

39. Palamakula, A.; Khan, M. A., Evaluation of cytotoxicity of oils used in coenzyme Q10 Self-Emulsifying Drug Delivery Systems (SEDDS). *Int. J. Pharm.* **2004,** *273* (1), 63-73.

40. Sridharan, R.; Cameron, A. R.; Kelly, D. J.; Kearney, C. J.; O'Brien, F. J., Biomaterial based modulation of macrophage polarization: a review and suggested design principles. *Materials Today* **2015,** *18* (6), 313-325.

41. Lee, D.; Cha, C., The combined effects of co-culture and substrate mechanics on 3d tumor spheroid formation within microgels prepared via flow-focusing microfluidic fabrication. *Pharmaceutics* **2018,** *10* (4), 229.

42. Noudeh, G. D.; Khazaeli, P.; Mirzaei, S.; Sharififar, F.; Nasrollahosaiani, S., Determination of the toxicity effect of sorbitan esters surfactants group on biological membrane. *J. Biol. Sci.* **2009,** *9*, 423-430.

43. Bilati, U.; Allémann, E.; Doelker, E., Sonication parameters for the preparation of biodegradable nanocapsulesof controlled size by the double emulsion method. *Pharm. Dev. Technol.* **2003,** *8* (1), 1-9.

44. Chen, l.; Zhang, Z.; Qiu, J.; Zhang, L.; Luo, X.; Jang, J., Chaperonin CCT-mediated AIB1 folding promotes the growth of ERα-positive breast cancer cells on hard substrates. *PLOS One* **2014,** *9* (5), e96085.

45. Weagel, E.; Smith, C.; Liu, P. G.; Robison, R.; O'Neill, K., Macrophage Polarization and Its Role in Cancer. *J. Clin. Cell. Immunol.* **2015,** *6* (4), 338.

46. Lewis, C. E.; Pollard, J. W., Distinct role of macrophages in different tumor microenvironments. *Cancer Res.* **2006,** *66* (2), 605-612.

47. Kalluri, R., The biology and function of fibroblasts in cancer. *Nat. Rev. Cancer* **2016,** *16*, 582.

48. Bhowmick, N. A.; Neilson, E. G.; Moses, H. L., Stromal fibroblasts in cancer initiation and progression. *Nature* **2004,** *432*, 332.

49. Machesky, L. M., Lamellipodia and filopodia in metastasis and invasion. *FEBS Lett.* **2008,** *582* (14), 2102-2111.

50. Jacquemet, G.; Hamidi, H.; Ivaska, J., Filopodia in cell adhesion, 3D migration and cancer cell invasion. *Curr. Opin. Cell Biol.* **2015,** *36*, 23-31.

51. Friedl, P.; Gilmour, D., Collective cell migration in morphogenesis, regeneration and cancer. *Nat. Rev. Mol. Cell Biol.* **2009,** *10*, 445.

52. Petrova, Y. I.; Schecterson, L.; Gumbiner, B. M., Roles for E-cadherin cell surface regulation in cancer. *Mol. Biol. Cell* **2016,** *27* (21), 3233-3244.

53. Andrews, J. L.; Kim, A. C.; Hens, J. R., The role and function of cadherins in the mammary gland. *Breast Cancer Res.* **2012,** *14* (1), 203.

54. Allavena, P.; Sica, A.; Solinas, G.; Porta, C.; Mantovani, A., The inflammatory micro-environment in tumor progression: The role of tumor-associated macrophages. *Crit. Rev. Oncol. Hematol.* **2008,** *66* (1), 1-9.

PART V

Cell subtype-dependent generation of breast tumor spheroids within 3D mechanically tunable microgels and their variable responses to chemotherapeutics

5.1. Introduction

Due to the limitations of conventional two-dimensional (2D) monolayer cell culture in recapitulating native tissues, there is a growing need for developing 3D cell culture models that allow for more complex and physiologically-relevant biological analyses. In order to create 3D tissue constructs, biocompatible and cell adhesive materials such as hydrogels and nanofibers are often used as scaffolds to culture various cells.[1-4] With recent advances in microfabrication technology, more precise manipulation of physical dimensions and complex architecture of the engineered tissues is possible.[5-7] However, it is still a significant challenge for scaffold-based tissues to closely mimic complex cell-cell and cell-ECM interactions and maintain their long-term viability with limited diffusivity. In addition, the technology for mass production of 3D tissue constructs for high-throughput screening applications are still in its infancy. For the cells that naturally form aggregates upon proliferation preferentially over substrate adhesion, such as embryonic stem cells and tumor cells, they are easily guided to form multicellular spheroids with a defined size, which are deemed more efficient, scalable, and readily-applicable 3D tissue constructs.[2, 8-12] Spheroids consisting of non-adherent cells can be easily developed in a liquid suspension culture (e.g. spinner flask), but it is not feasible to precisely control their size, uniformity and compositions. More uniform-sized spheroids with greater are generally developed by culturing cells within a confined space, such as hanging drop and microwell arrays.[13-15] More recently, microfabrication technology, such as 3D printing and microfluidics, is being adopted to generate spheroids with more uniformity and controlled cellular compositions.[16-18] Spheroids have a number of features that allow for closer resemblance to native 3D tissues, making them highly attractive models for biomedical investigation.[2, 8-12] First, spheroids consist of cells held together by extensive tight cell-cell junctions mimicking native tissue structures. Thus, biological phenomena could be analyzed in the context of complex tissue physiology. Second, the cells reside in varying levels of mass transportation along the depth of spheroids due to diffusional limitations, making it possible to analyze of the effect of soluble factors on tissues in spatiotemporal detail. Third, heterogeneous spheroids consisting of multiple cell types can be efficiently developed via co-culture for investigation of heterogeneous biological networks. Despite numerous studies on the development and applications of spheroids as 3D tissue models, there are a few deficiencies that need to be addressed before fully embraced with clinical

relevance. Most notably, the effect of microenvironmental factors on spheroids has not been extensively studied to date. Most spheroids are generated only with highly proliferative cells, devoid of ECM. Even though cells can express and deposit ECM to the surrounding, leading to cell-ECM interaction during spheroid generation, the role of ECM especially on the initial stages of cell behavior leading to spheroid formation is not well understood. In addition, it is challenging to maintain spheroids in a defined size for a long period of time. Spheroid generation mostly relies on the growth potential of a particular cell type, therefore they may continue to grow in size rather rapidly with the continued cell growth, making it difficult to develop smaller spheroids. This would critically complicate their analysis, as the concentric distribution of cells along the depth could vary with changing size. In this present study, a microfluidic flow-focusing device was adopted to create uniform-sized spherical micro-scale hydrogels ('microgels') encapsulated with spheroid-forming tumor cells, in order to investigate the effect of 3D microenvironment on the cellular behavior, leading to spheroid formation. [17,19-21] Owing to the ability of the microfluidic device to precisely control the size of microgels that act as a vessel confining the spheroids, the overall size of spheroids generated within the microgel could be controlled. Moreover, the mechanical properties of the microgels were controlled in a wide range to elucidate the role of biomechanical cues imparted by the microgels.[19, 20] Three different breast tumor cells, which are commonly categorized into three different subtypes based on malignancy, were used. [22, 23] The cell behavior and subsequent spheroid formation within the microgels showed highly characteristic dependence on microgel mechanics for each cell subtype, especially involving the formation of polyploidy.[24, 25] Finally, to further highlight the importance of microenvironmental consideration on spheroids, the variable efficacy of chemotherapeutic agents was evaluated against the tumor spheroids in the mechanically-tuned microgels.

5.2. Material and methods

5.2.1. Synthesis of methacrylic gelatin (MGel)

Gelatin (5 g, from porcine skin, Sigma Aldrich), 4-methoxyphenol(0.05g, Sigma Aldrich) and 4-dimethylaminopyridine (0.5 g, Sigma Aldrich) were dissolved in 50 mL dimethylsulfoxide at 50 °C. Glycidyl methacrylate (2 mL, Sigma Aldrich) was added dropwise and reacted for 48 hours at 50 °C under dry N_2.[26-28] The product was purified by dialysis against deionized (DI) water and dried by lyophilization. The methacrylation of gelatin was confirmed with ^{1}H-NMR spectroscopy (Figure 5.1)

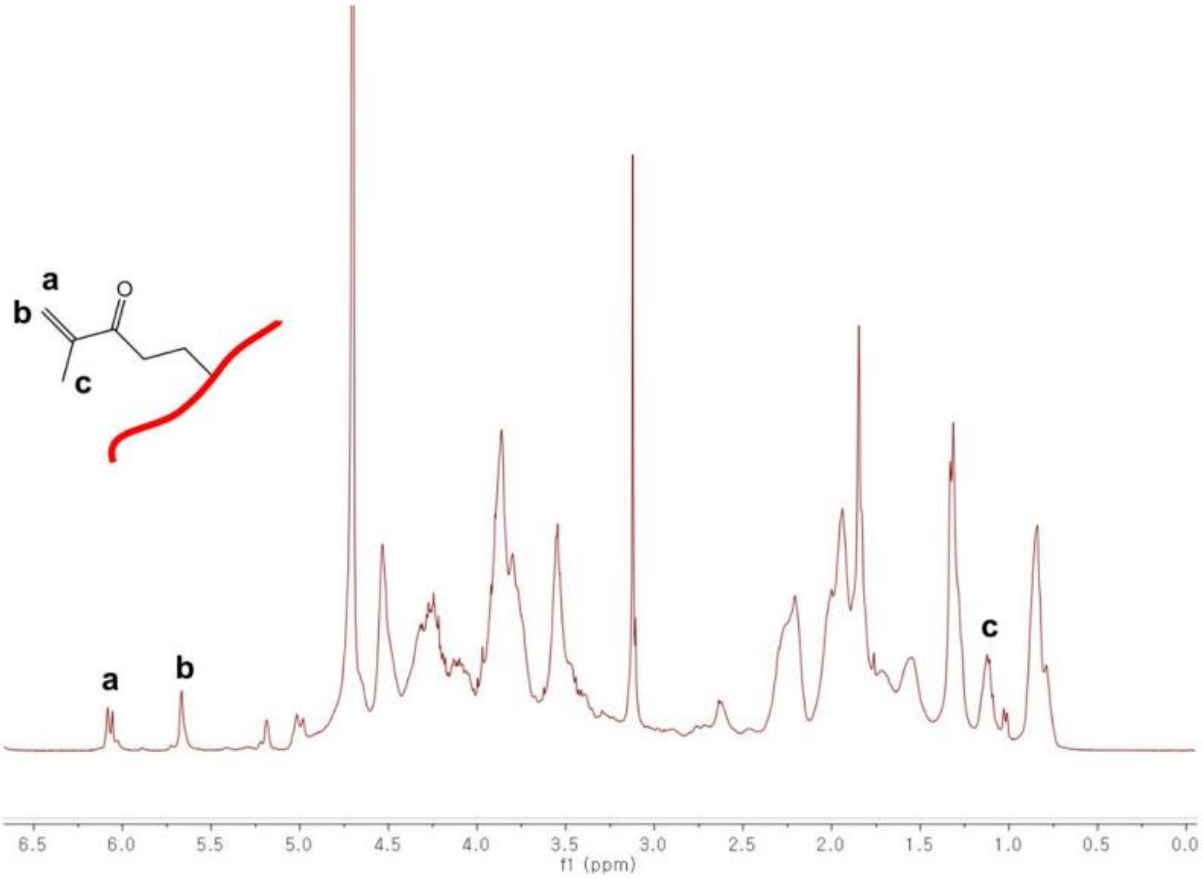

Figure 5.1. A representative 1H-NMR spectrum of methacrylic gelatin (MGel). Characteristic peaks corresponding to methacrylate are noted (a-c).

5.2.2. Microfluidic fabrication of cell-laden microgels

The flow-focusing microfluidic device was used to generate cell-laden droplets, which were photocrosslinked in situ to develop cell-laden microgels. The detailed device fabrication procedure is provided in detail elsewhere.[19, 20, 29] Aqueous solution phases 1 and 2 (*Aq*1 and *Aq*2) both consisted of MGel and 0.2 % (w/v) Irgacure 2959® in phosphate buffered saline (PBS, pH 7.4). The channel geometry allowed *Aq*1 to enter *Aq*2 prior to droplet generation, with *Aq*1 becoming the core of a droplet (Figure 5.2a). Oil phase (*O*) consisted of 20 % Span®80 (Sigma Aldrich) as a surfactant in mineral oil (Sigma Aldrich). In *Aq*1, breast tumor cells, MDA-MB-231, MCF-7, or SK-BR-3 (Korean Cell Line Bank, http://cellbank.snu.ac.kr), at 1×10^7 cells mL^{-1} were dispersed. The fluids were injected into the microfluidic device using electronic pumps (Legato®100, KD Scientific). Varying the ratio of flow rates of *Aq* and *O* resulted in the change in size of droplets (*Aq*1 and *Aq*2 were kept at the same flow rate). Here, the flow rates of *Aq* and *O* were 100 and 500 μL hr^{-1}, respectively, resulting in 100 μm average diameter. The droplets generated from the microfluidic device was immediately irradiated with

UV for 2 minutes (intensity: 200 mW, distance: 5 cm, emission filter: 250-450 nm, Model S1500, Omnicure®) to photocrosslink the droplets to develop cell-laden microgels. The microgels were washed extensively with PBS to remove residual oil, and incubated in the cell culture medium at 37 °C under 5 % atmospheric CO_2. The cell behavior and subsequent spheroid formation within microgels was monitored visually with inverted optical microscope at various times (XDS-3FL, Optika). The cell culture medium was RPMI1640 supplemented with 10 % heat inactivated fetal bovine serum (FBS), 2 mM L-glutamine, 25 mM HEPES and 25 mM $NaHCO_3$ (all purchased from Thermo Fisher) for all cell types.

5.2.3. In vitro evaluation of spheroids in microgels

5.2.3.1. Viability and proliferation

The viability of the cells encapsulated in the microgels were measured using LIVE/DEAD Cell Viability Assay kit (Thermo Fisher), following the manufacturer's instructions. Briefly, the cell-laden microgels were treated with calcein-AM and ethidium homodimer-1 to fluorescently label live (green) and dead (red) cells, and were visualized with fluorescence microscopy (XDS-3FL, Optika). The viability was reported as the percentage of live cells from the total number of cells.

The proliferation rate (k_P) of encapsulated cells was determined by counting the number of live cells at various time points up to 7 days, and the plot of the normalized number of viable cells (N_t/N_0) vs. time (t) was fitted with the following power-law equation,

$$\frac{N_t}{N_0} = 2^{k_P \cdot t} \qquad (1)$$

N_t was the number of viable cells at time, t, and N_0 was the initial number of viable cells at t=0. [19, 20, 27]

5.2.3.2. Fluorescent actin and nuclei visualization

To visualize the actin structure and nuclei of MDA-MB-231 cells during spheroid formation, the cells were labeled with fluorescein-labeled phalloidin (FITC-phalloidin, Thermo Fisher) and 4',6-diamidino-2-phenylindole (DAPI, Sigma Aldrich), respectively.[28, 30] Briefly, the cell-laden microgel sample taken at each time was first fixed in 4 % formaldehyde and washed with PBS. After treating with permeabilizing solution (0.5 % Triton™ X-100) for 5 minutes, followed by blocking solution (1 % bovine serum albumin and 0.1 % sodium azide) for 30 minutes, the sample was treated with FITC-phalloidin working solution (5 U mL^{-1}) for 30 minutes. After washing with PBS, the sample was then treated with DAPI (300 nM) for 5 minutes. The labeled sample was visualized using a confocal fluorescence microscope (FV1000, Olympus).

5.2.4. Chemotherapeutic screening

After 15 days of culture to develop large spheroids within microgels, they were treated with varying concentrations of chemotherapeutic agents, cisplatin and paclitaxel (Sigma Aldrich), up to 3 days. The viability of spheroids was measured using LIVE/DEAD Cell Viability Assay kit (Thermo Fisher), as stated above.

5.3. Results and Discussion

5.3.1. Fabrication of breast tumor cell-laden microgels

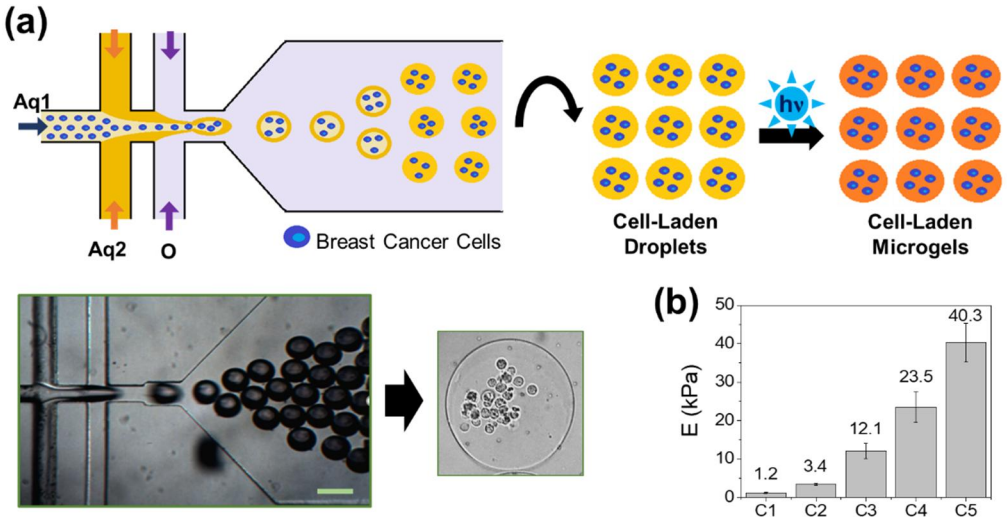

Figure 5.2. (a) A flow-focusing microfluidic fabrication of breast tumor cell-laden microgels. (b) Elastic moduli (*E*) of MGel hydrogels at various concentrations. (scale bar: 200 μm)

A flow-focusing microfluidic device was used to generate uniform-sized aqueous droplets dispersed with breast tumor cells. This particular microfluidic channel geometry allowed the formation of "core-shell" type droplets, in which one aqueous phase (*Aq*1) entered the other aqueous phase (*Aq*2) prior to droplet generation by the shear stress of oil phase (*O*) (Figure 5.2). By including the cells in *Aq*1, the cells were directed to the core region of droplets and minimized their contact with cytotoxic *O* during droplet generation.[19, 20, 29] *Aq*1 and *Aq*2 consisted of gel-forming polymer, methacrylic gelatin (MGel), along with a photo-initiator. Methacrylate groups were conjugated to gelatin backbone to MGel, which has been widely used as scaffolds for cell culture applications, as they retain cell-adhesive motifs (e.g. RGD peptide) as well as photocrosslinkability.[31-33] The MGel concentration in *Aq*2 was kept slightly higher than that of *Aq*1, so the polymer diffusion occurs inward and minimize the cells in the core region from moving outward, further prevent the cells from contacting the surrounding *O*.[19, 20, 29] The subsequent photo-crosslinking to generate cell-laden microgels indeed showed the cells mostly remained within the core region. Furthermore, the initial delineation between core and shell regions

eventually disappeared, demonstrating they became homogenously merged via diffusion. To assess the effect of microenvironmental mechanics on the cell behavior and spheroid formation, the rigidity of the microgels was controlled by varying the MGel concentration. Five different pairs of concentrations were explored as *Aq*1 and *Aq*2; 5 % and 8 %, 7 % and 10 %, 9 % and 12 %, 11 % and 14 %, and 13 and 16 %, which are denoted from 'C1' to 'C5'. The overall MGel concentration after the merging of core and shell regions were estimated to be 6.2 % (C1), 8.2 % (C2), 10.2 % (C3), 12.2 % (C4) and 14.2 % (C5), determined based on the relative amounts of core and shell regions.[19, 20] Their elastic moduli, determined from uniaxial compression of bulk hydrogels fabricated separately, ranged from 1.2 to 40.3 kPa (Figure 5.2b), while their swelling ratios showed corresponding decrease from 30 to 12.5 (Figure 5.3).

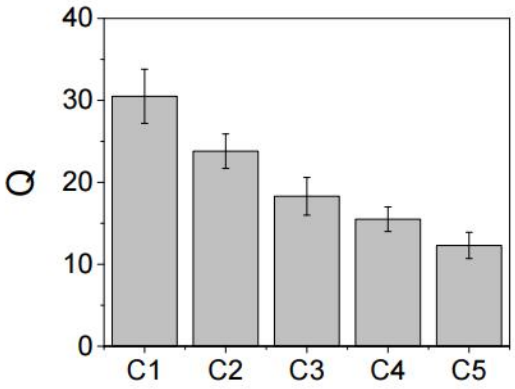

Figure 5.3. Swelling ratios (Q) of MGel hydrogels with varying rigidity **(C1-C5)**.

It was hypothesized that the effect of microgel mechanics on cell behavior and spheroid formation would vary widely based on cellular subtypes. Therefore, cells from three different breast tumor cell lines were explored; MDA-MB-231, SK-BR-3 and MCF-7. They are commonly categorized as "triple negative B", "HER2+" and "luminal A", respectively, in decreasing order of aggressiveness.[22, 23]

5.3.1.1. MDA-MB-231

MDA-MB-231 cells are classified as "triple negative B" (or "basal B"), identified by the lack of three characteristic markers, estrogen receptor (ER), progesterone receptor (PR) and human epithelial receptor 2 (HER2), and generally associated with a more aggressive form of tumor, accompanied by several genetic alterations.[22, 23, 34] The cells encapsulated in the microgels with varying rigidity maintained high viability (Figure 5.4a and 5.4b). Interestingly, the cell proliferation increased substantially with microgel rigidity, with increased number of smaller spheroids within the microgels, suggesting the increased mechanotransduction signals imparted by higher microgel rigidity promoted the cellular proliferation (Figure 5.4c and 5.4d). This is especially striking, considering the lower permeability of microgels at higher rigidity, which could limit media diffusion. At the lowest rigidity of

C1, the number of viable cells significantly decreased over time, almost devoid of cells in the microgels by day 9. At C2, there was a small increase in the number of cells up to day 5, but did not show further growth afterwards. It is widely known that many types of cells are heavily governed by mechanotransduction mediated by surrounding matrices transmitting biophysical cues.[35-37] In particular, increased mechanical properties of the matrices have been shown to enhance cell survival and proliferation. These results also highlighted the importance of providing sufficient mechanical stimuli for cell survival for sustaining cellular activities as well as promoting the proliferation of MDA-MB-231 cells in 3D microenvironment.

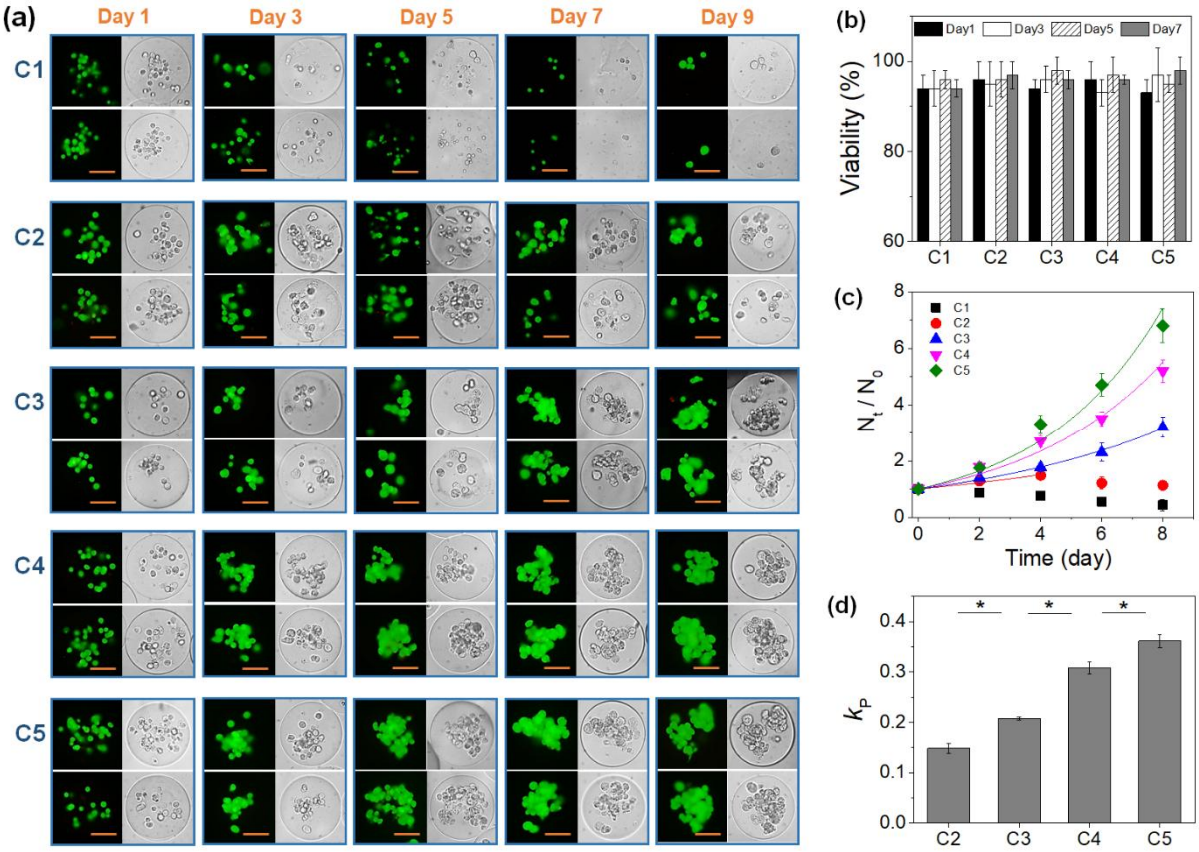

Figure 5.4. (a) Optical (right) and fluorescent (left) microscopic images of MDA-MB-231 cells in microgels with varying rigidity (C1-C5) (scale bar: 50 μm). (b) The cell viability was quantified as the percentage of live cells obtained from (a). (c) The plot of normalized number of live cells (N_t/N_0) vs. time was fitted with a power-law model to obtain the (d) proliferation rate (k_P) (*p<0.05).

The cellular morphology within the microgels was assessed in detail by fluorescently labeling cytoplasmic actin and nuclei. At C2, several cells were shown to spread and display lamellipodial projections, suggesting the increase in migratory potential (Figure 5.6a and 5.5a). In addition, the cells merged to form larger cells with multiple nuclei at earlier times at grew in size, while still demonstrating lamellipodial projections. This morphological changes suggested that the cells formed polyploid giant

cancer cells (PGCC), a hallmark of aggressive tumor progression.[24, 25] PGCC with lamellipodia were also shown at C3, though they were generally larger with lesser extent of lamellipodia (Figure 5.6b and 5.5b). With increased rigidity, the cell spreading became more limited but increased proliferation led to larger PGCC. At C4, the lamellipodia was not shown, and the size of PGCC was much smaller (Figure 5.6c and 5.5c). But the number of smaller PGCC increased more significantly in the same time. Due to the limited available space within microgels at higher rigidity, the cells likely could not spread effectively, and PGCC could not grow in size. But further increase in proliferative capacity of cells produced higher number of smaller PGCC.

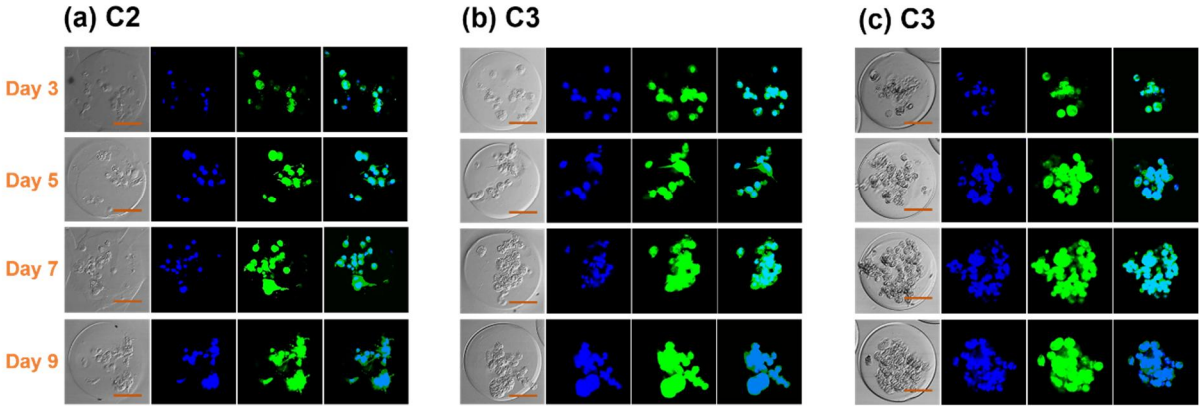

Figure 5.5. Fluorescent microscopic visualization of actin (green) and nuclei (blue) of MDA-MB-231 cells in microgels with varying rigidity over 9 days of culture; (a) C2, (b) C3, and (c) C4 (scale bar: 50 μm).

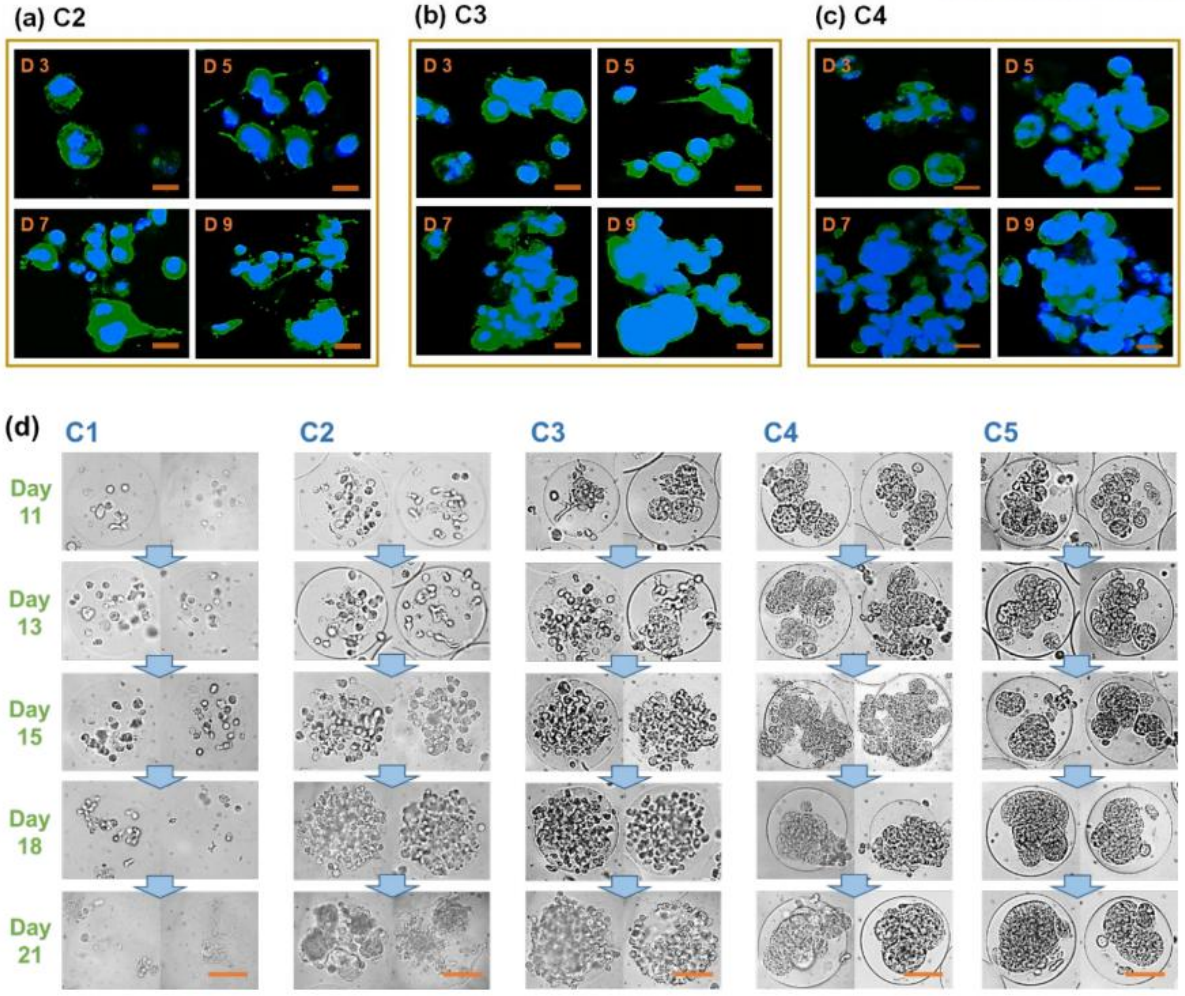

Figure 5.6. Fluorescent microscopic visualization of actin (green) and nuclei (blue) of MDA-MB-231 cells in microgels with varying rigidity over 9 days of culture; (a) C2, (b) C3, and (c) C4 (scale bar: 50 μm). (d) Microscopic images of MDA-MB-231 cells in microgels with varying rigidity (C1-C5) taken during a long-term culture for 21 days (scale bar: 50 μm).

As a control, the MDA-MB-231 cells were separately cultured on the surface of MGel hydrogels to identify the difference between 2D and 3D cultures (Figure 5.7).

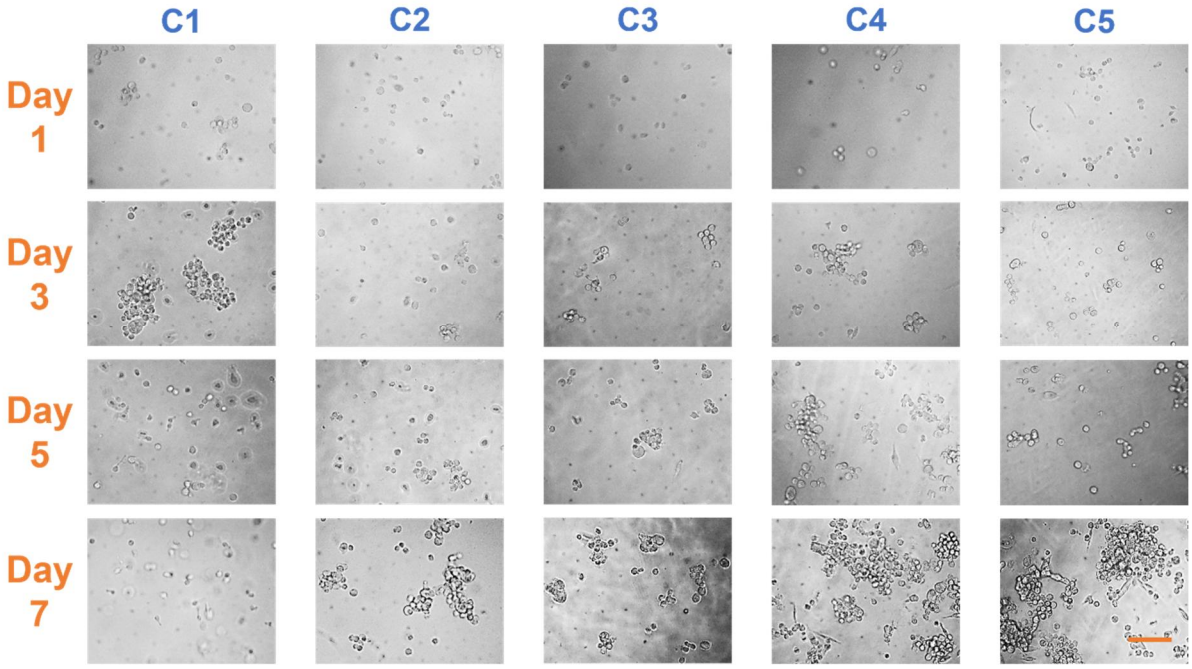

Figure 5.7. Microscopic images of MDA-MB-231 cells cultured on MGel hydrogels with varying rigidity (scale bar: 200 um).

Similar to those in microgels, the cell proliferation increased with hydrogel rigidity. Since there was no spatial restriction, the cells were highly migratory. However, PGCC were not shown and cell aggregation was much smaller. This result indicated that under restrictive environment with higher hypoxia of 3D microgels may have promoted PGCC formation and merging of cells, in line with similar findings that have been previously reported. [25, 38]

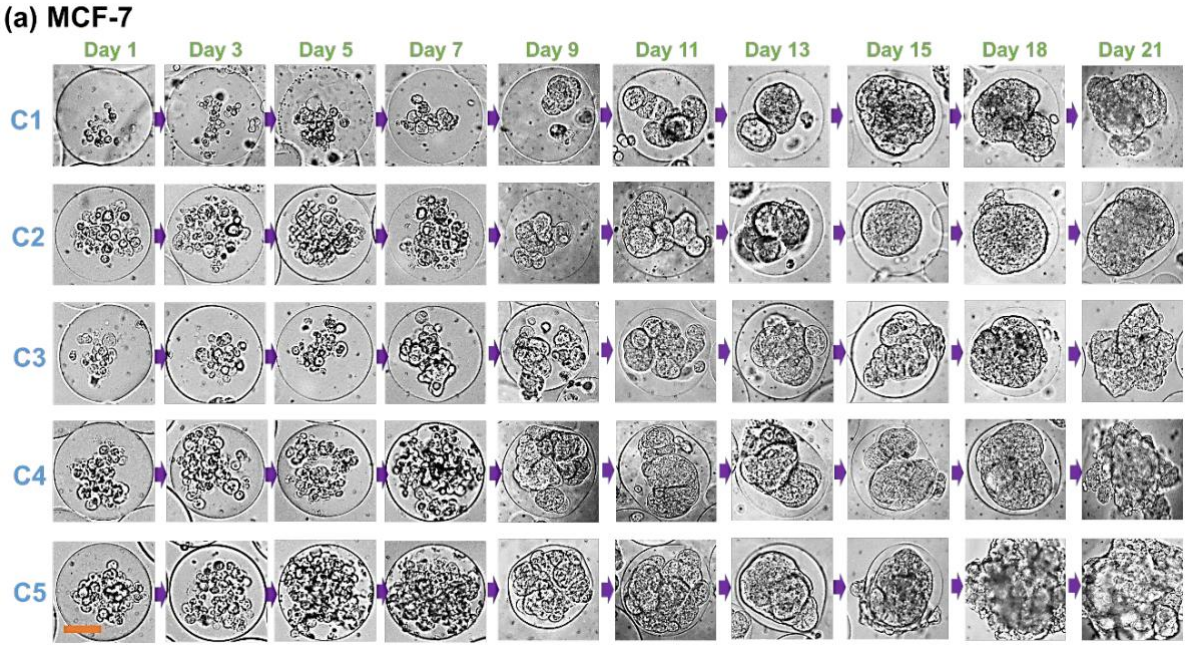

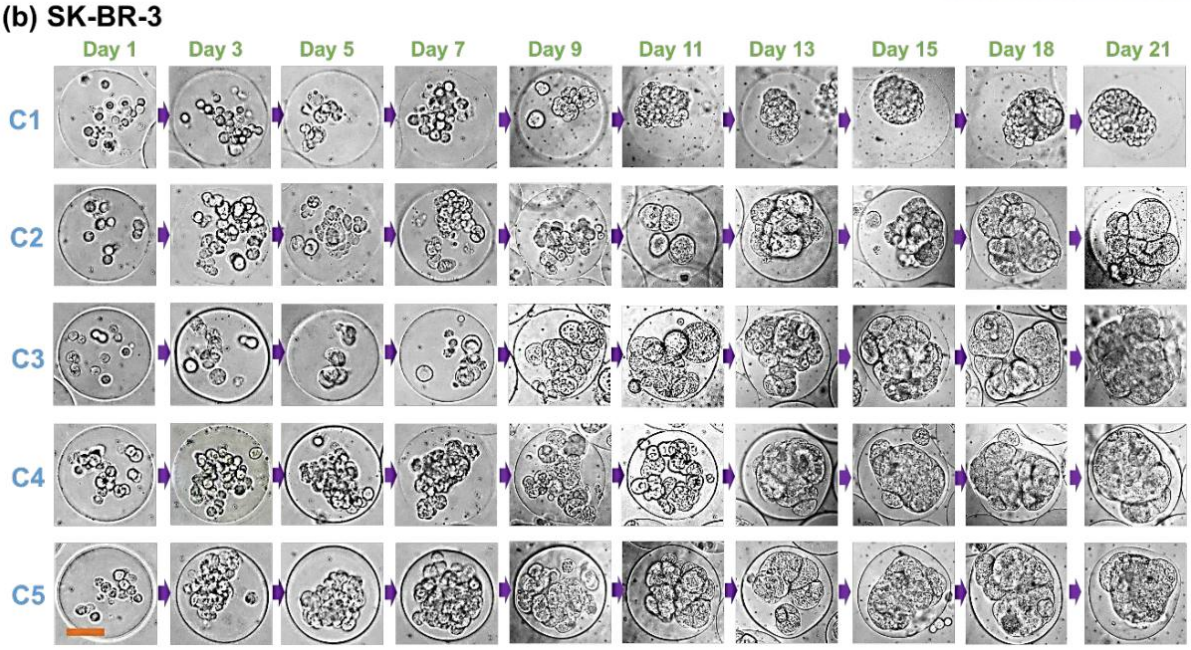

Figure 5.8. Microscopic images of (a) MCF-7 and (b) SK-BR-3 cells in microgels with varying rigidity (C1-C5) taken at various times up to 21 days (scale bar: 50 μm).

The cell-laden microgels were further cultured up to 21 days. At higher microgel rigidity of C4 and C5, the smaller cell aggregates merged and formed larger and more cohesive spheroids, occupying most of the microgels (Figure 5.6d). This was especially noteworthy given that MDA-MB-231 cells have been known to be highly aggressive and lack tight cell-cell adhesion, and as a result generally do not lead to larger cohesive spheroid formation, unless providing external stimuli such as hypoxia. It can be inferred that increased rigidity, coupled with restrictive environment elevating hypoxia, may have facilitated the spheroid formation. At intermediate C3, the number of smaller cell aggregates increased substantially and covered most of the microgel, but did not merge to form larger spheroids. Similar growth pattern was observed at C2, though at lower rate. Interestingly, the cell spreading with lamellipodia could still be shown at day 13, before significant proliferation occurred afterwards. At C1, the cell growth continued to decline, and the cells were mostly gone by 21 days. The microgel structure deteriorated over time due to low crosslinking density, which likely caused the cell death. Taken together, these results further reinforced the importance of microenvironmental mechanics, imparted by the microgels, on promoting tumor spheroid formation in 3D. It should also be noted that while the number of cells and size of spheroids grew exponentially, the overall size of microgels did not change, which indicated the cells within the microgels could significantly remodel the surrounding polymeric matrices to accommodate increased number of cells.

5.3.1.2. MCF-7 and SK-BR-3

In addition to MDA-MB-231, two other commonly used breast tumor cells, MCF-7 and SK-BR-3,

were encapsulated in the microgels and their activities were evaluated in the same manner. MCF-7 is classified as “luminal A” having ER positivity and HER2 negativity, with variable PR expression.[22, 23] Luminal A cells are less aggressive (i.e. low migration, tight cell-cell junctions) than other subtypes. SK-BR-3, on the other hand, is classified as “HER2” having HER2 positivity and ER negativity. HER2 cells possess intermediate aggressiveness between luminal A and basal B. Initial stage of cell culture, up to 7 days, showed the proliferation of MCF-7 cells increased with microgel rigidity, as similarly shown for MDA-MB-231 cells (Figure 5.8a). Unlike MDA-MB-231, MCF-7 cells did not show prominent lamellipodia, indicating the lesser degree of migratory potential, but cell aggregation and PGCC formation were more prominent at all microgel rigidity. Especially at higher rigidity of C4 and C5, a collection of smaller spheroids was formed. Similar results were observed for SK-BR-3 cells, though the proliferation rate was slightly lower. The size of PGCC for both MCF-7 and SK-BR-3 was smaller than that of MDA-MB-231 cells (Figure 5.8b). Interestingly, further culture up to 21 days demonstrated significant spheroid formation within microgels at all microgel rigidity for both MCF-7 and SK-BR-3 cells, unlike MDA-MB-231 cells which only became larger and cohesive spheroids at higher microgel rigidity. For MCF-7, spheroids significantly increased in size and fused with one another to form large, singular cohesive spheroids occupying most of the microgels, rather than creating new, smaller spheroids, even at low microgel rigidity of C1 and C2 (Figure 5.8a). The size of spheroids became larger with microgel rigidity, and they eventually outgrew the size of the microgels, migrating out and invading the surrounding. Similar dependence of spheroid growth on the microgel rigidity was observed for SK-BR-3 cells (Figure 5.8b). The size of SK-BR-3 spheroids was generally smaller than those of MCF-7, and singular cohesive spheroids were formed in microgels with higher rigidity. At lower rigidity, although the spheroids grew in size substantially, they did not lead to a singular cohesive spheroid in a microgel, especially at C1 in which only the collection of very small spheroids was shown.

MCF-7 and SK-BR-3 cells were also cultured on MGel hydrogel surface as a control (Figure 5.9 and 6.10). Similar to MDA-MB-231, the proliferation rates of both MCF-7 and SK-BR-3 cells increased with hydrogel rigidity. SK-BR-3 cells increased in numbers without forming larger aggregates or spheroids, only showing “grape-like” clusters, demonstrating their lack of tight cell-cell junctions. On the other hand, MCF-7 cells naturally formed spheroids during proliferation, more so at higher rigidity. These results highlight the greater tendency of MCF-7 cells to develop spheroids than other cell types, and it was similarly displayed in 3D microgels as well. It is also noteworthy that even though both MDA-MB-231 and SK-BR-3 cells did not form spheroids in 2D culture, they did form spheroids within microgels with varying degrees, which highlight the critical role of 3D microenvironment. The mechanisms of cell behavior and spheroid generation of three cell types within microgels are comprehensively illustrated in Figure 5.11.

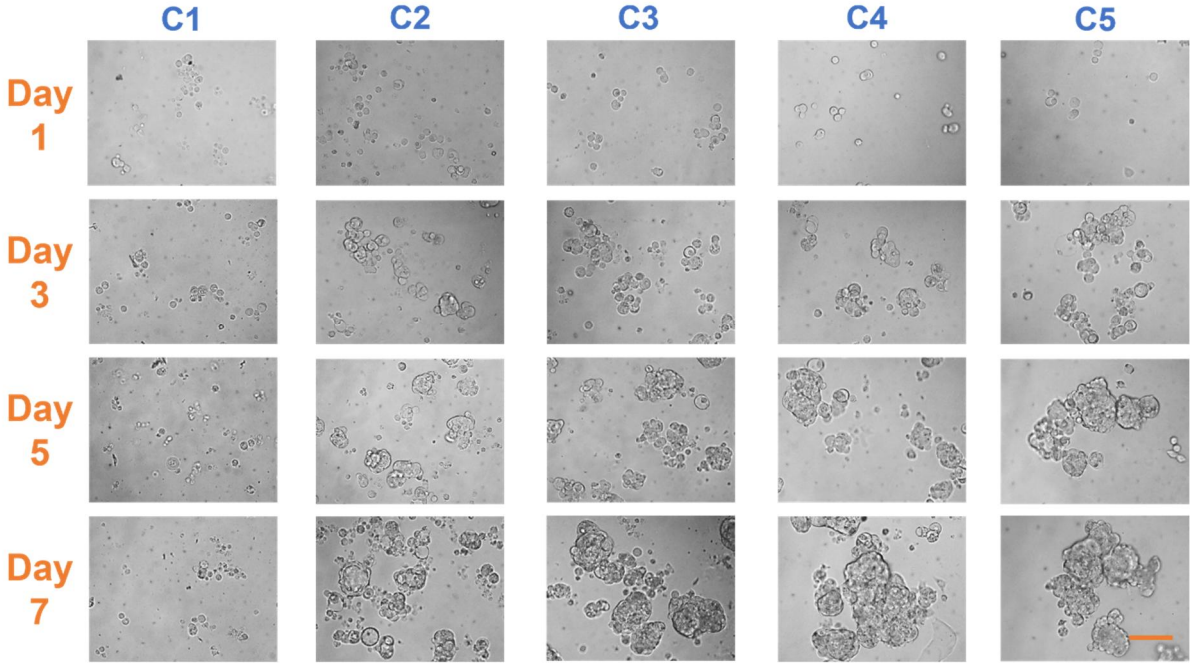

Figure 5.9. Microscopic images of MCF-7 cells cultured on MGel hydrogels with varying rigidity (scale bar: 200 um).

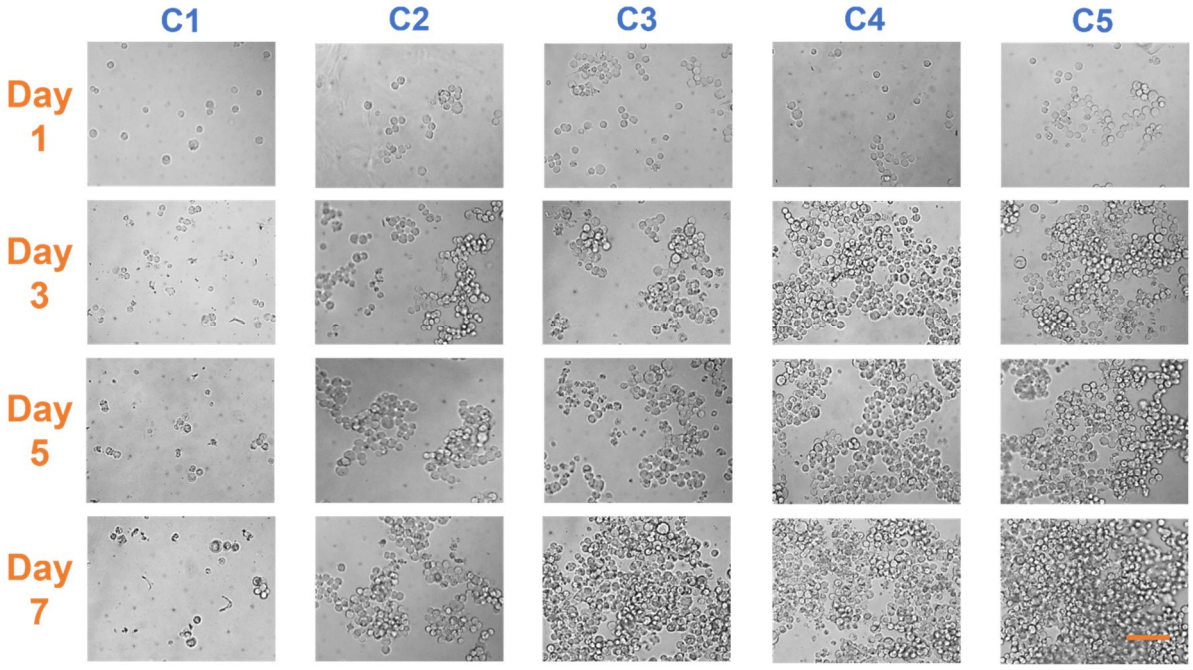

Figure 5.10. Microscopic images of MCF-7 cells cultured on MGel hydrogels with varying rigidity (scale bar: 200 um).

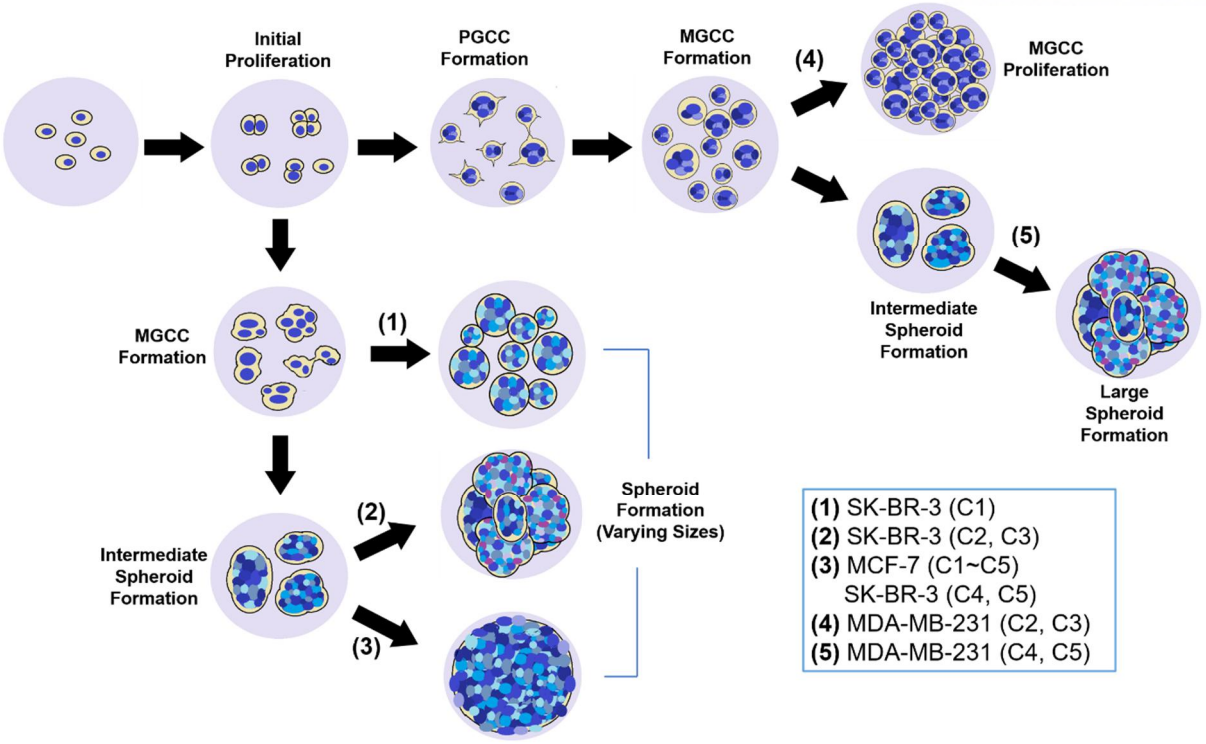

Figure 5.11. Schematic illustration of spheroid formation mechanisms of MDA-MB-231, MCF-7 and SK-BR-3 cells in microgels with varying rigidity (C1-C5).

5.3.2. Chemotherapeutic response of spheroids in microgels

Spheroids have been long considered a valuable tissue model for various biological investigations with implications in 3D tissue physiology; cell-cell interaction and concentric distribution.[39-41] More recently in pharmaceutical industry, there has been a growing emphasis on developing more physiologically-relevant and patient-specific testing platforms for drug discovery. Therefore, miniaturized tissue constructs are increasingly investigated as a drug screening platform, with the ultimate goal of replacing traditional 2D monolayer cell cultures. In this regard, spheroids are considered especially attractive for efficient fabrication. However, conventional spheroids are generally created by the proliferative capacity of the constituting cells, without considering the effect of microenvironmental factors, limiting more accurate and expansive representation of native tissues. Therefore, the spheroids generated within mechanically-tunable microgels developed in this study would provide more in-depth context of mechanical microenvironment in determining the influence of chemotherapeutics. To account for the effect of microgel mechanics on the chemotherapeutic efficacy against breast tumor spheroids, varying concentrations of widely used drugs, paclitaxel and cisplatin, were applied to the spheroids. The ranges of concentrations for paclitaxel and cisplatin were 1-100 nM and 30-500 μM, respectively, which was first determined by applying them to 2D monolayer cultures (Figure 5.12).

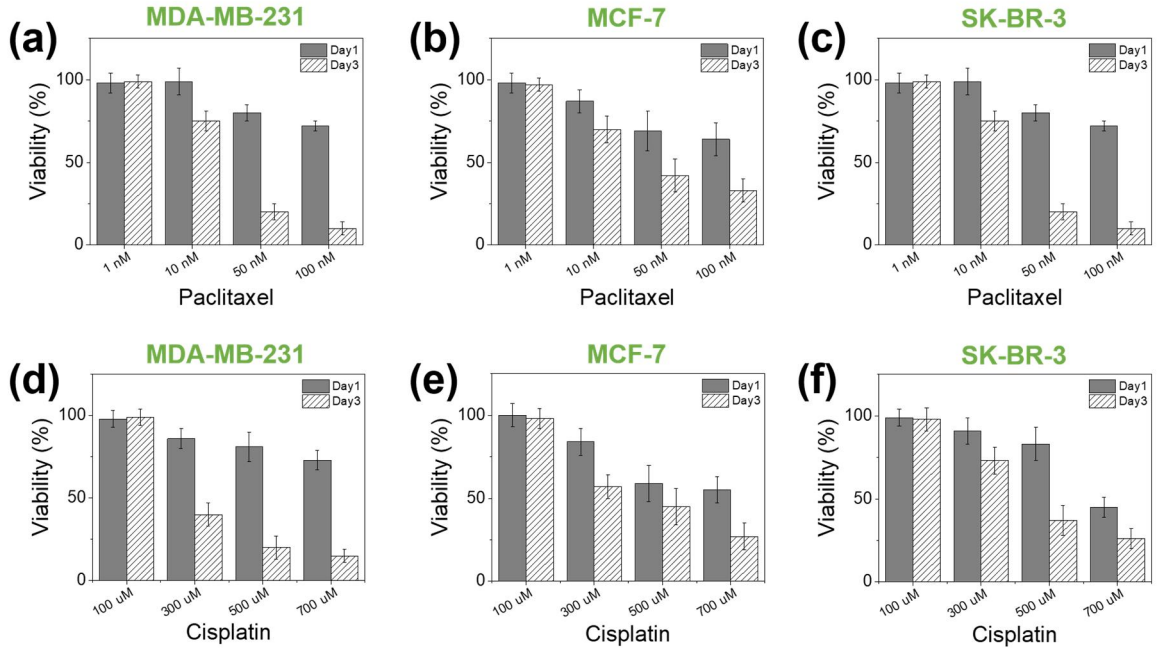

Figure 5.12. Cytotoxicity of varying concentrations of chemotherapeutic agents, paclitaxel and cisplatin, against 2D monolayer cultures of (a, d) MDA-MB-231, (b, e) MCF-7, and (c, f) SK-BR-3 cells, measured at day 1 and 3 of exposure.

In these ranges, concentration-dependent cytotoxicity was demonstrated when treated up to 3 days, and interestingly was not significantly affected by the cell type. The spheroids developed using the same cell types after 15 days of culture, which had mostly fully grown to cover the inner space of microgels (due to the insufficient growth, C1 was not tested).

5.3.2.1. MDA-MB-231

The cytotoxicity of paclitaxel or cisplatin against MDA-MB-231 cells within microgels with varying rigidity (C2-C5) was assessed 1 day or 3 days after treatment by measuring their cell viability.

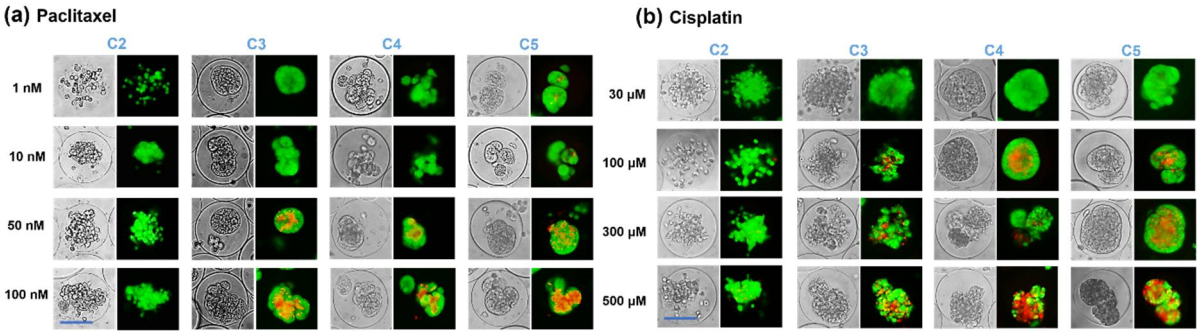

Figure 5.13. Fluorescent imaging of live (green) and dead (red) MDA-MB-231 cells of spheroids in microgels with varying rigidity (C2-C5) taken after 1 day of exposure to different concentrations of (a) paclitaxel and (b) cisplatin (scale bar: 50 μm).

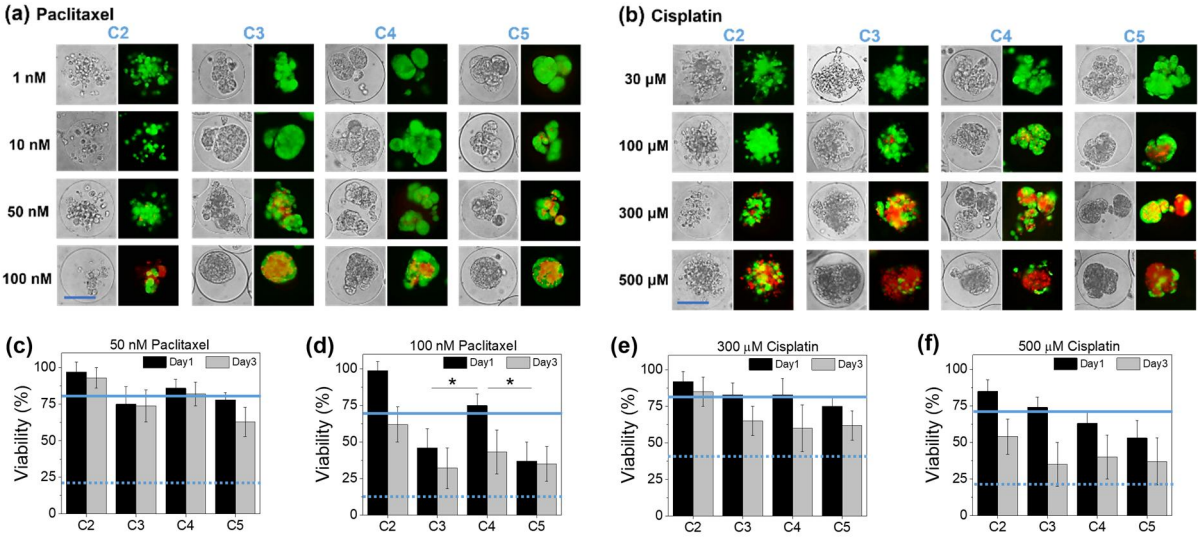

Figure 5.14. Fluorescent imaging of live (green) and dead (red) MDA-MB-231 cells of spheroids in microgels with varying rigidity (C2-C5) taken after 3 days of exposure to different concentrations of (a) paclitaxel (1nM, 10nM, 50 nM and 100 nM) and (b) cisplatin (30 μM , 100 μM, 300 μM and 500 μM) (scale bar: 50 μm). (c-f) The cell viability of MDA-MB-231 spheroids in microgels with varying rigidity (C2-C5) measured after 1 or 3days of exposure to different concentrations of paclitaxel (50 nM, 100 nM) and cisplatin (300 μM, 500 μM) (*$p<0.05$). Solid and dotted lines represent the viabilities of monolayer cultures of MDA-MB-231 cells exposed to the same concentration at day 1 and 3, respectively.

For paclitaxel, the decrease in viability became noticeable above 50 nM at day 1 for all microgels except C2 (Figure 5.14a and 5.14c, Figure 5.13a). At 100 nM, there was greater cytotoxicity at all microgels, as expected (Figure 5.14a and 5.14d, Figure 5.13a). Interestingly, there was a biphasic trend in cell viability, in which the viabilities significantly decreased for C3 and C5, 42 % and 34 %, respectively, compared to that of 2D monolayer culture, whereas the viability at C4 did not decrease as much, similar to that of 2D monolayer culture, at 73 %. This result highlighted that the spheroids within microgels having different mechanical properties significantly influenced their responses to chemotherapeutic agents. Higher permeability of microgel at lower rigidity of C3 allowed greater influx of paclitaxel, whereas limited permeability at higher rigidity of C5 increased the hypoxia in the microgels. Both factors contributed to enhancing the chemotherapeutic effects of paclitaxel. It should be noted that the viability at C2 was much higher than other conditions regardless of concentrations and exposure duration, closer to that of 2D monolayer culture, likely due to the insufficient formation of spheroids. Further treatment of paclitaxel for 3 days resulted in significant reduction in cell viability at all microgel condition, as expected, but they were still higher than that of monolayer culture(Figure 5.14a and 5.14d), indicating the cells in spheroids could further resist the chemotherapeutic effect. Several previous studies have demonstrated similar multicellular resistance mediated by tight cell-cell junctions.[42-45]

Unlike paclitaxel, the cell viability decreased continuously with increasing microgel rigidity at day 1 against cisplatin, more prominently at higher concentration (Figure 5.14e and 5.14f, Figure 5.13b). This suggested that the increased hypoxia within microgels at higher rigidity had significant synergistic effect on the cytotoxic effect of cisplatin, but increased diffusion at lower rigidity (C3), which had contributed to decrease cell viability for paclitaxel, did not show the same effect. Due to the lower chemotherapeutic potency of cisplatin as compared to paclitaxel, as evidenced by the requirement of high concentration (tens to hundreds of micromolar range), increased infusion of cisplatin to the microgel at C3 did not have the same contributing effect.

5.3.2.2. MCF-7

The cytotoxic effects of paclitaxel and cisplatin at the same concentrations were also explored with MCF-7 spheroids in microgels, as done with MDA-MB-231 (Figure 5.16, Figure 5.15).

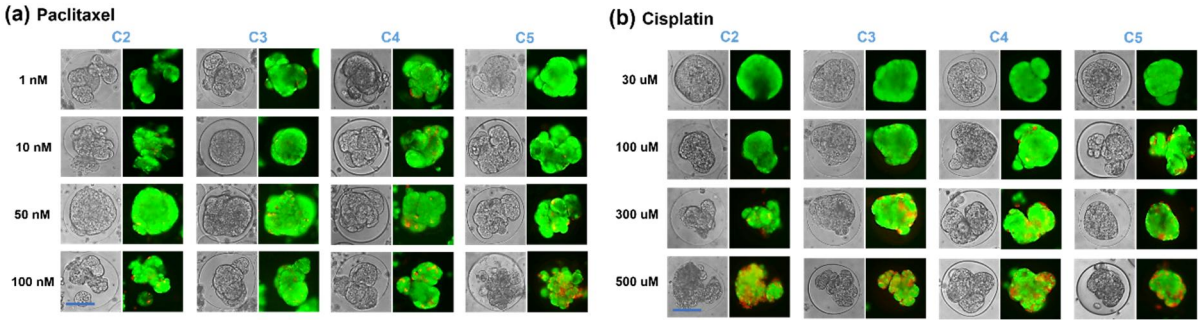

Figure 5.15. Fluorescent imaging of live (green) and dead (red) MCF-7 cells of spheroids in microgels with varying rigidity (C2-C5) taken after 1 day of exposure to different concentrations of (a) paclitaxel and (b) cisplatin (scale bar: 50 μm).

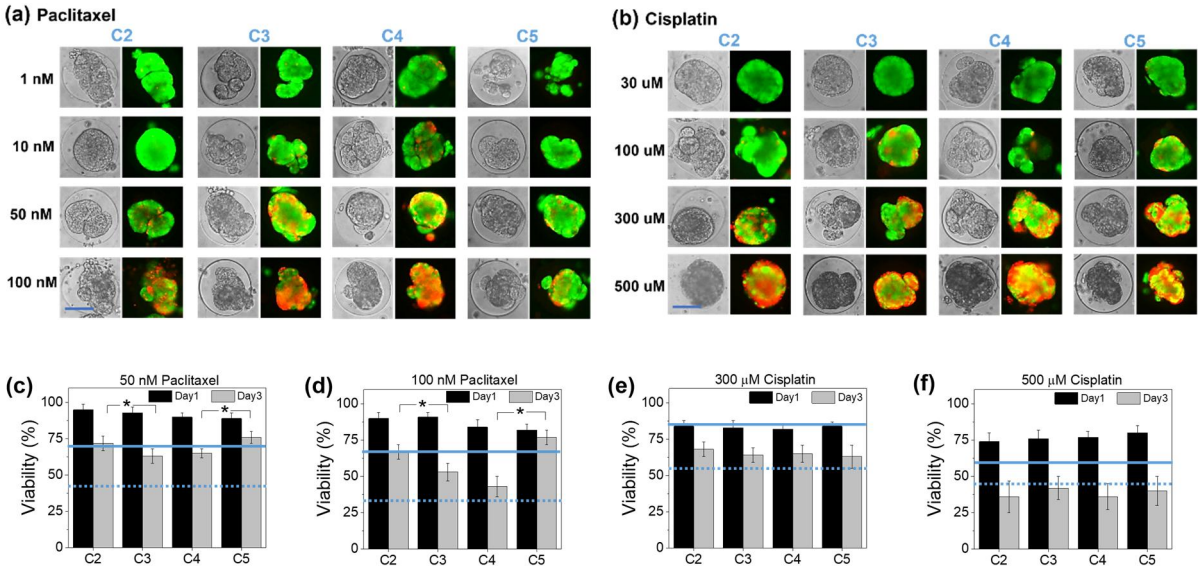

Figure 5.16. Fluorescent imaging of live (green) and dead (red) MCF-7 cells of spheroids in microgels with varying rigidity (C2-C5) taken after 3 days of exposure to different concentrations of (a) paclitaxel (1nM, 10nM, 50 nM and 100 nM) and (b) cisplatin (30 μM , 100 μM, 300 μM and 500 μM) (scale bar: 50 μm). (c-f) The cell viability of MCF-7 spheroids in microgels with varying rigidity (C2-C5) exposed to paclitaxel and cisplatin, calculated from (a) and (b) (*p<0.05). Solid and dotted lines represent the viabilities of monolayer cultures of MCF-7 cells exposed to the same concentration at day 1 and 3, respectively.

At day 1, the cells were generally more resistant to chemotherapeutics at the same concentrations as compared to MDA-MB-231 regardless of microgel rigidity, all similar or higher than that of 2D monolayer culture (Figure 5.16c and 5.16d, Figure 5.15). In addition, for both paclitaxel and cisplatin, lower concentrations did not result in meaningful dependence of the cell viability on microgel rigidity. Since MCF-7 cells more readily became cohesive spheroids than MDA-MB-231 cells, their overall chemoresistance probably became more prominent.

The exposure of paclitaxel at higher concentration (100 nM) at day 3 revealed an interesting biphasic dependence on microgel rigidity; higher cell viabilities at highest (C5) and lowest (C2) microgel rigidity, and lower cell viabilities at intermediate microgel rigidity (C3 and C4) (Figure 5.16a and 5.16d). This trend was opposite to that of MDA-MB-231 spheroids, shown in Figure 5.14d. Moreover, the cell viability was the largest at the highest microgel rigidity (C5) having the lowest permeability. It can be explained that with increasing microgel rigidity, increased hypoxia within the microgels caused further cytotoxicity along with paclitaxel. This was further supported by the observation that the cell death predominantly occurred from the periphery of spheroids, indicating greater chemotherapeutic effect to those more immediately exposed to the drug. However, highly chemoresistant spheroids formed at the highest microgel rigidity, coupled with limited diffusion of drug molecules, significantly reduced the cytotoxic effect of paclitaxel, especially compared to MDA-MB-231 spheroids.[43, 46] On the other hand, the cell death occurred from the core of MDA-MB 231 spheroids regardless of microgel rigidity and type of drugs, even though the cells on the periphery were more readily contacted (Figure 5.14). This suggested that unlike MCF-7 cells, the MDA-MB 231 spheroids were not as cohesive and as a result, the drug molecules could more easily diffuse into the spheroids and cause cytotoxicity from the core aided by increased hypoxia. The cytotoxic effect of cisplatin on the MCF-7 spheroids was not influenced by the microgel rigidity even at day 3 (Figure 5.16e and 5.16f). Unlike MDA-MB-231 spheroids whose viability decreased with microgel rigidity in response to cisplatin, likely promoted by increased hypoxia, it was probably not as significant factor for more cohesive MCF-7 spheroids, supported by the majority of cell death occurring at the spheroid periphery.

5.3.2.3. SK-BR-3

SK-BR-3 cells were able to form cohesive spheroids within microgels with varying rigidity, much like MCF-7 cells. Their response to paclitaxel and cisplatin at day 1 was also similar to that of MCF-7 spheroids, all demonstrating high cell viability regardless of microgel rigidity (Figure 5.18c, Figure 5.18d and Figure 5.17). In addition, the cell death also occurred from the periphery rather than the core. These findings also highlight the chemoresistance of cohesive spheroids.

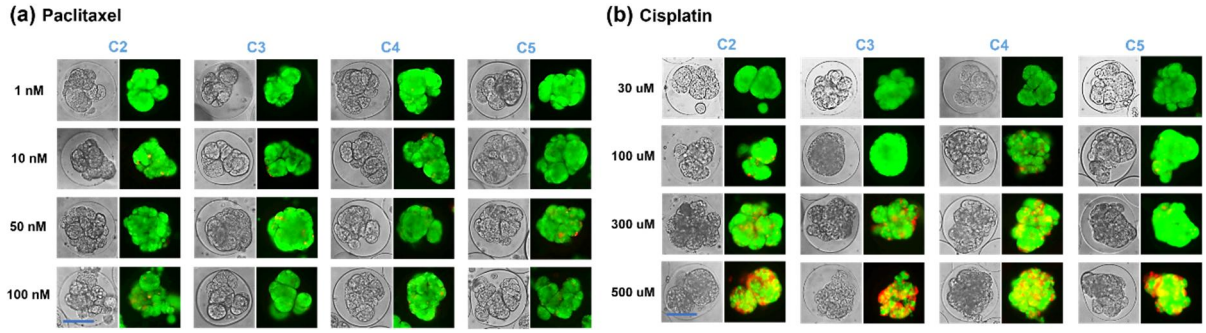

Figure 5.17. Fluorescent imaging of live (green) and dead (red) SK-BR-3 cells of spheroids in microgels with varying rigidity (C2-C5) taken after 1 day of exposure to different concentrations of (a) paclitaxel and (b) cisplatin (scale bar: 50 μm).

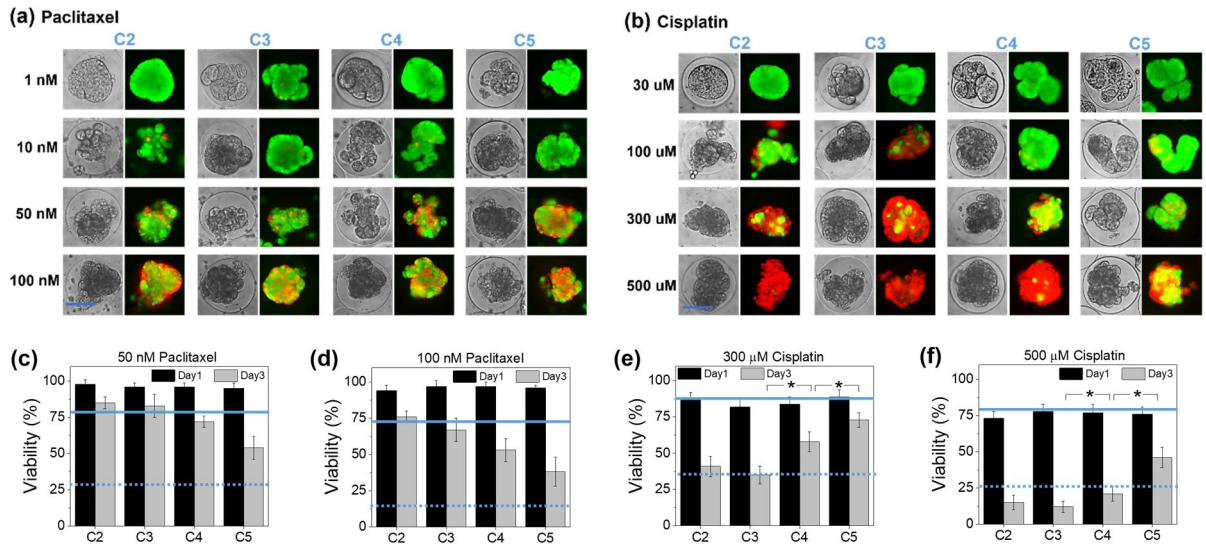

Figure 5.18. Fluorescent imaging of live (green) and dead (red) SK-BR-3 cells of spheroids in microgels with varying rigidity (C2-C5) taken after 3 days of exposure to different concentrations of (a) paclitaxel (1nM, 10nM, 50 nM and 100 nM) and (b) cisplatin (30 μM , 100 μM, 300 μM and 500 μM) (scale bar: 50 μm). (c-f) The cell viability of SK-BR-3 spheroids in microgels with varying rigidity (C2-C5) exposed to paclitaxel and cisplatin, calculated from (a) and (b) (*p<0.05). Solid and dotted lines represent the viabilities of monolayer cultures of SK-BR-3 cells exposed to the same concentration at day 1 and 3, respectively.

Interestingly, the cell viability of SK-BR-3 spheroids in response to paclitaxel at day 3 showed that the cytotoxicity increased significantly with increasing microgel rigidity, which became more prominent at higher concentration (Figure 5.18a, Figure 5.18c and Figure 5.18d). At higher microgel rigidity, there was greater increase in cell death around the core of spheroids, compared to those at lower microgel rigidity, which suggested the role of hypoxia in enhancing the chemotherapeutic effect. Since MCF-7 cells formed more cohesive spheroids at all microgel conditions as compared to SK-BR-3, it could be inferred that less cohesive SK-BR-3 spheroids became more susceptible to paclitaxel especially at higher microgel rigidity having greater hypoxia than MCF-7 spheroids at the same microgel rigidity. Similarly, given very low viability at all microgel conditions, coupled with predominant cell death at the periphery of microgels, the increased diffusion of cisplatin at lower rigidity of microgels resulted in greater cytotoxicity (Figure 5.18b, Figure 5.18e and Figure 5.18f). It was also evident that at the same concentration, the cytotoxic effect of cisplatin was more pronounced against SK-BR-3 spheroids than both MCF-7 and MDA-MB-231 spheroids.

5.4. Conclusion

In this study, uniform-sized spherical gelatin microgels encapsulated with different types of breast cancer cells were engineered using a flow-focusing microfluidic technology. The cells within the microgels spheroids proliferated and turned into spheroid structures, demonstrating the biocompatible and bioactive properties of microgels. Importantly, their degrees of formation showed highly complex dependence on the cell subtypes and mechanical properties of microgels. The cellular behavior and subsequent spheroid formation of three breast tumor cells, MDA-MB-231, SK-BR-3 and MCF-7, categorized as “triple negative B”, “HER2+” and “luminal A” in decreasing order of aggressiveness, respectively, showed that more cohesive and large spheroids regardless of microgel rigidity were generated by MCF-7 cells, while MDA-MB-231 cells only became spheroids in microgels at higher rigidity. SK-BR-3 cells also readily formed spheroids, though more cohesive and larger spheroids were shown in microgels at higher rigidity. Interestingly, more aggressive MDA-MB-231 cells formed larger and more migratory polyploid giant cancer cells (PGCC) as they continued to proliferate, whereas PGCCs of MCF-7 and SK-BR-3 cells were generally smaller but they proliferated faster and more readily formed spheroids. Furthermore, chemotherapeutic efficacies of paclitaxel and cisplatin evaluated on these spheroids also highlighted that their cytotoxic effects were heavily influenced by the complex interplay between cell subtype and 3D mechanical microenvironment. Taken together, the results of this study highlight the importance of both cellular and extracellular factors on the formation and pathophysiology of 3D tumor spheroids, and provide biomaterial-based design criteria for generating tumor spheroids and their application in drug screening.

5.5. Reference

1. Ravi, M.; Paramesh, V.; Kaviya, S. R.; Anuradha, E.; Solomon, F. D. P., 3D cell culture systems: Advantages and applications. *Journal of Cellular Physiology* **2015,** *230* (1), 16-26.

2. Thoma, C. R.; Zimmermann, M.; Agarkova, I.; Kelm, J. M.; Krek, W., 3D cell culture systems modeling tumor growth determinants in cancer target discovery. *Advanced Drug Delivery Reviews* **2014,** *69-70*, 29-41.

3. van Duinen, V.; Trietsch, S. J.; Joore, J.; Vulto, P.; Hankemeier, T., Microfluidic 3D cell culture: from tools to tissue models. *Current Opinion in Biotechnology* **2015,** *35*, 118-126.

4. W., H. J., 3D Cell Culture: A Review of Current Approaches and Techniques 1. In *3D Cell Culture: Methods and Protocols*, W., H. J., Ed. Humana Press: 2011; Vol. 695, pp 1-15.

5. Huh, D.; Hamilton, G. A.; Ingber, D. E., From 3D cell culture to organs-on-chips. *Trends in Cell Biology* **2011,** *21* (12), 745-754.

6. Vaezi, M.; Seitz, H.; Yang, S., A review on 3D micro-additive manufacturing technologies. *The International Journal of Advanced Manufacturing Technology* **2013,** *67* (5-8), 1721-1754.

7. Zorlutuna, P.; Annabi, N.; Camci-Unal, G.; Nikkhah, M.; Cha, J. M.; Nichol, J. W.; Manbachi, A.; Bae, H.; Chen, S.; Khademhosseini, A., Microfabricated biomaterials for engineering 3D tissues. *Advanced Materials* **2012,** *24* (14), 1782-1804.

8. Bartosh, T. J.; Ylöstalo, J. H.; Mohammadipoor, A.; Bazhanov, N.; Coble, K.; Claypool, K.; Lee, R. H.; Choi, H.; Prockop, D. J., Aggregation of human mesenchymal stromal cells (MSCs) into 3D spheroids enhances their antiinflammatory properties. *Proceedings of the National Academy of Sciences* **2010,** *107* (31), 13724-13729.

9. Hirschhaeuser, F.; Menne, H.; Dittfeld, C.; West, J.; Mueller-Klieser, W.; Kunz-Schughart, L. A., Multicellular tumor spheroids: An underestimated tool is catching up again. *Journal of Biotechnology* **2010,** *148* (1), 3-15.

10. Kim, J. B.; Stein, R.; O'Hare, M. J., Three-dimensional in vitro tissue culture models of breast cancer — a review. *Breast Cancer Research and Treatment* **2004,** *85* (3), 281-291.

11. Lin, R.-Z.; Chang, H.-Y., Recent advances in three-dimensional multicellular spheroid culture for biomedical research. *Biotechnology Journal* **2008,** *3* (9-10), 1172-1184.

12. Mehta, G.; Hsiao, A. Y.; Ingram, M.; Luker, G. D.; Takayama, S., Opportunities and challenges for use of tumor spheroids as models to test drug delivery and efficacy. *Journal of Controlled Release* **2012,** *164* (2), 192-204.

13. Fennema, E.; Rivron, N.; Rouwkema, J.; van Blitterswijk, C.; de Boer, J., Spheroid culture as a tool for creating 3D complex tissues. *Trends in Biotechnology* **2013,** *31* (2), 108-115.

14. Gong, X.; Lin, C.; Cheng, J.; Su, J.; Zhao, H.; Liu, T.; Wen, X.; Zhao, P., Generation of multicellular tumor spheroids with microwell-based agarose scaffolds for drug testing. *PLOS ONE* **2015,** *10* (6), e0130348.

15. Tung, Y.-C.; Hsiao, A. Y.; Allen, S. G.; Torisawa, Y.-s.; Ho, M.; Takayama, S., High-throughput 3D spheroid culture and drug testing using a 384 hanging drop array. *Analyst* **2011,** *136* (3), 473-478.

16. Faulkner-Jones, A.; Greenhough, S.; King, J. A.; Gardner, J.; Courtney, A.; Shu, W., Development of a valve-based cell printer for the formation of human embryonic stem cell spheroid aggregates. *Biofabrication* **2013,** *5* (1), 015013.

17. Kim, C.; Chung, S.; Kim, Y. E.; Lee, K. S.; Lee, S. H.; Oh, K. W.; Kang, J. Y., Generation of core-shell microcapsules with three-dimensional focusing device for efficient formation of cell spheroid. *Lab on a Chip* **2011,** *11* (2), 246-252.

18. Vadivelu, R. K.; Kamble, H.; Shiddiky, M. J. A.; Nguyen, N.-T., Microfluidic technology for the generation of cell spheroids and their applications. *Micromachines* **2017,** *8* (4), 94.

19. Lee, D.; Cha, C., The combined effects of co-culture and substrate mechanics on 3d tumor spheroid formation within microgels prepared via flow-focusing microfluidic fabrication. *Pharmaceutics* **2018,** *10* (4), 229.

20. Lee, D.; Lee, K.; Cha, C., Microfluidics-assisted fabrication of microtissues with tunable physical properties for developing an in vitro multiplex tissue model. *Advanced Biosystems* **2018,** *2* (12), 1800236.

21. Siltanen, C.; Yaghoobi, M.; Haque, A.; You, J.; Lowen, J.; Soleimani, M.; Revzin, A., Microfluidic fabrication of bioactive microgels for rapid formation and enhanced differentiation of stem cell spheroids. *Acta Biomaterialia* **2016,** *34*, 125-132.

22. Dai, X.; Cheng, H.; Bai, Z.; Li, J., Breast cancer cell line classification and its relevance with breast tumor subtyping. *Journal of Cancer* **2017,** *8* (16), 3131-3141.

23. Holliday, D. L.; Speirs, V., Choosing the right cell line for breast cancer research. *Breast Cancer Research* **2011,** *13* (4), 215.

24. Fei, F.; Zhang, D.; Yang, Z.; Wang, S.; Wang, X.; Wu, Z.; Wu, Q.; Zhang, S., The number of polyploid giant cancer cells and epithelial-mesenchymal transition-related proteins are associated with invasion and metastasis in human breast cancer. *Journal of Experimental &*

Clinical Cancer Research **2015,** *34* (1), 158.

25. Zhang, S.; Mercado-Uribe, I.; Xing, Z.; Sun, B.; Kuang, J.; Liu, J., Generation of cancer stem-like cells through the formation of polyploid giant cancer cells. *Oncogene* **2013,** *33*, 116.

26. Cha, C.; Shin, S. R.; Gao, X.; Annabi, N.; Dokmeci, M. R.; Tang, X.; Khademhosseini, A., Controlling mechanical properties of cell-laden hydrogels by covalent incorporation of graphene oxide. *Small* **2014,** *10* (3), 514-523.

27. Hong, J.; Shin, Y.; Kim, S.; Lee, J.; Cha, C., Complex tuning of physical properties of hyperbranched polyglycerol-based bioink for microfabrication of cell-laden hydrogels. *Advanced Functional Materials* **2019,** *29* (13), 1808750.

28. Kim, S.; Sim, S. B.; Lee, K.; Cha, C., Comprehensive examination of mechanical and diffusional effects on cell behavior using a decoupled 3D hydrogel system. *Macromolecular Bioscience* **2017,** *17* (9), 1700162.

29. Kim, S.; Oh, J.; Cha, C., Enhancing the biocompatibility of microfluidics-assisted fabrication of cell-laden microgels with channel geometry. *Colloids and Surfaces B: Biointerfaces* **2016,** *147*, 1-8.

30. Huang, X.; Teng, X.; Chen, D.; Tang, F.; He, J., The effect of the shape of mesoporous silica nanoparticles on cellular uptake and cell function. *Biomaterials* **2010,** *31* (3), 438-448.

31. Hoque, M. E.; Nuge, T.; Yeow, T. K.; Nordin, N.; Prasad, R. G. S. V., Gelatin based scaffolds for tissue engineering - A review. *Polymers Research Journal* **2015,** *9* (1), 15-32.

32. Kang, H.-W.; Tabata, Y.; Ikada, Y., Fabrication of porous gelatin scaffolds for tissue engineering. *Biomaterials* **1999,** *20* (14), 1339-1344.

33. Santoro, M.; Tatara, A. M.; Mikos, A. G., Gelatin carriers for drug and cell delivery in tissue engineering. *Journal of Controlled Release* **2014,** *190*, 210-218.

34. Hendrix, M. J. C.; Seftor, E. A.; Kirschmann, D. A.; Seftor, R. E. B., Molecular biology of breast cancer metastasis Molecular expression of vascular markers by aggressive breast cancer cells. *Breast Cancer Research* **2000,** *2* (6), 417.

35. Ingber, D. E., Cellular mechanotransduction: putting all the pieces together again. *The FASEB Journal* **2006,** *20* (7), 811-827.

36. Kumar, S., Stiffness does matter. *Nature Materials* **2014,** *13*, 918.

37. Wei, S. C.; Fattet, L.; Tsai, J. H.; Guo, Y.; Pai, V. H.; Majeski, H. E.; Chen, A. C.; Sah, R. L.; Taylor, S. S.; Engler, A. J.; Yang, J., Matrix stiffness drives epithelial–mesenchymal transition and tumour metastasis through a TWIST1–G3BP2 mechanotransduction pathway.

Nature Cell Biology **2015,** *17*, 678.

38. Lopez-Sánchez, L. M.; Jimenez, C.; Valverde, A.; Hernandez, V.; Peñarando, J.; Martinez, A.; Lopez-Pedrera, C.; Muñoz-Castañeda, J. R.; De la Haba-Rodríguez, J. R.; Aranda, E.; Rodriguez-Ariza, A., $CoCl_2$, a mimic of hypoxia, induces formation of polyploid giant cells with stem characteristics in colon cancer. *PLOS ONE* **2014,** *9* (6), e99143.

39. Chu, C.; Schmidt, J. J.; Carnes, K.; Zhang, Z.; Kong, H. J.; Hofmann, M.-C., Three-Dimensional Synthetic Niche Components to Control Germ Cell Proliferation. *Tissue Engineering Part A* **2009,** *15* (2), 255-262.

40. Kunz-Schughart, L. A.; Freyer, J. P.; Hofstaedter, F.; Ebner, R., The use of 3-D cultures for high-throughput screening: The multicellular spheroid model. *Journal of Biomolecular Screening* **2004,** *9* (4), 273-285.

41. LaBarbera, D. V.; Reid, B. G.; Yoo, B. H., The multicellular tumor spheroid model for high-throughput cancer drug discovery. *Expert Opinion on Drug Discovery* **2012,** *7* (9), 819-830.

42. Fang, Y.; Sullivan, R.; Graham, C. H., Confluence-dependent resistance to doxorubicin in human MDA-MB-231 breast carcinoma cells requires hypoxia-inducible factor-1 activity. *Experimental Cell Research* **2007,** *313* (5), 867-877.

43. Imamura, Y.; Mukohara, T.; Shimono, Y.; Funakoshi, Y.; Chayahara, N.; Toyoda, M.; Kiyota, N.; Takao, S.; Kono, S.; Nakatsura, T.; Minami, H., Comparison of 2D- and 3D-culture models as drug-testing platforms in breast cancer. *Oncology Reports* **2015,** *33* (4), 1837-1843.

44. Maruhashi, R.; Akizuki, R.; Sato, T.; Matsunaga, T.; Endo, S.; Yamaguchi, M.; Yamazaki, Y.; Sakai, H.; Ikari, A., Elevation of sensitivity to anticancer agents of human lung adenocarcinoma A549 cells by knockdown of claudin-2 expression in monolayer and spheroid culture models. *Biochimica et Biophysica Acta (BBA) - Molecular Cell Research* **2018,** *1865* (3), 470-479.

45. Yang, T.-M.; Barbone, D.; Fennell, D. A.; Broaddus, V. C., Bcl-2 family proteins contribute to apoptotic resistance in lung cancer multicellular spheroids. *American Journal of Respiratory Cell and Molecular Biology* **2009,** *41* (1), 14-23.

46. Reynolds, D. S.; Tevis, K. M.; Blessing, W. A.; Colson, Y. L.; Zaman, M. H.; Grinstaff, M. W., Breast cancer spheroids reveal a differential cancer stem cell response to chemotherapeutic treatment. *Scientific Reports* **2017,** *7* (1), 10382.

PART VI

Facile generation hollow fiber to mimic blood vessel using human endothelial cells via GelMa and Alginate combination by controlled hydrogel stiffness in 3D culture

6.1. Introduction

Tissue Engineering can provide some solutions in various fields such as biomaterials, biological factors, usage of cells in order to restore or replace the abnormal condition. Generally, 3D cell printing is regarded as versatile technique for tissue engineering because of the high freedom for assigning cells and a lot of biomolecules are patterned geometrically.[1] In this technique, one limitation required for biomaterials which can instant gelation behavior. The methods usesd a lot of tool, such as 3D printer, nozzle and so on. However, in our study, we used two kind of needle which made modified by me, that is facile generated method for hollow fiber compare to 3D printing. In, Alginate case, the deficiency of binding sites such as RGDs for cell attachment and migration in alginate dramatically impairs activities for encapsulated cells.[2] In this study, we can solve the problem as I mentioned before, we use alginate and GelMa which is biomaterial derived collagen in naturally polymer, in order to mimic blood vessel. Alginate maintains the shape of blood vessels by physically crosslinking with calcium, and then irradiates with UV, allowing GelMa to bond chemically. After using citrate (chelating method) to remove all of the calcium bound to the alginate, the alginate diffuses out of the vessel, forming a pore, and the vessel can only form the GelMa backbone. And we have observed that endothelial cells differentiate or proliferate best under certain conditions using hydrogels of varying concentration. Also, endothelial progenitor cells (EPCs) are attractive cell source for treatment of ischaemia disease for their potentials in neovascularization.[3] Therefore, it is very important to seek an endothelial cell inspired material for this engineering fields.

6.2. Material and methods

6.2.1. Synthesis of methacrylic gelatin (MGel)

Gelatin (5 g, from porcine skin, Sigma Aldrich), 4-methoxyphenol(0.05g, Sigma Aldrich) and 4-dimethylaminopyridine (0.5 g, Sigma Aldrich) were dissolved in 50 mL dimethylsulfoxide at 50 °C. Glycidyl methacrylate (2 mL, Sigma Aldrich) was added dropwise and reacted for 48 hours at 50 °C

under dry N_2. The product was purified by dialysis against deionized (DI) water and dried by lyophilization. The methacrylation of gelatin was confirmed with ^{1}H-NMR spectroscopy.

6.2.2. Microgel using Semi IPN and IPN structure

Sodium Alginate (Junsei) and MGel are mixed in order to final concentration Alginate 0.5%, 1% and MGel 4%, 6%, 8%, 10%, 15%. Move the solution into the syringe and total volume is 1mL. After then dropping to the well plate included Calcium Chloride (0.1M) in DI water. The Endothelial cells were dispersed in the MGel and Alginate solution at 1 x 10^6 cell mL^{-1}. Semi-IPN or IPN is different with or without UV exposure (320nm) during 1 min.

6.2.3. In vitro evaluation of Gels using Semi IPN and IPN structure

6.2.3.1. Viability and proliferation

The viability of the cells encapsulated in the microgels were measured using LIVE/DEAD Cell Viability Assay kit (Thermo Fisher), following the manufacturer's instructions. Briefly, the cell-laden gel was treated with calcein-AM and ethidium homodimer-1 to fluorescently label live (green) and dead (red) cells, and were visualized with fluorescence microscopy (XDS-3FL, Optika). The viability was reported as the percentage of live cells from the total number of cells. The proliferation rate (k_P) of encapsulated cells was determined by counting the number of live cells at various time points up to 7 days, and the plot of the normalized number of viable cells (N_t/N_0) vs. time (t) was fitted with the following power-law equation,

$$\frac{N_t}{N_0} = 2^{k_P \cdot t} \qquad (2)$$

N_t was the number of viable cells at time, t, and N_0 was the initial number of viable cells at t=0.[8-10]

6.2.4. Facile generation of cell-laden hollow fiber

We made a new needle formation which can allow to generate hollow fiber as shown Figure X. Inside of tube consisted of hollow formation using Calcium Chloride 0.05M, FBS 10% and HEPES 25mM in Distilled water. Outer phase which are Alginate and MGel mixture is included endothelial cell. As shown Figure X. The syringe pump flow rates are same both inner and outer phase 800 μl/min. Calcium Chloride concentration is 0.3M, FBS 10% and HEPES 25mM in Distilled water.[4]

6.3. Results and Discussion

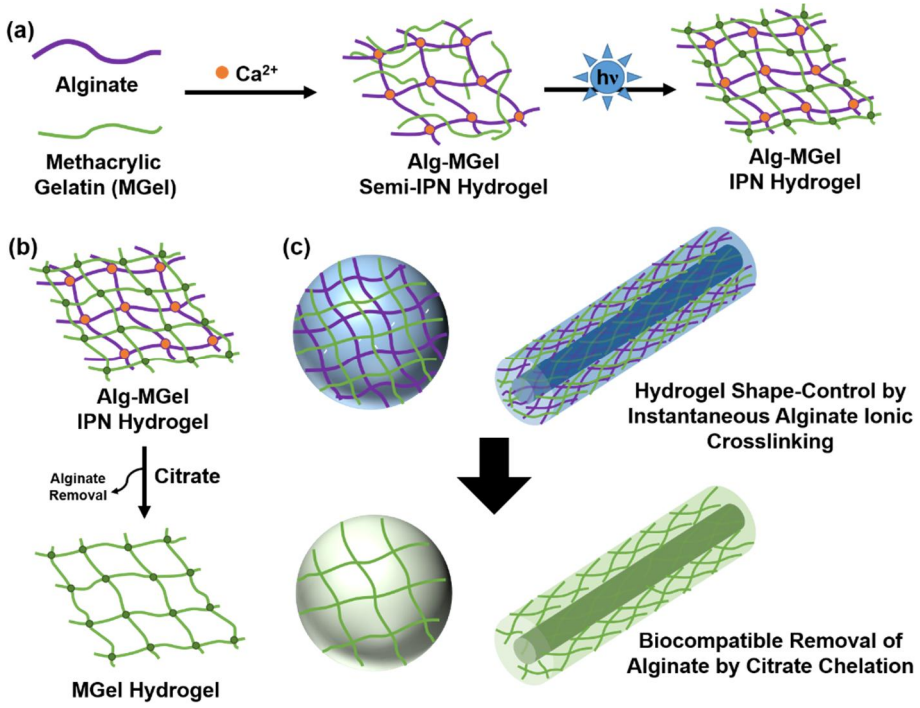

Figure 6.1. This schematic represents overall experiments. (a) Alginate and MGel mixed Ca^{2+} as a physical cross-linking using Alginate (Semi-IPN) after then chemical cross-linking by UV exposure using MGel (IPN). (b) IPN structure can be removed physically cross-linked Alginate by Sodium Citrate. (c) Generating of hollow fiber using same methods.

6.3.1. Fabrication of endothelial cell laden gel

In this study, we explored various having stiffness gel and compare to semi-IPN or IPN. We performed cell encapsulated gel using syringe. Semi-IPN and IPN can be separated condition by with or without UV exposure. When UV exposure to the gel, which can convert to IPN condition. However, when UV not exposure to the gel, which can maintain semi-IPN formation (Figure 1a). With IPN gel formation, Alginate can be made pore through removed alginate via Sodium Citrate. Therefore, the structure remained MGel backbone (Figure 1b). At first, we can generate cell laden gel in order to check elastic modulus or swelling ratio. With same method, we performed to mimic blood vessel using endothelial cell (Figure 1c).

6.3.2. Physical properties of Microgel using Semi IPN and IPN structure

6.3.2.1. Elastic modulus and swelling ratio

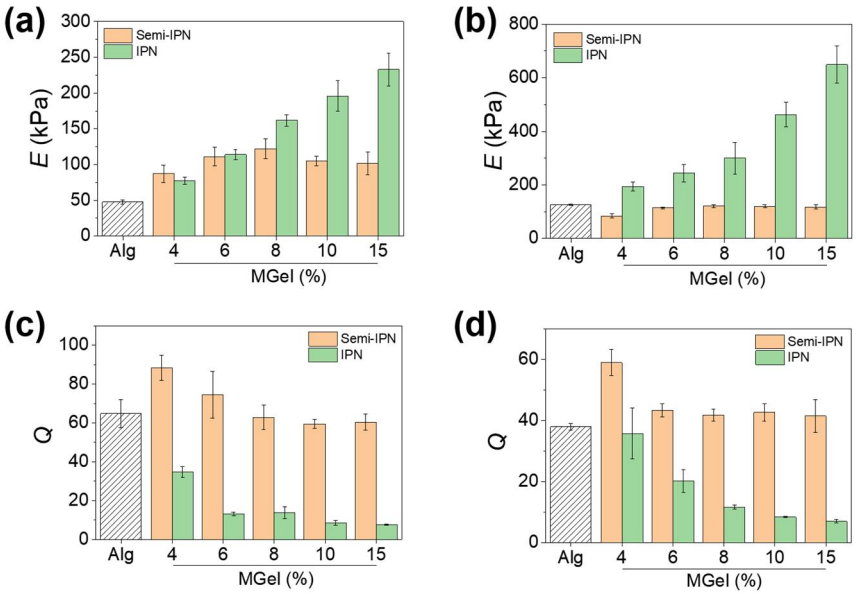

Figure 6.2. (a) and (c) Elastic moduli (*E*) and Swelling ratios (*Q*) of Alginate 0.5% and MGel mixed Semi-IPN and IPN (b) and (d) Elastic moduli (*E*) and Swelling ratios (*Q*) of Alginate 1% and MGel mixed Semi-IPN and IPN.

One of the advantages of hydrogel is that we can control the stiffness by changing hydrogel concentration. Figure 2 indicates that Elastic modulus and swelling ratios with Alginate and MGel at various concentration. As expected, Alginate concentration is higher as well as elastic modulus also increased. MGel concentration is higher as well as elastic modulus also increased. However, the trend in swelling ratio was opposite to that of elastic modulus since the porosity within the hydrogel becomes reduced with increasing crosslinking density.

6.3.2.2 SEM structure of IPN structure

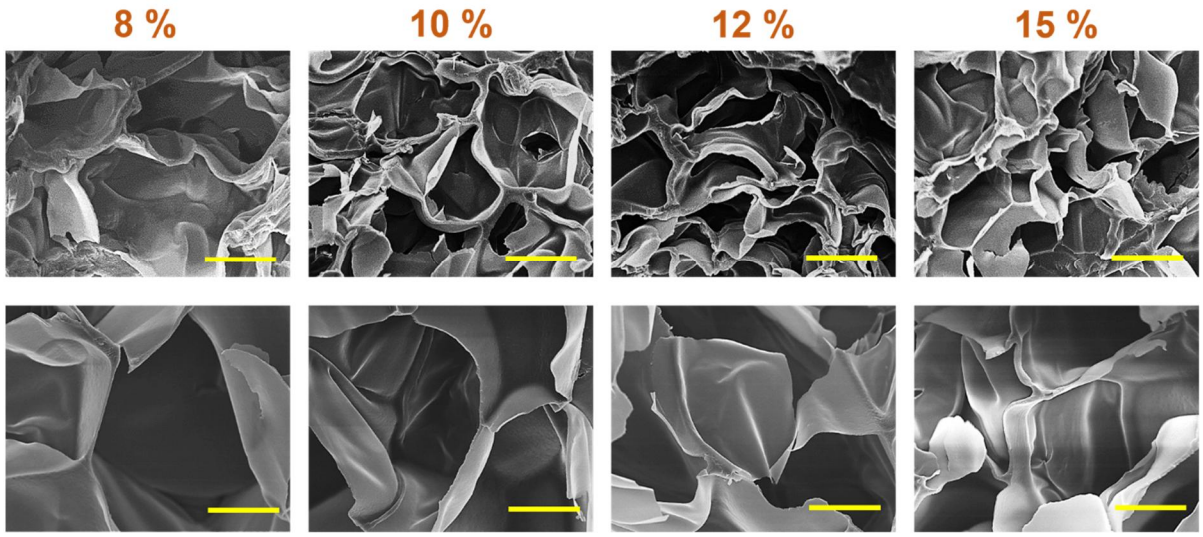

Figure 6.3. SEM images of IPN structure (Alginate 1% and MGel 8%, 10%, 12%, 15%) (scale bar: 10 μm)

Figure 3 shows that SEM images of IPN structure at various MGel concentration. MGel concentration is increased as well as the pore size is decreased because of high cross-linking density. These results were correlated with the modulus and swelling ratio results mentioned above.

6.3.3. In vitro evaluation of Microgels using Semi IPN and IPN structure

6.3.3.1 Viability and proliferation

It is well established that the mechanical cues imparted by the surrounding matrices exert significant effects on residing cells by signal transduction through focal adhesion.[5] Therefore, it was hypothesized that the mechanical properties of the microgels, controlled by the concentration of MGel, would influence the 3T3 activities. The viability of 3T3 cells encapsulated within the microgels having different rigidity was assessed at various time points (Figure 4a and 4b) with or without UV exposure in order to make Semi-IPN or IPN structure. The initial viability, taken at day 1, were very low live cell observed in all conditions. At higher MGel concentrations, there was increased cell viability regardless Semi-IPN or IPN structure. This was made possible because the microgel consisted of crosslinked network of gelatin, which is derived from natural collagen and retains cell responsive moieties such as Arg-Gly-Asp (RGD) peptide and matrix metalloproteinase (MMP) recognition domains.[6, 7] The proliferation rate of 3T3 in microgels at various MGel concentrations was calculated to assess the effect of mechanical properties on the encapsulated cells (Figure 4c and 4d). The increase in the number of live cells (N_t/N_0) were counted at different times up to 7 days. The proliferation rate (k_P) was obtained by fitting the plot with a power-law model (Figure 4e). The k_P value was increased as well as MGel concentration increased. Interestingly, Semi-IPN microgel is higher cell viability rather than IPN microgel. This could be the result of diminished permeability of the microgels with increased crosslinking density preventing further growth, similar to previous studies demonstrating the combined effects of mechanical and diffusional properties of hydrogels on the cells in 3D.

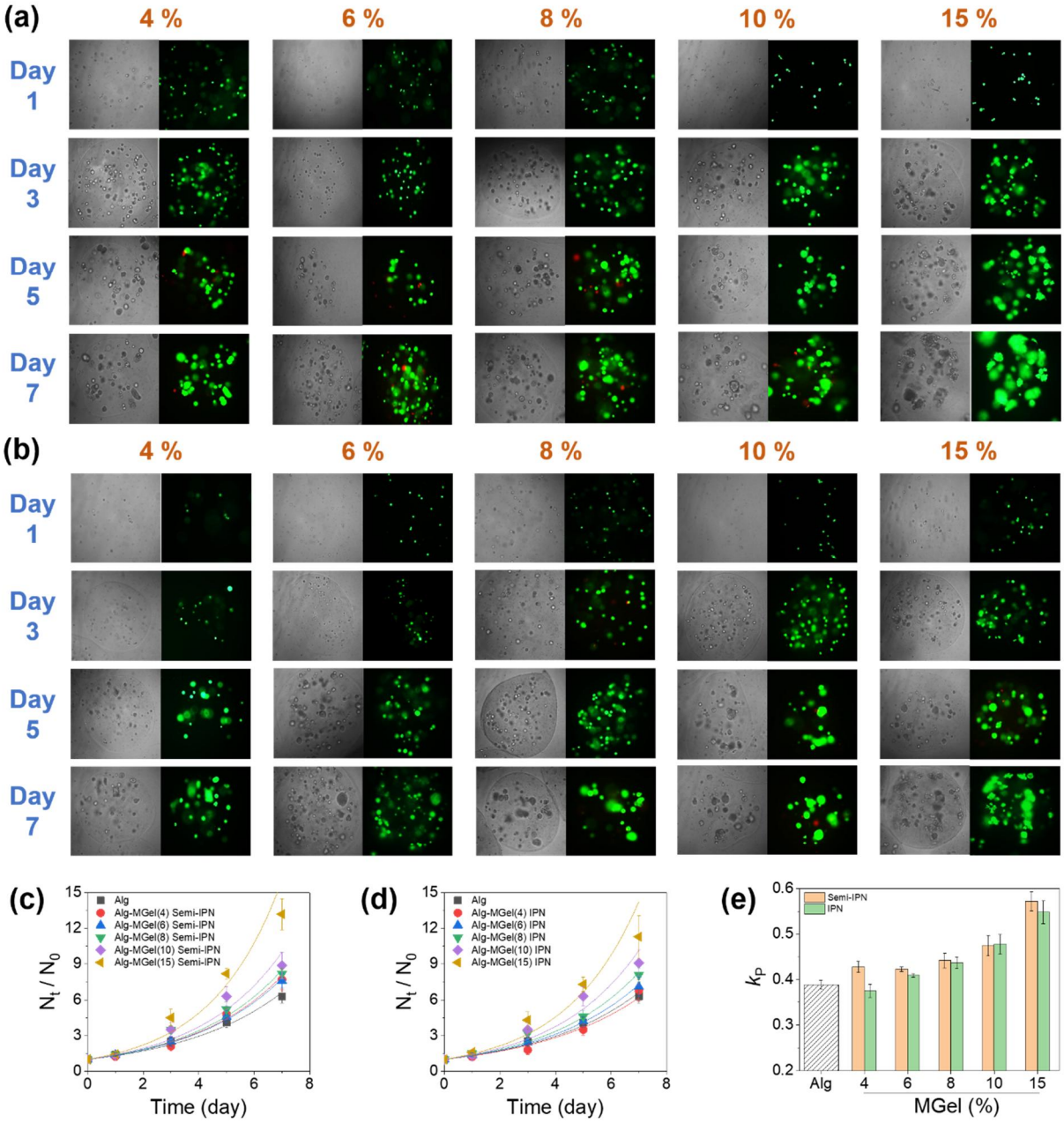

Figure 6.4. Cell viability and proliferation in microgel. Representative microscopic(left) and fluorescent (right) images of 3T3 encapsulated in microgel taken at various times up to 7days. The cells were fluorescently stained to identify live (green) and dead (red) cells. (a) Semi-IPN structure (b) IPN structure (c) and (d) The normalized number of viable cells (N_t/N_0) in microgel was measured over time (N_t: number of viable cells at time, t, N_0: number of initial viable cells) Semi-IPN and IPN. (e) The plot in panel (c) and (d) were fitted with a power-law model to obtain the proliferation rate (k_P).

6.3.4. Effect of Sodium Citrate (Removing Alginate)

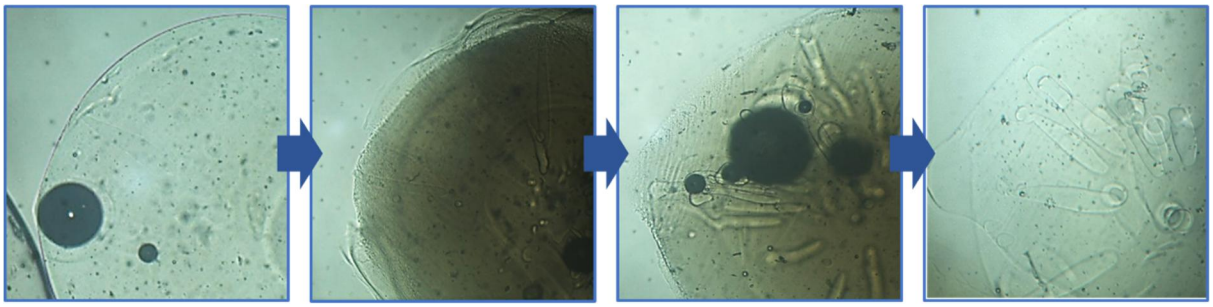

Figure 6.5. These images show the process which is removed alginate from IPN microgel in various time.

Figure 5 represents the process which is removed alginate from IPN microgel in various time. First image is alginate and MGel mixed microgel after UV exposure. Second image shows when sodium citrate (0.1M) exposed into the IPN microgel. At that time, the microgel was stared blur because of removing alginate and simultaneously generating porosity. Overtime, however, the opaque microgels became transparent again after the alginate was completely drained.

6.3.5. Facile generation of cell-laden hollow fiber

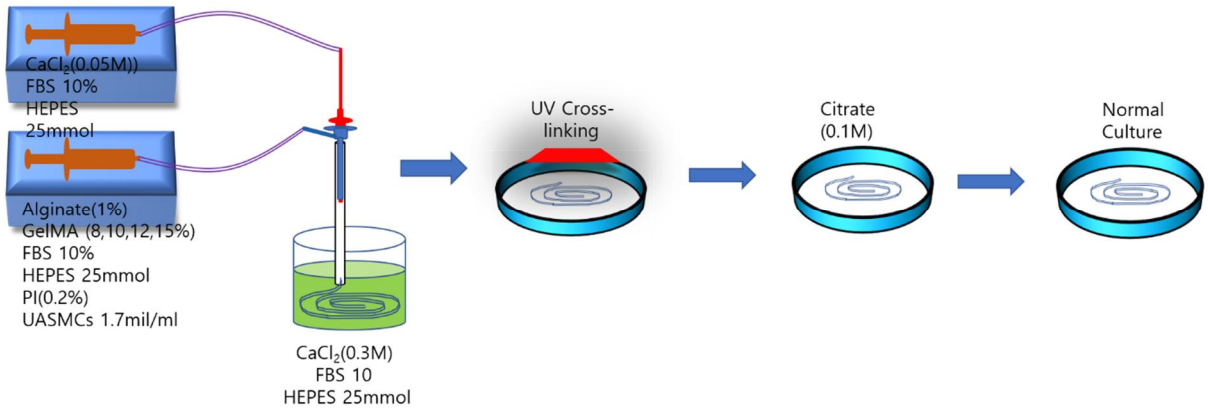

Figure 6.6. Scheme of generation of hollow fiber using alginate and MGel with HUVECs outer phase and inner phase 0.05M calcium chloride, 10% FBS, 25mM HEPES.

Figure 6 indicates that how to generate hollow fiber using needle and borosilicate glass. We performed two kind of blood vessel such as Semi-IPN or IPN structure by with or without UV exposure. We try to cut off the vessel about 1cm fragmentation. After then, we cultured up to 7days and observed cell viability through live/dead assay. Figure 7 (a) shows mimic blood vessel image and Figure 7 (b) is observed by microscopic to confirm whether hollow fiber or not. As a result, that has hollow fiber

formation.

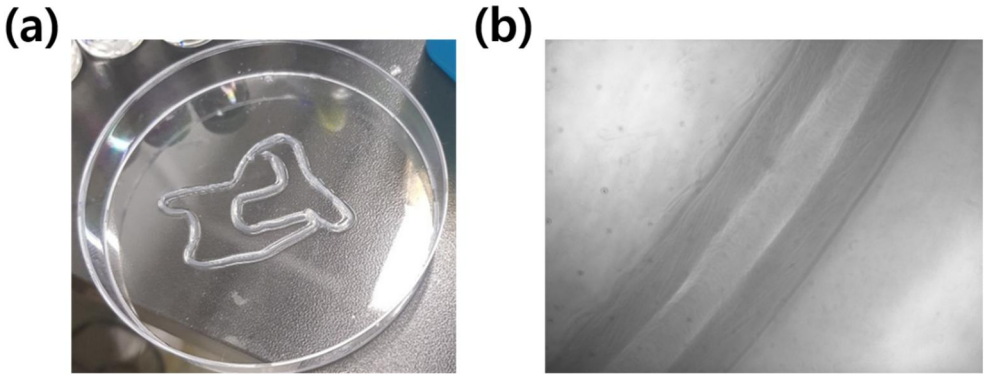

Figure 6.7. (a) Hollow fiber to mimic blood vessel using Alginate and MGel. (b) Microscopic image of hollow fiber.

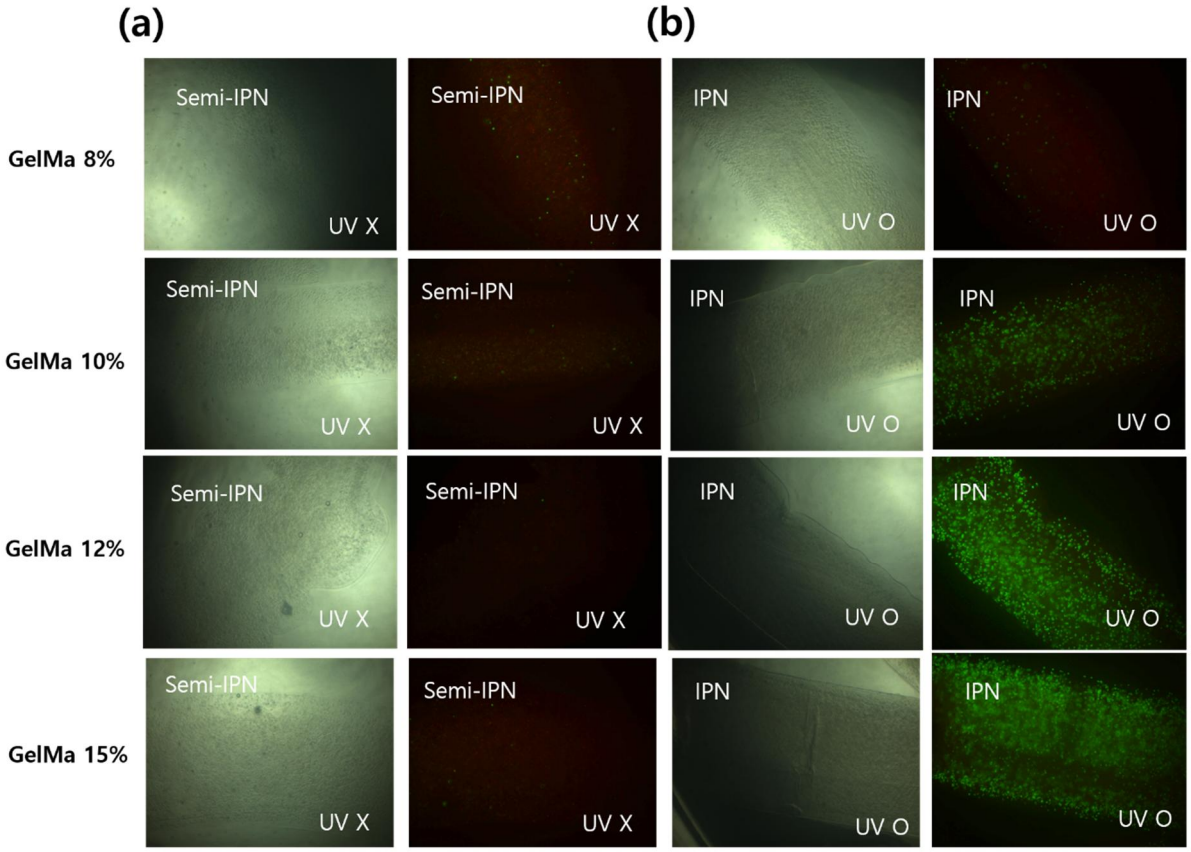

Figure 6.8. Cell viability and proliferation in hollow fiber with HUVECs. Representative microscopic(left) and fluorescent (right) images of HUVECs encapsulated in microgel taken at various times up to 7days. These images show at 7days. The cells were fluorescently stained to identify live (green) and dead (red) cells. (a) Semi-IPN structure (b) IPN structure.

As I mentioned before, we performed two kind of hollow fiber to mimic blood vessel such as Semi-IPN or IPN structure by with or without UV exposure. Figure 8 (a) is mimicking blood vessel having

Semi-IPN structure and Figure 8 (b) is mimicking blood vessel having IPN structure. The cell viability is very depended on hydrogel stiffness. At low stiffness having hydrogels, there are low cell viability observed regardless of semi-IPN or IPN structure. In all conditions, cell encapsulated microgels at semi-IPN did not proliferate because of very low elastic modulus. However, hydrogel stiffness increased as well as the cell viability also increased.

6.4. Conclusion

We try to generate hollow fiber to mimic blood vessel using semi-IPN or IPN structure. By controlling concentration of Alginate and MGel mixture, we can obtain tunable cell encapsulated microgel. At first, we observed cell viability which is encapsulated microgel by dripping method. Alginate concentration is higher as well as elastic modulus also increased. MGel concentration is higher as well as elastic modulus also increased. However, the trend in swelling ratio was opposite to that of elastic modulus since the porosity within the hydrogel becomes reduced with increasing crosslinking density. The cell viability is very depended on hydrogel stiffness regardless semi-IPN or IPN structure. The proliferation rate (k_P) was obtained by fitting the plot with a power-law model. The k_p value was increased as well as MGel concentration increased. Interestingly, semi-IPN microgel is higher cell viability rather than IPN microgel. This could be the result of diminished permeability of the microgels with increased crosslinking density preventing further growth. To mimic blood vessel case, also shows same result. At low stiffness having hydrogels, there are low cell viability observed regardless of semi-IPN or IPN structure. However, hydrogel stiffness increased as well as the cell viability also increased. We observed by microscopic to confirm whether hollow fiber or not. As a result, that has hollow fiber formation. We have planned to closer mimic blood vessel using Smooth muscle cell.

6.5. Reference

1. Park, J. H.; Jang, J.; Lee, J. S.; Cho, D. W., Three-Dimensional Printing of Tissue/Organ Analogues Containing Living Cells. *Ann Biomed Eng* **2017,** *45* (1), 180-194.

2. Gao, G.; Lee, J. H.; Jang, J.; Lee, D. H.; Kong, J.-S.; Kim, B. S.; Choi, Y.-J.; Jang, W. B.; Hong, Y. J.; Kwon, S.-M.; Cho, D.-W., Tissue Engineered Bio-Blood-Vessels Constructed Using a Tissue-Specific Bioink and 3D Coaxial Cell Printing Technique: A Novel Therapy for Ischemic Disease. *Advanced Functional Materials* **2017,** *27* (33).

3. Asahara, T.; Kawamoto, A.; Masuda, H., Concise review: Circulating endothelial progenitor cells for vascular medicine. *Stem Cells* **2011,** *29* (11), 1650-5.

4. Zhang, X.; Kim, G. J.; Kang, M. G.; Lee, J. K.; Seo, J. W.; Do, J. T.; Hong, K.; Cha, J. M.; Shin, S. R.; Bae, H., Marine Biomaterial-Based Bioinks for Generating 3D Printed Tissue Constructs. *Mar Drugs* **2018,** *16* (12).

5. Wang, N.; Tytell, J. D.; Ingber, D. E., Mechanotransduction at a distance: mechanically coupling the extracellular matrix with the nucleus. *Nat Rev Mol Cell Biol.* **2009,** *10*, 75-82.

6. Ugarte-Berzal, E.; Vandooren, J.; Bailon, E.; Opdenakker, G.; Garcia-Pardo, A., Inhibition of MMP-9-dependent Degradation of Gelatin, but Not Other MMP-9 Substrates, by the MMP-9 Hemopexin Domain Blades 1 and 4. *J Biol Chem* **2016,** *291* (22), 11751-60.

7. Vandooren, J.; Geurts, N.; Martens, E.; Van den Steen, P. E.; Jonghe, S. D.; Herdewijn, P.; Opdenakker, G., Gelatin degradation assay reveals MMP-9 inhibitors and function of O-glycosylated domain. *World J Biol Chem* **2011,** *2* (1), 14-24.

8. Lee, D.; Cha, C., The combined effects of co-culture and substrate mechanics on 3d tumor spheroid formation within microgels prepared via flow-focusing microfluidic fabrication. *Pharmaceutics* **2018,** *10* (4), 229.

9. Lee, D.; Lee, K.; Cha, C., Microfluidics-assisted fabrication of microtissues with tunable physical properties for developing an in vitro multiplex tissue model. *Advanced Biosystems* **2018,** *2* (12), 1800236.

10. Hong, J.; Shin, Y.; Kim, S.; Lee, J.; Cha, C., Complex tuning of physical properties of hyperbranched polyglycerol-based bioink for microfabrication of cell-laden hydrogels. *Advanced Functional Materials* **2019,** *29* (13), 1808750.

Acknowledgement

It has been three years and six months since I entered the Laboratory for Integrative Biomaterials Engineering in Ulsan National Institute of Science and Technology (UNIST). As a Ph.D. candidate and as the member of the lab., it was really worthwhile and enjoyable time. Now, as a Ph.D., I want to dedicate my doctoral dissertation to many people who helped me successfully finishing the course.

First of all, I feel grateful to Professor Chaenyung Cha, Professor Jiyun Kim, Professor Hyun-Wook Kang, Professor Tae Eun Park, and Professor Seung Yun Yang who attended as the committee members. Their insights and suggestions were helpful not only to broaden my knowledge but also to give me upcoming ideas to be studied in my career further.

I did not have any experience in biomaterials and bio-related research during my undergraduate and master's course in Chemistry at College of Natural Sciences. However, Professor Chaenyung Cha, who has granted and directed my Ph.D. course, kindly allowed me to be the member of his lab. and work with good people. His sharp comments improved me, so it was absolutely a great honor for me to be the first student in his group to get the Ph.D. degree. In addition, he supported me in being accepted in a post-doctoral program at Harvard Medical school.

I would like to appreciate some graduate students in UNIST who I have met since September 2016: Kangseok as the lab-mate shared his knowledge of bio-experiments. Suntae, Mirae, Jisu and Cholong discussed the research through a number of meetings. Other lab. members including Wonwoo, Min Kyeong, Seunggyu, and Jeonghyun, or Seunguk, InCheol, Soo-chan, Yeonsoo, Byung Hoon, Youngmu, Yonghwan, Seoyoon, and Yungyeong and so on in School of Materials Science and Engineering were warm and friendly to me.

I also cannot help but thank to whom I met in prior to the Ph.D. course. I consulted Professor Jaegeun Noh who advised my master's degree in Hanyang University on my concerns. Dr. Ji yoon Kang in KIST always welcomed me with a bright smile. Dr. Kyung-Sik Shin always bought me dinner and listened to me. Dr. Youngdo Jeong, Dr. Yijae Lee, Dr. Hong Nam Kim and Dr. Nakwon Choi gave me a lot of advice.

Lastly, I really appreciate my lovely wife Minjung, my healthy sons -Junwon and Junyoung-, and my parents who greatly supported me with their in-depth belief, proud and pray. My mother-in-law and father-in-law encouraged me as well. Thank you all of the other family members.